Master Thesis

Concept design of a foldable Cold Water pipe for a 10 MW OTEC installation

R. C. Martens

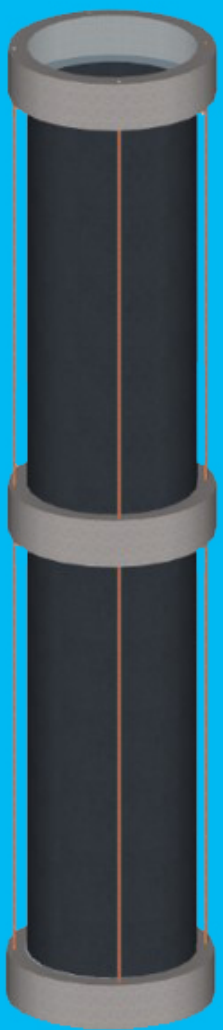

Master Thesis

Concept design of a foldable Cold Water pipe for a 10 MW OTEC installation

by

R. C. Martens

to obtain the degree of Master of Science
at the Delft University of Technology.

Company:

Student number:	4298233	
Project duration:	September 1, 2019 – September 18, 2020	
Thesis committee:	Prof. dr. ir. A. Metrikine,	TU Delft
	Dr. Ir. H. Hendrikse,	TU Delft
	Ir. B.J. Kleute,	Allseas
	Ir. A. Posthuma,	Allseas

Preface

This master thesis contains a concept design of a foldable cold water pipe for a 10 MW OTEC installation. The thesis serves as an exploratory study in order to understand the challenges that are related to a foldable concept design for OTEC technology.

This master thesis is my end work for my master in Offshore and Dredging Engineering. After one year of hard work, I am proud of this thesis. I never would have thought to have learned so much in one year. From learning how to start my day at work, to learning how to do research day-in-day-out. It truly has been an experience with a lot of learning points for myself. Asking enough questions when you get stuck, preparing meetings for myself, setting feasible goals for myself, creating structure in my laptop folders, to name only a few. The skill I am most grateful for to have learned during this graduation period, is to have developed a structured working method for myself in which I stay motivated and in which I keep an overview of what I am doing.

During my graduation I have been supervised by Dr. Ir. H. Hendrikse and Prof dr. ir. A. Metrikine, from the TU Delft. I would like to thank both of them for their support and useful feedback during my graduation period. From the company Allseas, Ir. B.J Kleute and A. Posthuma have supervised me. I would like to thank both B.J Kleute and A. Posthuma for their feedback and support as well, both in good times as well as in somewhat more difficult times. I greatly appreciate the support all of you have given me during my graduation.

Finally, I would like to say a special thanks to all my friends and family. My close friends and family have really helped me to keep going forward with my thesis. This support has been of much added value and I really appreciate all of the support you have given me.

R. C. Martens
Delft, September 2020

Abstract

Ocean Thermal Energy Conversion (OTEC) has been heavily researched and developed over the last decade. However, no commercial scale for OTEC has been reached yet. OTEC is a clean and renewable source of energy which utilizes the seawater temperature difference between the upper and deep ocean layers to generate electricity. The heat exchangers and the cold water pipe design are considered to be the most challenging part. The cold water pipe is often stated to be the largest risk. The installation of the cold water pipe, the high investment costs of the cold water pipe and the large forces acting upon the cold water pipe are crucial factors for the future success of OTEC. In this thesis, a new kind of cold water pipe concept is introduced: the foldable FLEX-hose concept.

The FLEX-hose concept consists of a thin sheet of nylon, supported by concrete rings and polyester cables. The total length of the foldable concept design is 1000 m. The nylon sheet is attached to the concrete rings and the cables are attached to the concrete rings. The cables run through the concrete rings and can be used during installation to lower the pipe. Deployment of the foldable pipe is expected to be relatively easy thereby lowering the installation costs. The Multi Criteria Analysis performed in this thesis show the FLEX-hose foldable concept to be attractive compared to a foldable spiral concept, a flexible composite concept, a rigid composite pipe and a HDPE pipe. However, the inclination angle occurring while pumping may not become significant, meaning above 7.5 degrees, since this will lead to lower energy efficiency. In addition, no current design is available on the market, meaning heavy research and development is needed for the foldable concept to succeed.

Possible challenges for the FLEX-hose concept that have been established through this research include instability occurring due to buckling and a pressure drop becoming larger than 0.6 bar, thereby significantly reducing the net power of the OTEC plant. The maximum allowed angle of inclination of the sheet to stay below 0.6 bar is calculated to be 7.5 degrees at a flow speed of 2 m/s. During pumping a discharge of 20.000 kg/s is pumped through a thin walled pipe with a diameter of 3.5 m, which leads to a radial displacement of the nylon sheet. Collapse and too significant deformations of the thin walled sheet are prevented by applying 10 MN of pre-tension in the thin walled sheet. However, in order for the nylon sheet to stay in the linear elastic regime, the calculated wall thickness is 0.04 m, thereby making foldability questionable. A total of 200 concrete rings is present in the design, one every 5 m over the total length of 1000 m of the pipe. In addition, a large clump weight of 12 MN is needed at the bottom of the pipe. The total system weight of the foldable pipe with concrete rings is calculated to be 1840 mT, which could be installed by an offshore installation vessel. Finally, creep has also been established to be a challenge due to the life-time of 30 years for the cold water pipe. A synthetic plastic material such as nylon experiences relaxation of the material when stressed for a longer period of time, leading to large deformations.

Executive Summary

Ocean Thermal Energy Conversion is a clean and renewable source of energy which utilizes the sea-water temperature difference between the upper and deep ocean layers to generate electricity. OTEC has been heavily researched and developed over the last decade. However, until today no commercial scale for OTEC has been reached yet. The heat exchangers and the cold water pipe are considered to be the most challenging part. The free hanging cold water pipe in the water is considered to be one of the largest challenges for OTEC. This can be explained by the fact that large forces will act upon the vertical pipe and its dynamic behaviour is difficult to fully predict in harsh offshore conditions. From the OTEC projects in the past and the failures that have occurred in these projects, it is concluded that the installation of the cold water pipe, the investment costs and the large forces acting upon the cold water pipe are crucial factors for the future success of OTEC. In this thesis, a new kind of cold water pipe concept is introduced: a foldable FLEX-hose concept.

The FLEX-hose concept consists of a thin sheet of nylon, supported by concrete rings and cables made from polyester. The nylon sheet is attached to the concrete rings and the cables are attached to the concrete rings. The cables run through the concrete rings and can be used during installation to lower the pipe. The force distribution in the cables and the sheet respectively is determined by the axial stiffness of the nylon sheet and the cables. The design requirements for the foldable concept design in this thesis are: pressure drop needs to be below 0.6 bar, the unity checks for the nylon sheet and the cables for the stresses should be acceptable, the cable tension force should be positive and the displacement of the sheet should not be in contact with the cables. The FLEX-hose concept design comprises a cold water pipe with a seawater flow through of 20.000 kg/s, which comes down to 19 m^3/s. A relatively low flow speed of 2 m/s is favourable such that the diameter is below 4 m and the head losses are not above 0.6 bar. The major losses are accomplished by the friction losses. The nominal net power of the OTEC plant after taking into account all the pressure losses and process energy losses is 10.34 MW of a gross energy supply of 15 MW.

A Multi-Criteria Analysis has been performed on five different cold water pipe concept designs in order to compare the foldable concept to other current concepts. The foldable FLEX-hose concept and the HDPE pipe have scored the best in the MCA. The FLEX-hose concept is expected to be a good concept due to easy deployment with the foldable concept and relatively low material costs. However, the inclination angle while pumping may not become above 7.5 degrees at a flow speed of 2 m/s since this will lead to lower energy efficiency. In addition, no current design is available on the market, meaning research and development is needed. Concept 5, the reference HDPE pipe, also performs well in the MCA. The current market that is focused on HDPE as well as the relatively low material costs are considered to be the main advantages. Installation is expected to be relatively difficult, since large parts of pipe will have to be joined together offshore. In order to provide easy installation and lower investments costs for the future of OTEC, the foldable cold water pipe concept is concluded to be a hopeful and good concept.

The final foldable concept design consists of a total of 200 rings over 1000 m, a nylon sheet thickness of 0.04 m and three polyester cables of 0.07 m. The foldability of a nylon sheet of 0.04 m has not been quantified. Identified challenges for the FLEX-hose concept that have been established through the modelling in this thesis include the pressure drop becoming > 0.6 bar, collapse of the thin walled sheet and creep of the nylon sheet. The results of the model show that the pressure drop in the foldable cold water pipe due to the displacement of the sheet is very important for the design. In order to have a pressure drop below 0.6 bar and have a foldable design which is below 2000 mT in weight, a high pre-tension of at least 10 MN is needed in the sheet for every 5 m. In addition, the pressure drop in the cold water pipe increases significantly when the sheet contracts in the upper region from the sea surface until -200 m. Using a span distance of 5 m between the concrete rings is advised since the inclination angle

stays below 7.5 degrees. However, a large pre-tension of 10 MN is still needed, leading to a large clump weight of approximately 12 MN. The second main challenge for the FLEX-hose foldable concept is to prevent buckling collapse from happening. Since the hoop stress becomes negative during pumping of the water and the thickness is only 0.04 m, buckling instability could occur at stresses below the elastic limit or yield strength of the material. The calculated collapse pressure for a thin walled flexible nylon sheet without axial tension varies between 0.13 kN/m^2 and 103.50 kN/m^2, depending on the thickness t and length L between the rings. Since this is relatively low, axial tension by introducing pre-tension in the sheet is advised to prevent instabilities from occurring. The last established main challenge for the foldable design is creep happening in the nylon sheet. Creep is the tendency of a solid material to deform permanently under the influence of constant stress. As time passes by, creep could lead to failure of the material. It could therefore be beneficial to locally increase the strength of the pipe by means of reinforcements thereby reducing the maximum stress in the pipe.

Contents

List of Figures

List of Tables

List of Symbols and Abbreviations

AFRP	Aramid Fibre Reinforced Polymer
CAPEX	Capital Expenditure
CDF	Cumulative Density Function
CFRP	Carbon Fibre Reinforced Polymer
CWP	Cold Water Pipe
DSM	Deep Sea Mining
FRP	Fiber Reinforced Polymer
GFRP	Glass Fibre Reinforced Polymer
HDPE	High Density Polyethylene
HFO	Heavy Fuel Oil
ICE	Internal Combustion Engine
IMO	International Maritime Organization
MCA	Multi Criteria Analysis
MDO	Marine Diesel Oil
OTEC	Ocean Thermal Energy Conversion
PA	Polyamide
PEMFC	Proton exchange membrane fuel cell
PP	Polypropylene
PU	Polyurethane
PVC	Polyvinylchloride
PVDF	Polyvinylidene Fluoride
TLP	Tension Leg Platform
TPE	Thermoplastic elastomers
ULS	Ultimate Limit State
XLPE	Cross Linked Polyethylene

$\dot{m}$	Mass flow
ϵ	Strain
η	Efficiency
ρ_a	Ambient density seawater

ρ_c	Density cold seawater
ρ_s	Density warm (surface) water
σ_a	Axial stress
σ_h	Hoop stress
σ_r	Radial stress
σ_{VM}	Von Mises stress
A	Surface area
D	Diameter
dP	Pressure loss
E	Young's Modulus
f	Friction factor
F_c	Axial cable force
F_s	Axial sheet force
g	Gravitational constant (=9.81 m/s^2)
K	Constant
L	Length
mT	Metric Ton (=1000 kg)
P	Power consumption
p_e	External pressure
p_i	Internal pressure
Q	Discharge
T	Tension
t	Thickness
T_c	Cold water temperature
T_w	Warm water temperature
u_f	Flow speed
W_c	Collapse pressure

1 Introduction

1.1. Background

The global energy demand has been rising steadily in the last decade due to the rising population on Earth. From 2017 to 2050 the global economy is expected to grow by 130 % [13]. In addition, the growing need for renewable energy has been acknowledged by governments in order to be able to lower the global CO_2 footprint and meet the goals of the Paris Agreement. As a logical consequence, it has become more important to produce renewable energy in the current society.

1.1.1. Energy transition

In the last decade, the energy transition has become an important subject in our society. The Paris Agreement, signed in 2016, has forced governments and business to be made aware and act accordingly on the subject of climate change. The long term goal of the Paris Agreement is to keep the global warming below 1.5 °Celsius, which can only be achieved with strong enforced policies lowering the carbon footprint of society [14]. A forecast of the world primary energy supply by source is shown in Figure 1.1. It is clear to see that fossil fuels such as coal and oil, which are the main producers of CO_2, are predicted to decline in production, following from the stricter climate regulations. Natural gas, also implying LNG, is predicted to grow in volume. Renewable sources such as wind, solar energy, hydro-power, biomass and nuclear fuels are also expected to grow in volume, as can be seen in Figure 1.1.

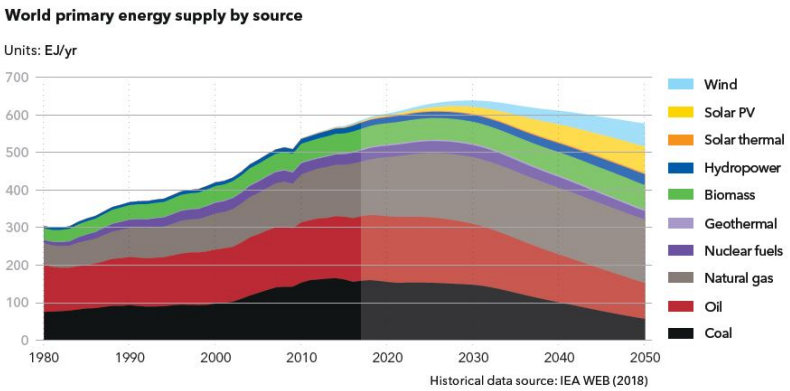

Figure 1.1: World primary energy supply by source [13]

The Paris Agreement implies both limiting global warming, as well as preventing air pollution by improving air quality. Limiting global warming can be achieved by lowering greenhouse gas intensities in our economy. The main greenhouse gas that contributes to global warming is CO_2, which accounts for 76 % of the total emitted greenhouse gasses [2]. Other greenhouse gasses include methane (CH_4), nitrous oxide (N_2O) and fluorinated gases. An overview of all the greenhouse gasses is shown in Table 1.1. In addition, the main substances that contribute to air pollution are PM (particulate matter), ozone, NO_2, CO and SO_2 [29]. PM is a term used to described small solid particles and liquid droplets suspended in the air. Particulate matter mainly comes from motor vehicles, wood burning heaters and industry activities. For the maritime sector in particular, the emissions of NO_2 and SO_2 are of importance since these gasses are produced while using marine diesel oil.

Greenhouse gas	**Relative percentage (%)**
Carbon dioxide (CO_2)	76
Methane (CH_4)	16
Nitrous oxide (N_2O)	6
Fluorinated gases (CFC's)	2

Table 1.1: Greenhouse gasses in relative contribution [2]

Energy transition in maritime industry

Since 13 April 2018, the International Maritime Organization (IMO) agreed upon a strategy for handling climate change in the maritime sector as a result of the Paris Agreement. This agreement is called *IMO 2050*. The IMO is responsible for measures to improve the safety and security of international shipping and to limit marine pollutants from ships. In total, it is estimated that the maritime industry emits around 940 million tonnes of CO_2 on a yearly basis, accounting for about 2.5 % of the global greenhouse gas emissions. Shipping emissions represent about 13 % of the transport industry of the overall EU greenhouse gas emissions [9]. Therefore, it is inevitable that the energy mix consumption in the maritime industry has to change in the future.

IMO 2020 is the first enforcement that is applied. This enforcement contains agreements concerning limits for sulphur in fuel oil used on board of ships, to comply to new standards for air quality. The sulphur content in fuel oil may not exceed 0.50 %, starting from 1 January 2020. This can be achieved by using a compliant fuel oil with a sulphur content that does not exceed 0.50 %, or by using a so called scrubber (Exhaust Gas Cleaning System). Alternatively, another fuel such as LNG or methanol can be used. A more in detailed explanation of *IMO 2020* is provided in Appendix B.

The agreement of the *IMO 2050* contains the following objectives [23]:

1. Making the Energy Efficiency Index (EEI) standards more strict, meaning an increase in the number of more energy-efficient built vessels.
2. Reducing the transport performance of a ship, which is measured in CO_2 emissions per kilometre.
3. Reduction of greenhouse gases of at least 50 % by 2050.

These three objectives as proposed by the IMO for *IMO 2050* are ambitious, meaning it is important that all stakeholders take responsibility for achieving those goals. In addition, it is also important that more research and development is performed regarding alternative fuels. There are two possible ways that are suggested by the DNV-GL to be able to reach these goals. The first strategy focuses on design requirements for new build ships, arguing that a complete fuel shift should happen from 2040 onwards. Option two focuses on operational requirements, arguing that alternative fuels such as biodiesel and liquefied biogas should be introduced more gradually [36]. In the end, it are flag states and port states that have rights and responsibilities to enforce compliance.

In 2038, it is predicted that half of the maritime energy use will be non-oil. A possible energy use and projected fuel mix for the simulated IMO ambitions is shown in Figure 1.2. In order to reach the climate goals of *IMO 2050*, a decline in the use of heavy fuel oils and scrubber (HFO) has to be accomplished and new and more renewable energy sources should be used. In Figure 1.2 it is clear that HFO and scrubber are expected to decline heavily in use.

Fuels such as low-sulphur fuel oil (hybrid) together with LNG and ammonia in combination with diesel as a dual fuel are expected to increase in use as a consequence of the IMO regulations. Other examples of renewable energy sources that are suitable on an offshore vessel are fuel cells, nuclear energy and Ocean Thermal Energy Conversion (OTEC). More explanation about the energy transition is provided in Appendix A, including an MCA about possible new energy sources for the maritime industry.

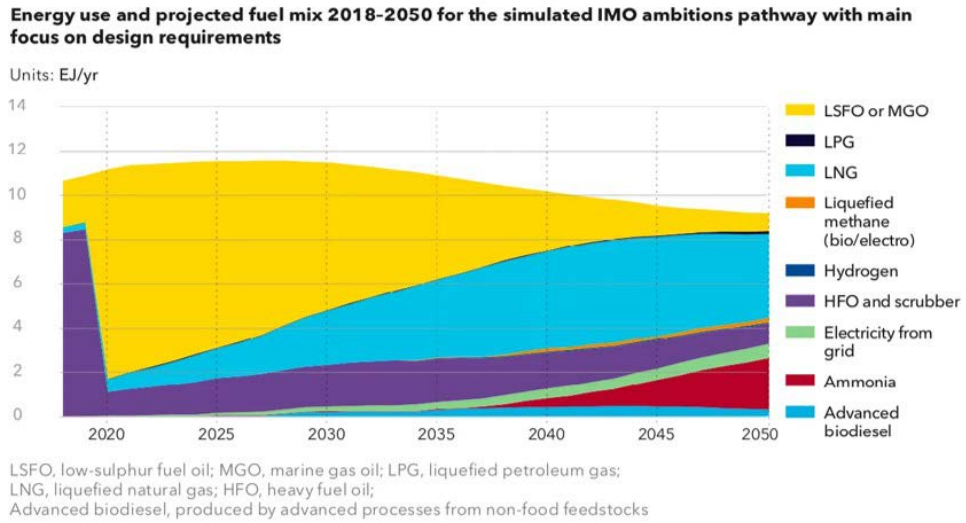

Figure 1.2: Energy use and projected fuel mix in maritime industry [14]

1.2. Ocean Thermal Energy Conversion

OTEC is a clean and renewable source of energy which utilizes the seawater temperature difference between the upper and deep ocean layers to generate electricity. It can be used to produce a base-load electricity without emitting CO_2. The net efficiency of an OTEC system is relatively low around 3 %. However, OTEC is a free source of energy since it is solar energy that is conserved in the ocean. In addition, the temperature gradient is relatively constant during the day, meaning OTEC energy produces a base load electricity throughout the year. Lastly, the LCOE of an offshore OTEC plant is calculated to be €0.19/kWh , which is competitive in comparison to other energy sources [5]. Figure 1.3 presents a graph of the costs associated with OTEC in comparison to other energy sources such as oil.

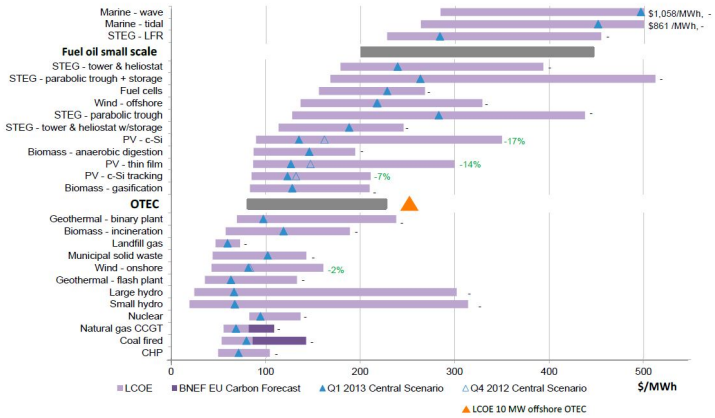

Figure 1.3: LCOE of different energy sources [5]

OTEC is most applicable around the equator in tropical and coastal regions, where the temperature differential is at least 20 degrees. Since more than half of the world's population lives within 100 km from the coast and roughly 1 billion people live in tropical regions, OTEC is considered to be a good potential source of energy for these areas. The largest OTEC resource is available offshore reaching larger ocean depths, in which an offshore floating OTEC plant is needed to generate the electricity.
In tropical areas the surface water can reach temperatures which are higher than 25 degrees, whereas the temperature at 800 - 100 m depth is as low as 4 - 5 degrees [12]. The red areas in Figure 1.4 present the best possible locations for OTEC with the largest temperature difference. A larger temperature difference is favorable since this means a higher efficiency for the generated electricity. The total global potential is estimated to be 7 TW, which is more than two times the global electricity demand [7].

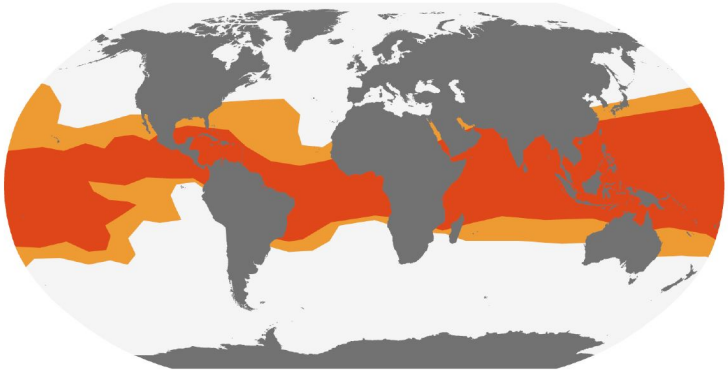

Figure 1.4: Ocean's resource for OTEC [5]

1.2.1. Working principle OTEC

The working principle of OTEC is a thermodynamic Rankine Cycle that converts thermal energy into electricity. In a Rankine cycle, a particular working fluid is used comparable to the working fluids used in heat pumps in household refrigerators. First, the working fluid is pressurized, after which it is heated in the heat exchangers by the warm water that is extracted from the ocean's upper layer. The working fluid expands and this results in pressurized vapour which drives a turbine to generate electricity. Usually, ammonia is used as the working fluid. After this, the cold water is used to condense the ammonia back to the liquid phase at lower pressure. In this way a closed cycle is created with a working fluid which is pumped throughout the closed cycle. In general, an OTEC plant requires the following parts to function properly: two inlet pipes (cold and warm), one large outlet discharge pipe, three pumps (cold, warm, cycle), an evaporator and a condenser. The working principle of an OTEC system can be seen in Figure 1.5.

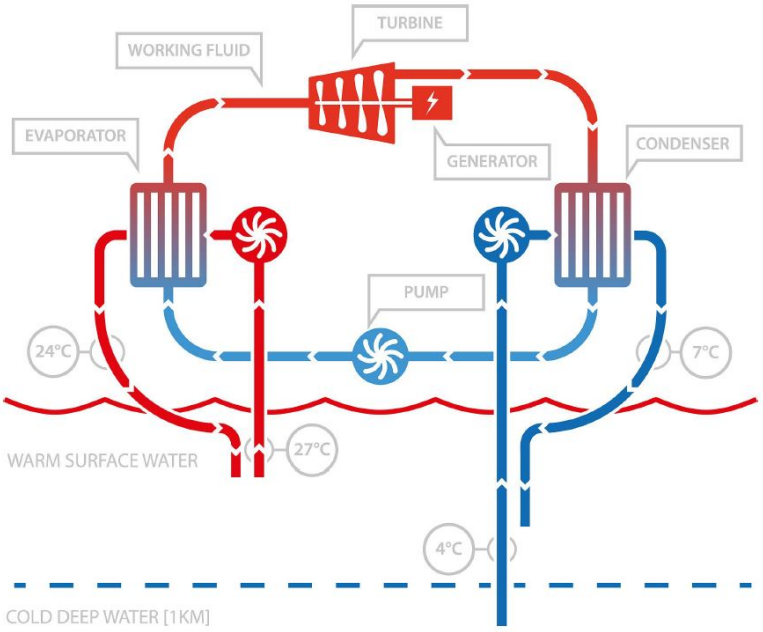

Figure 1.5: Working principle of OTEC [22]

There are three possible cycles that can be used in an OTEC system: a closed cycle, an open cycle and a hybrid cycle [4]. The closed cycle uses a working fluid such as ammonia to be evaporated. The advantage of ammonia instead of other working fluids is that it has a relatively low boiling point due to which it evaporates relatively quickly. In the open cycle warm seawater is used for evaporation. The open cycle, however, has lower efficiencies due to the fact that it takes more energy to warm up water. In the hybrid cycle a mix of water and a working fluid is used.

1.2.2. History of OTEC

In 1930, George Claude was the first person to build a land-based OTEC plant. After three failed attempts he finally succeeded to install a deep water pipeline at Matanzas bay in Cuba. Later in the year, unfortunately, the OTEC pipeline installation was destroyed by a storm. In 1935, Claude constructed a new plant aboard a 10.000 ton cargo vessel which was called Tunisie. This plant had an inlet pipe of 2.5 m steel in diameter and it was 650 m long. Unfortunately, the weather and the waves destroyed the OTEC pipe before it could generate power.

OTEC technology was heavily developed in the 80s, when the offshore industry was mainly being driven by the offshore oil and gas industry. In 1979, a first "Mini OTEC" of 50 kW was produced with a High Density Poly-ethylene (HDPE) tube of 670 m in length and 0.7 m in diameter. The "Mini OTEC" project was located in Hawaii and it was the first OTEC project to generate more electricity than was needed for running the electricity plant, meaning it had a positive net energy output. A few years later, in 1981, another experiment called "OTEC-1" was carried out on the same location. Three HDPE pipes having a diameter of 1.2 m were installed. It was a successful operation and the test site was used to test the technology. The years after this OTEC technology was on the rise, which lead to a 1 MW OTEC floating plant being installed in India in 2006. Unfortunately, the plant was unsuccessful due to failed installation of the deep sea cold water pipe.

More recently, in 2014, DCNS announced the funding for the NEMO project. DCNS developed a large diameter foldable pipe. However, the project failed because there were problems with certifying a new pipe and it was considered to be too expensive. One year later, in 2015, a collaboration between Makai Ocean engineering and Lockheed Martin resulted in the realization of an OTEC power plant in Hawaii. This is the first land-based closed OTEC cycle connected to the grid which is capable of generating 105 kilowatts, enough to power about 120 homes. The cold water pipe is made from HDPE. A total overview of previous OTEC projects can be seen in Table 1.2.

From the OTEC projects in the past and the failures that have occurred, it can be concluded that the installation of the cold water pipe, the investment costs and the large forces acting upon the cold water pipe are crucial factors for the future success of OTEC.

Year	Project/Location	Onshore/Offshore	Power	Pipe material	Length	Diameter	Result
1930	Matanzas Bay, Cuba	Onshore	22 kW	Steel	2000 m	1.6 m	Pipe destroyed by a storm
1933	La Tunisie, Brazil	Offshore	2.2 MW	Steel	1000 m	2.5 m	Attempt to deploy pipe failed
1979	Mini-OTEC, Hawaii	Offshore	50 kW	HDPE	670 m	0.7 m	Successful operation
1980	OTEC -1, Hawaii	Offshore	1 MW	bundle HDPE	670 m	1.2 m	Successful operation
1983	Hawaii	Test facility	-	FRP	122 m	2.4 m	Successfully demonstrated
2006	India	Offshore	1 MW	HDPE	800 m	1 m	2 attempts to deploy pipe failed
2014	DCNS - NEMO	Test facility	-	foldable concept	15 m	1.5 m	Problems with certifying and too expensive
2015	Makai, Hawaii	Onshore	105 kW	HDPE	670 m	1.0 m	Successful operation, still in use
2019	South Korea	Offshore	1 MW gross	HDPE	100 m	1.2 m	Unknown

Table 1.2: Previous OTEC projects [12] [22] [21]

1.3. Problem description

The energy transition is changing industries globally, including the maritime sector. This means new energy concepts including renewable energies are becoming more important in the maritime sector. As described in the previous section, OTEC technology has been heavily researched and developed over the last decade. However, no commercial scale for OTEC has been reached yet. The heat exchangers and the cold water pipe are considered to be the most challenging part [4]. The cold water pipe is often stated to be the largest risk of OTEC. Immature design and unsettled technology of the cold water pipe are considered to be the main reasons why OTEC developments get stuck in pilot projects [1]. Especially the free hanging pipe in the water is a large challenge, as large forces will act upon this vertical pipe and its dynamic behaviour is difficult to fully predict in harsh offshore conditions. In addition, OTEC requires large seawater flows at low pressure losses which is a large challenge. As a result, it can be concluded that the optimization of the design of the cold water pipe is of crucial importance for the future success of OTEC.

1.4. Subject of thesis

The subject of this thesis is a concept design of a foldable pipe for a 10 MW offshore OTEC plant, similar to the schematic drawing in Figure 1.6. The main components of the offshore OTEC plant consist of a floating vessel structure, seawater pipes, pumps and moorings. The process components on-board of the OTEC plant are the heat exchangers, working fluid piping, working fluid pump and the turbine. Connection to the shore is provided by a cable which transports the produced electricity from the platform to the shore.

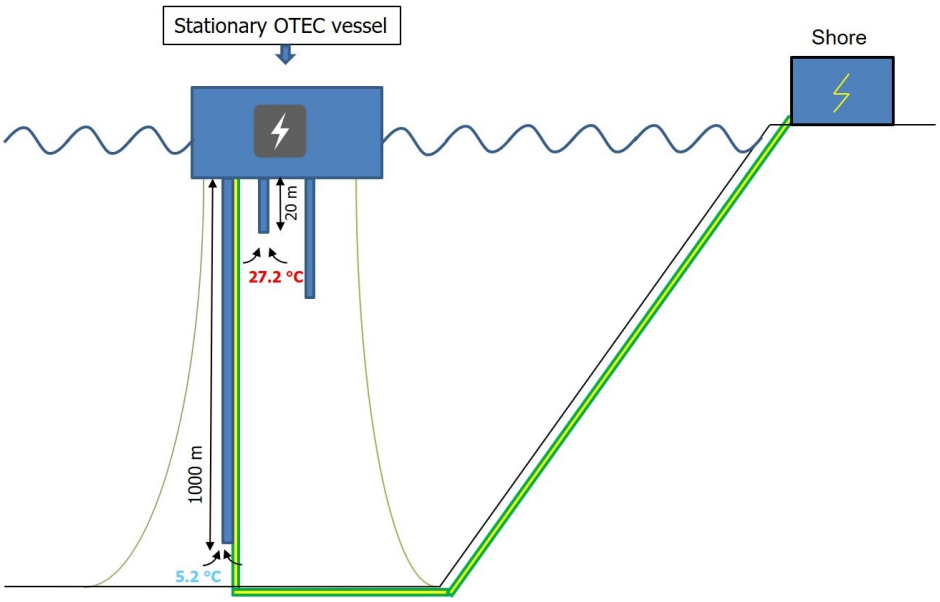

Figure 1.6: Schematic drawing offshore OTEC plant

The design goals for the cold water pipe in this thesis are:

- Enough strength and stiffness during operation, such that the cold water pipe does not collapse when water is being pumped through the pipe.
- Easy installation of the cold water pipe by introducing a foldable or flexible concept.
- High flow rates and low pressure losses should be achieved for the upscaling of OTEC.
- Costs of the cold water pipe should be as low as possible.

1.5. Research question

The main research question of this thesis is:

- **To what extend is a foldable OTEC pipe concept technically feasible for a 10 MW offshore plant and how does a foldable pipe compare to current cold water pipe concepts?**

The sub-questions that will help answer the research question are:

- What are the key design requirements of a Cold Water OTEC pipe for a 10 MW OTEC plant?
- How does a foldable OTEC pipe compare to current cold water pipe concepts?
- What are the main technical risks that influence the technical feasibility in the situation of operation and to what extent can these risks be mitigated?

1.6. Thesis outline

The thesis is divided into 4 main parts: introduction, analysis, modelling and conclusions. An overview of the thesis outline is shown in Figure 1.7.

Part I contains the analysis phase of the thesis done through literature study. The literature study is split up into the cold water pipe design analysis and the flexible concept designs. Subsequently, chapter 2 discusses the OTEC system requirements which are used as input values for the foldable cold water pipe design. Chapter 3 discusses the current research and developments in relation to material choice for the cold water pipe. Chapter 4 presents the multi criteria analysis for the different possibilities for the cold water pipe. The theory which is of importance for the chosen concept design is discussed in chapter 5.

Part II contains the modelling and calculations of the foldable FLEX-hose pipe. In Chapter 6, the model description is provided by discussing the assumptions and implications of the modelling. Chapter 7 presents the results of the modelling, concluding with a suggestion of the most optimal final design.

Finally, Part III contains the conclusions and recommendations of the thesis. In Chapter 8 the conclusions of the thesis are drawn. Finally, Chapter 9 presents the recommendations for future work that could be conducted.

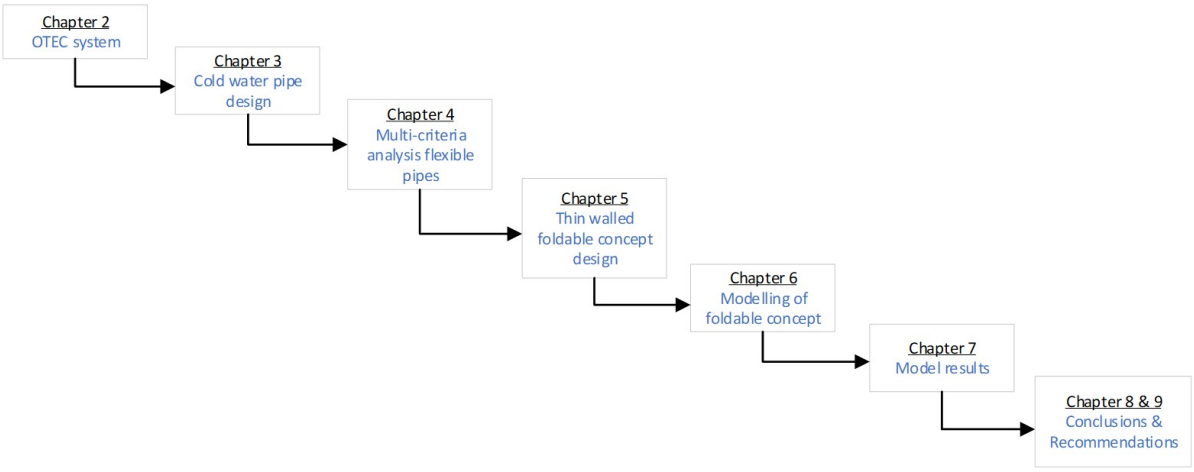

Figure 1.7: Thesis outline

I

Analysis

2

OTEC system

In this chapter, the basis of design parameters of the OTEC system are presented. This includes the temperature of the cold water and warm water pipe, the expected energy output, flow discharges and the length of the cold water pipe. First, the main OTEC sensitivities and the different OTEC configurations are discussed through literature research. After this, the chosen design requirements for the OTEC system in this thesis are presented and discussed.

2.1. OTEC system efficiency

There are many factors that influence the total net system efficiency of the OTEC plant. The main OTEC parameters that influence the net energy output are presented in Figure 2.1. The temperature difference of an OTEC system clearly has the largest impact on the energy output, which is why it is important to have a location with enough temperature difference potential. A minimum difference of temperature between the cold and warm water pipe of 20 degrees is desired. Other factors that play an important role in the net energy output are turbine efficiency and generator efficiency. However, the turbine efficiency and generator are limited by the industry turbines and generators. Lastly, the pressure drop in the cold water pipe and the pipe diameter play an important role in the net energy output. These two factors can be influenced by the design choices made for the cold water pipe. A design of the cold water pipe leading to a relatively low pressure drop and a relatively small pipe diameter is therefore the most desirable.

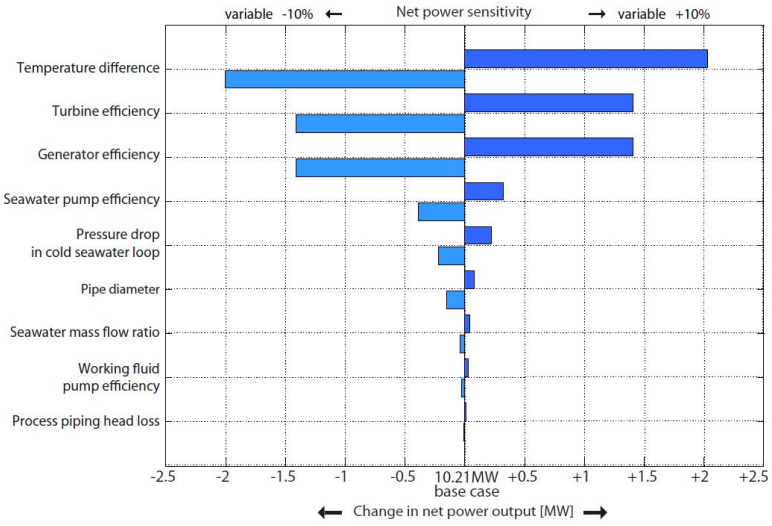

Figure 2.1: Sensitivity of OTEC system [22]

2.2. OTEC system configuration offshore

There are multiple OTEC design configurations possible, differing in size as well as in use: ship moored with swivel, barge with spread mooring, semi-submersible, cell spar and Tension Leg Platform (TLP). A schematic overview including the advantages, disadvantages, limitations, challenges and opportunities is presented in Figure 2.2. The cell spar concept and the TLP are mostly stated to be the best concepts for OTEC technology. The spar concept is excellent in stability and has a good pipe connection, whereas the TLP is low weight and also has an excellent pipe connection.

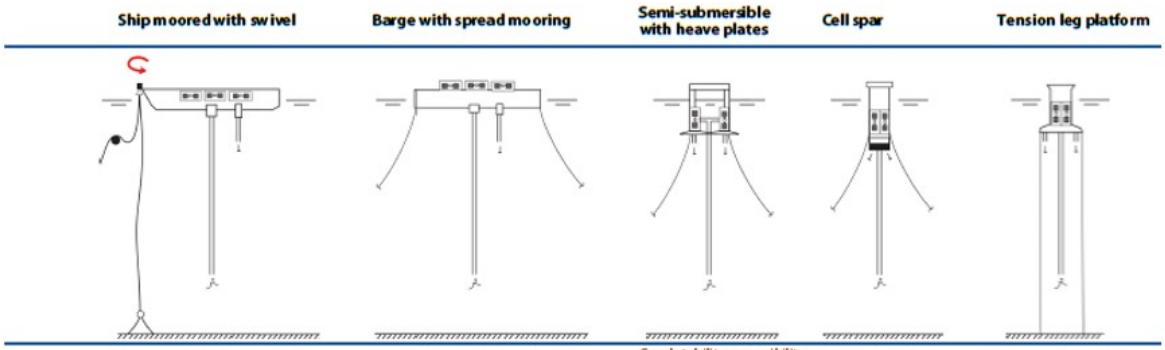

	Ship moored with swivel	Barge with spread mooring	Semi-submersible with heave plates	Cell spar	Tension leg platform
Advantages	Easy to mobilize; low cost hull; accessibility; off-the-shelf available	Simple hull and mooring design; low cost; off-the-shelf available	Good stability; accessibility; lower pumping requirements	Excellent stability; compact; good pipe connection	Low weight; excellent pipe connection
Disadvantages	Ship motions; higher pumping requirements	Barge motions; unstable behavior in beam seas; higher pumping requirements	High engineering needs; labor intensive fabrication	Heavy weight; dedicated installation vessel required	Complex transport and installation
Limitations	Lower availability in rough weather conditions; design flexibility	Lower availability in rough weather conditions; low economy of scale; design flexibility	Less applicable to one-off plant design	Less applicable to one-off and very large plant design	Water depth; scalability
Challenges	Swivel mooring of ship; connection to pipes and power cable	Motions and stability; connection to pipes and power cable	Layout optimization	Vortex induced platform motions	Vortex induced platform motions
Opportunities	Conversion of existing ship possible; readily available for pilot plant	Conversion of existing barge possible; readily available for pilot plant	Standardizing design and mass fabrication	Standardizing design and mass fabrication	Extreme weather resistant design

Figure 2.2: Different possibilities in offshore OTEC configurations [5]

2.3. Design requirements OTEC system

The design requirements of the OTEC system in this thesis are determined in consultation with Allseas. The design requirements are listed below:

- 10 MW of net electricity should be generated (W_{net}).
- The temperature difference between the cold and the warm water should be at least 20 °C(ΔT).
- The thermal energy efficiency of the overall OTEC system should be 2.5 % - 3 % (η_{net})
- The design life of the OTEC system is 30 years in operational state.

2.3.1. Basis of design values

The values presented in Table 2.1 are chosen for the design of the OTEC system. A maximum pump loss of 30 % in the OTEC system is determined to be a reasonable estimate [6]. As a logical consequence, it is necessary to pump 15 MW of gross OTEC energy through the system. The discharges through the OTEC cycle are respectively 19 m^3/s through the cold water pipe, 38 m^3/s through the warm water pipe and 57 m^3/s through the discharge pipe.

Example values for the water temperature that is pumped up are used from the location of Bonaire. All the environmental parameters are explained in Appendix F. The cold water that is pumped up from 1000 m has a temperature of 5.2 °C, whereas the warm water that is pumped up from 20 m has a temperature of 27.2 °C. This means the temperature difference of at least 20 °C, is sufficient for OTEC

technology. The temperature profile is presented in Appendix F. The values corresponding to general environmental conditions are summarized in Table 2.2.

OTEC system	Value	Unit
W_{gross}	15	MW
W_{net}	10.34	MW
Allowed pump loss	30.00	%
Q_{cwp} = $Q_{c,c}$	19	m^3/s
Q_{wwp} = $Q_{w,e}$	38	m^3/s
Q_{out}	57	m^3/s
$P_{t,warm}$	419	MWt

Table 2.1: Basis of design OTEC parameters

Environmental conditions	Value	Unit
T_c	5.2	°C
T_w	27.2	°C
ΔT	22	°C
$Depth$	1200	m

Table 2.2: Environmental conditions general Bonaire

2.3.2. Thermodynamic efficiency

OTEC converts thermal energy into electricity by applying a thermodynamic Rankine cycle. By applying the fundamentals of thermodynamics, the thermal efficiency can be calculated. This theoretical maximum is determined by the Carnot cycle. The thermal Carnot efficiency can be calculated by equation 2.1 [22]. Both the cold and warm water are important input parameters since both have a direct influence on the Carnot efficiency.

$$\eta_{\text{Carnot}} = 1 - \frac{T_{\text{c}}}{T_{\text{w}}} \tag{2.1}$$

in which:

- T_c is the temperature in the cold water pipe [°C]
- T_w is the temperature in the warm water pipe [°C]

For the parameters of Bonaire, a Carnot efficiency of 7.32 % is achieved. However, the gross thermal efficiency is lower in the system. In total, the gross efficiency is described by equation 2.2.Typically, the exergy of the system is 64 %, the turbine efficiency is 85 % and the generator efficiency is 90 % [22]. This leads to a gross thermal efficiency of 3.58 % of the OTEC system for Bonaire.

$$\eta_{\text{gross}} = \eta_{\text{carnot}} \cdot \eta_{\text{exergy}} \cdot \eta_{\text{turbine}} \cdot \eta_{\text{generator}} \tag{2.2}$$

in which:

- η_{carnot} is the Carnot efficiency [%]
- η_{exergy} is the exergy efficiency [%]
- $\eta_{turbine}$ is the turbine efficiency [%]
- $\eta_{generator}$ is the generator efficiency [%]

As a disadvantage of OTEC, it is often stated that the thermal efficiency of the OTEC system is relatively low. However, the thermal efficiency is not a good indicator to compare OTEC with different energy sources, as the ”cost” of the fuel for OTEC is zero. The energy that is stored in the ocean is sustainable, available and free. Besides, there are a number of possibilities to improve the overall efficiency of the OTEC system: using novel working fluids, using different thermodynamic cycles, optimization of heat exchanger design and customized turbine design [22].

2.3.3. Pump losses in the OTEC system

As stated in section 2.3.1 , the pump energy that is lost due to pumping the water throughout the OTEC system is 30 % of the gross power, which is a significant loss. There are four different causes considered for this pump loss leading to a pressure drop, which are listed below.

1. **Cold water power consumption**

   The cold water power consumption is dependent on the pressure drop and the discharge in the cold water pipe. The higher the pressure drop and the discharge through the cold water pipe, the higher the cold water power consumption. In Figure 2.3 and in equation 2.3, the cold water power consumption is represented by P_3.

2. **Warm seawater power consumption**

   The warm water power consumption is dependent on the pressure drop and the discharge in the warm water pipe. The higher the pressure drop and the discharge through the warm water pipe, the higher the warm water power consumption. In Figure 2.3 and in equation 2.3, the warm water power consumption is represented by P_1.

3. **Working fluid power consumption**

   The working fluid power consumption can be approximated as 4.2 % of the gross power [6]. In Figure 2.3 and in equation 2.3, the working fluid consumption is represented by P_2.

4. **Heat exchangers power consumption**

   The total heat exchangers power consumption can be determined by a summation of the pressure drops in the evaporator and the condenser. Both heat exchangers have a pressure drop in the order of magnitude of 0.3 bar [22]. In Figure 2.3, the heat exchanger power consumption is represented by E and C. In equation 2.3, the heat exchanger components are represented by P_c and P_e.

The total pump loss can be described by equations 2.3 and 2.4. The pressure drop resulting from the heat exchangers is not included. A schematic representation of the system is displayed in Figure 2.3.

$$P_1 + P_2 + P_3 + P_e + P_c = 0.3 * W_{gross} \tag{2.3}$$

$$(\Delta p_1 * Q_1 + \Delta p_e * Q_e + 0.042 * W_{gross} + \Delta p_3 * Q_3 + \Delta p_c * Q_c) * 0.1 = 0.3 * W_{gross} \tag{2.4}$$

in which:

- P_1, P_2 and P_3 denote the energy loss due to respectively the warm seawater consumption, working fluid and cold water consumption $[MW]$
- P_e denotes the energy loss due to the evaporator $[MW]$
- P_c denotes the energy loss due to the condenser $[MW]$
- W_{gross} denotes the gross energy input $[MW]$
- Δp_1, Δp_2 and Δp_3 denote the pressure drop due to respectively the warm seawater pipe, working fluid and cold seawater pipe $[bar]$
- Δp_e and Δp_c denote the pressure drop in respectively the evaporator and the condenser (=0.3 bar) $[bar]$
- Q_e and Q_c denote the discharge in the evaporator and the condenser $[m^3/s]$

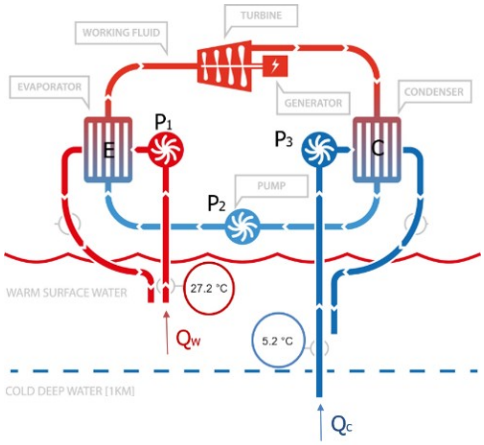

Figure 2.3: OTEC system [5]

2.3.4. Total cycle efficiency

With equation 2.4, the total maximum head loss in the cold water pipe is determined to be 0.6 bar, in order to stay above an OTEC efficiency of 70 %. This is also shown in Figure 2.4. The net thermal efficiency of the OTEC system, after taking into account the pump losses of the system, is determined to be 2.51 %.

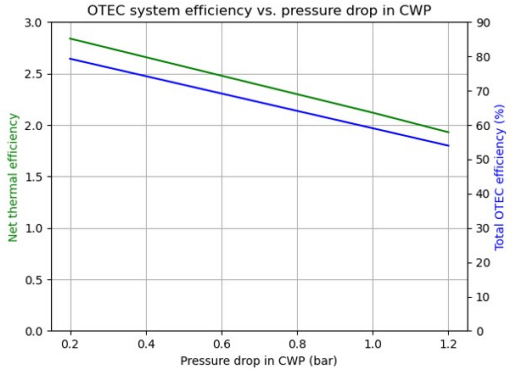

Figure 2.4: OTEC system efficiency as a function of head loss in cold water pipe

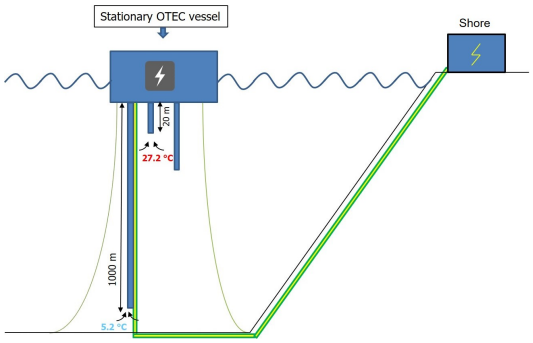

Figure 2.5: Overview OTEC system

2.4. Summary OTEC system values

The general operation conditions for the design of the OTEC plant are summarized in Table 2.3. Regarding the OTEC system configuration, a preliminary choice is made for a barge with spread mooring because of its large water surface area leading to a higher buoyancy force, making it possible to lift relatively easier with smaller cranes. In addition, Allseas is in possession of multiple vessels which characterize a barge with spread mooring, making an OTEC installation plant more attractive. An overview picture of the total OTEC system is given in Figure 2.5

OTEC system operating conditions	**Value**	**Unit**
Gross energy	15	MW
Temperature cold seawater	5.2	°C
Temperature warm seawater	27.2	°C
Heat flow warm water	419	MWt
Length cold water pipe	1000	m
Carnot efficiency	7.3	%
Turbine efficiency	85	%
Generator efficiency	90	%
Exergy efficiency	64	%
Gross thermal efficiency	3.6	%
Net thermal efficiency	2.5	%
Pressure drop cold water pipe	0.6	bar
Total power consumption	4.62	MW
Nominal net power	10.34	MW
OTEC system efficiency	69.20	%

Table 2.3: Summary of OTEC system values

3

Literature review on cold water pipe design

In this chapter, the current research in cold water pipe design is discussed . First, non-flexible materials such as steel, HDPE and composites are discussed. After this, the applicability of flexible materials into the cold water pipe design are discussed.

3.1. Cold water pipe materials

Up to today, there is no consensus what kind of pipe configuration is the best for the cold water pipe. HDPE is often mentioned as the best material choice. Other materials that are usually mentioned for the cold water pipe are steel, concrete, fiber-reinforced plastic (FRP), glass-reinforced plastic (GRP) and more flexible materials such as polyamides [12] [22].

Cold water pipes that have been installed up until now are relatively small compared to the length of 1000 m that is needed for the cold water pipe in OTEC. Next to this, the current upper limit of a pipe diameter is 4 m [22]. Other criteria that are important to take into consideration when choosing the cold water pipe material are : yield strength of the material, complexity of installation, availability in larger diameters, costs, corrosion resistance, thermal conductivity, surface roughness, resistance to fatigue and sensitivity to biofouling. A lower thermal conductivity means the cold water in the pipe will remain colder during operation and a a lower surface roughness means a higher efficiency of the OTEC system.

3.1.1. HDPE

HDPE is often mentioned as the best material choice due to high flexibility, lightness, stability, long life-time in both fatigue and corrosion and cheap to average material prices. In offshore environment, HDPE is mostly used for the transmission of water over longer distance and it is most well known for its high strength-to-density ratio. HDPE pipes are generally available in diameters up to 3 m and with lengths up to 500 m . The maximum diameter available of HDPE is 4 m [22]. The segments of HDPE can be fused or flanged together. One of the disadvantages of HDPE is that the yield strength is time dependent, since HDPE experiences creep over a longer period of time. Next to this, HDPE has a density that ranges from 939 to 960 kg/m^3, meaning ballast is needed to prevent buckling from happening in the pipe and provide stability. Lastly, relatively low material strength and today's limited size of manufacturing reduce the options of upscaling of HDPE. In Figure 3.1, the most important material properties of HDPE are summed up [21].

Material property	Value	Unit
Density	960	kg/m^3
Design stress after 50 years	6.3 / 8.0 *	MPa
Design stress at time zero	9.4 /12.0 *	MPa
Modulus of elasticity after 50 years	200	MPa
Poisson's ratio	-	0.4 - 0.5
Average coefficient of thermal expansion	0.2 * $10^{-}3$	$°C^{-}1$

* Safety Factors are 1.6 and 1.25 respectively

Table 3.1: HDPE characteristics [20]

HDPE concepts

In the past, two types of HDPE concept designs have been researched: one large HDPE pipe and a bundle of smaller HDPE pipes. A schematic presentation of these concepts can be seen in Figure 3.1 Size limitation of HDPE pipes requires small bundles of HDPE pipes. A bundle of HDPE is easy to manufacture, transport and deploy. However, previous studies have shown that a HDPE bundle of pipes of around 2.5 m leads to higher pressure drops and a higher added mass being too large. For example, The pressure drop is almost six times as large compared to a single large pipe [12] [22]. A HDPE design with a pipe and a bundle of pipes is shown in Figure 3.1. A large diameter HDPE pipe could, however, be a suitable option.

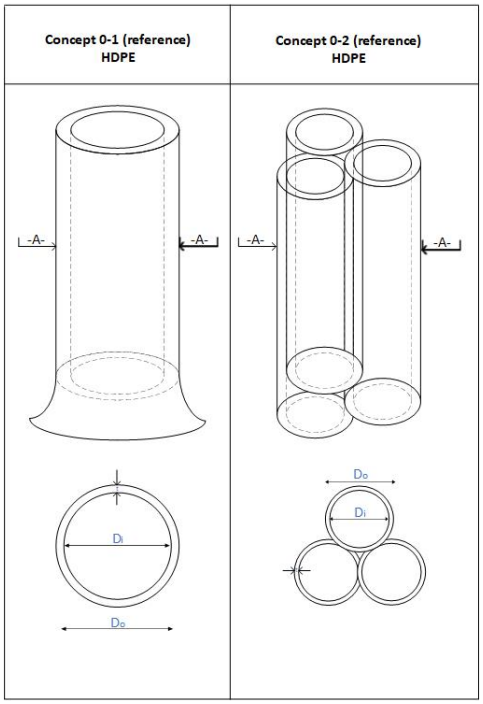

Figure 3.1: Concept drawings HDPE cold water pipe

3.1.2. Concrete and steel

Concrete and steel are materials which are used in various offshore applications, such as the pipeline industry and offshore monopiles due to high impact resistance and relatively low costs. However, both materials have a relatively high density, making the foreseen installation more complex with heavy loads thereby increasing the costs [22]. Steel pipes are currently available in large diameters ranging up to 11 m and having a wall thickness of 250 mm. However, since steel is a highly corrosive material, proper internal and external coating as well as cathodic protection are necessary.

3.1.3. Composites

Composites have been developing rapidly lately, providing new material solutions addressing the requirement for high performance [32]. Composites are materials made from two or more materials having different mechanical properties. Composites such as fiber-reinforced plastic (FRP) and glass-reinforced plastic (GRP) are light, strong and known for good fatigue and corrosion resistance [32]. FRP consists of a compound material, such as an epoxy, and a reinforcing material, such as fibers. Fibers add higher structural stiffness and strength to the material compared to glass fibers. The compound material can either be made from a thermoset or from a thermoplastic. Thermosets are cured irreversibly through a chemical reaction. Examples of thermosets include epoxy and phenolic. Thermoplastics require only heat and pressure in order to form the product, meaning it is a non reactive solid. Examples include PP, HDPE and PA11. PA11 is a polyamide nylon material.

Composite materials have been extensively incorporated into the marine industry, the main reason being the high strength to weight ratio and the resistance against corrosion. Examples are naval applications such as smaller boats, hovercrafts and catamarans . However, within the offshore industry composites have little operational experience. For instance, pipe segment joining techniques still have to be determined. Composites are currently only used for repair of gas pipelines and other offshore components such as risers and tendons. Smart drill pipes of composite are under development within the offshore environment. Metal remains the main choice in pipeline due to good performance in hazardous environments and more knowledge. Besides, the material costs of composite structures are relatively high, making it less attractive. [32]

Composite concepts

1. **Lockhead Martin composite concept**

   Lockheed Martin has developed a new advanced composite pipe, which can be seen in Figure 3.2 [27]. The concept comprises a composite pipe that is built while it is deployed vertically offshore. The idea is to make a continuous pipe and reduce the installation risk. The main challenge is the integration of the whole composite structure. The fibre rolls that are produced are completely continuous since they are not cut out in the process, which is a significant advantage. The disadvantage of the composite pipe is that the whole installation process has to be done offshore.

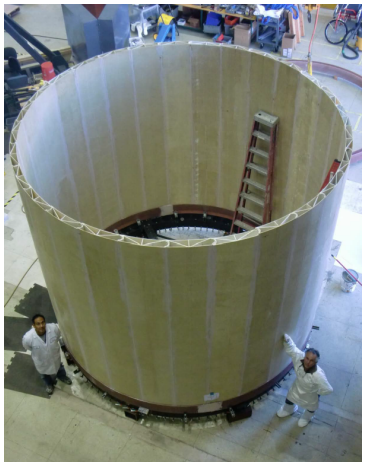

Figure 3.2: Composite concept Lockhead Martin [32]

The installation of the composite pipe is done in the following sequence:

(a) Core ring is being made by joining pultruded planks.

(b) Core is being covered with reinforcement and infused.

(c) When the resin is cured, the mould is removed and the composite is lowered vertically so that a new ring can be attached.

2. **Modular composite pipe**

   Another interesting cold water pipe concept is the modular composite concept, which can be seen in Figure 3.3 [3]. The idea is to pre-fabricate composite modules onshore and deploy the pipe offshore, thereby reducing cost and risk significantly. The concept is provided extra stability by the use of rings along the length of the pipe. In Figure 3.4, it can be seen that using more rings along the length of the pipe may reduce the risk of buckling form occurring.

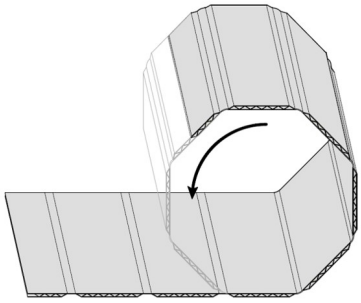

Figure 3.3: Modular composite concept [3]

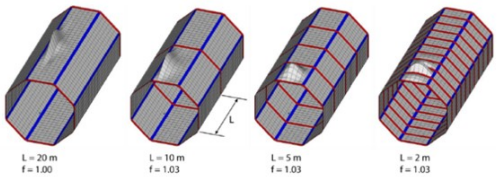

Figure 3.4: First buckling mode of modular composite concept [3]

3. **FRP sandwich pipe with stiffened rings**

   The last composite concept that is discussed is the fiber-reinforced plastic sandwich pipe [18]. Fiber reinforced plastic is combined with balsa wood to form the core of the pipe. Installation could be done with ballast in the pipe. The pipe itself could be pre-fabricated completely onshore. The FRP is resistant against seawater and has a low density. The total costs are estimated to be $ 26.8 M. A schematic picture of the concept can be seen in Figure 3.5.

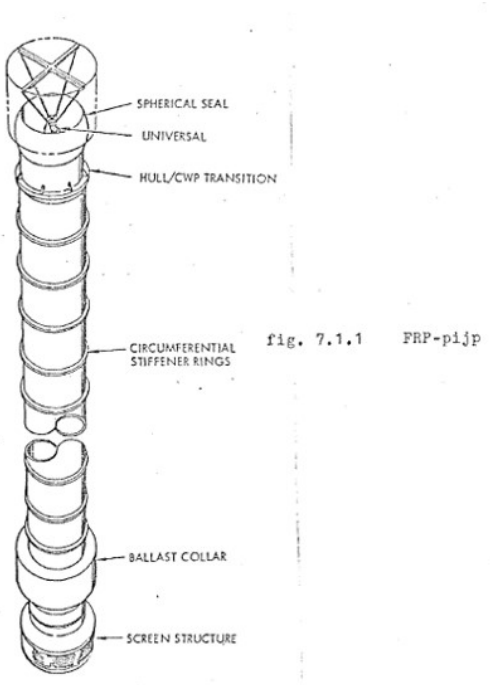

Figure 3.5: FRP pipe [18]

3.2. Alternative flexible cold water pipe materials

Other flexible materials that are considered for the use of the cold water pipe are specific polymers and elastomers such as polyamides (nylons) and thermoplastics having flexible properties. Nylons, TPU and PA are good alternatives for HDPE due to high performance and the possibility of increasing installation capabilities for larger OTEC scale plants[20].

Polymers can be subdivided into thermoplastics and thermosets. An elastomer is a polymer with the property of “elasticity,” generally having a low Young’s modulus and high yield strain compared with other materials. Figure 3.6 illustrates the relation between density and Young’s modulus for the full spectrum of materials. The graph is taken from the program CES Edupack. A lower density means more ballast will be needed in order to guarantee the same stability, whereas a higher flexibility will mean a higher probability of significant deformations. A higher Young’s modulus is mostly accompanied by a higher allowed yield stress, also meaning a higher maximum strain is allowed. The flexibility of a material is directly related to the Young’s Modulus (E). The relation of stress (σ) and strain (ϵ) in the linear phase is given by equation 3.1.

$$E = \frac{\sigma}{\epsilon} \tag{3.1}$$

in which:

- σ denotes the stress in a material [N/mm^2]
- ϵ denotes the strain in the material [%]

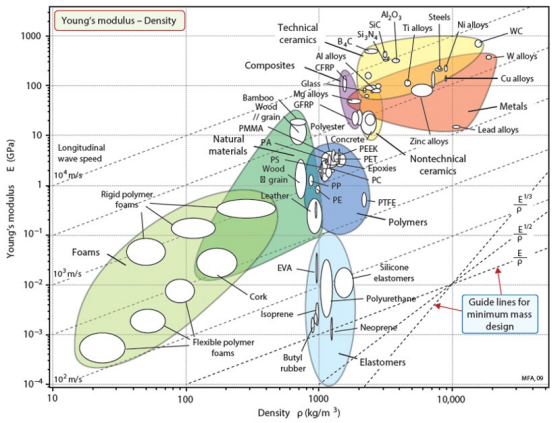

Figure 3.6: Material properties density vs. Young’s Modulus [21]

3.2.1. Polyamides

Polyamide materials that are seen as favorable for the cold water pipe are nylons, due to their lightness which makes it easy to install as well as easy to manufacture. There are many different sort of nylon, ranging from rigid nylon to flexible nylon. Flexible nylons typically have mechanical properties as summarized in Table 3.2.

Nylon concepts

A soft nylon pipe with a flexible membrane, held under tension by ballasted weights and supported by longitudinal cables is an interesting concept due to relative easy installation. The concept comprises a flexible membrane, such as a synthetic textile, with modular rings to create a cylindrical zone. The cables could for instance be made of high tenacity poly ethylene and are being inclined in the circumferential direction in both directions to form a mesh. The cables are arranged in a sleeve to the membrane, which is made from the same material as the membrane. If enough cables are attached to the membrane, the concept will form like a hyperbole shape, which can be seen in Figure 3.7 and

Material Property	Value	Unit
ρ	1045	kg/m^3
E	355	MPa
f_y	26	MPa
elongation at yield	37	%
price	10.55	$€/kg$
tensile strength	48	MPa

Table 3.2: Material properties flexible nylon

Figure 3.8. The total costs of a flexible cold water pipe could be as low as $ 13.3 M, which makes it an interesting concept [18]. A disadvantage of this concept is that the deformation of the sheet is expected to induce relatively large pressure drops, lowering the efficiency of the OTEC system. Next to this, nylon itself is relatively expensive. However, fewer material is expected to be necessary for this concept. A schematic drawing of a soft nylon pipe is shown in Figure 3.7.

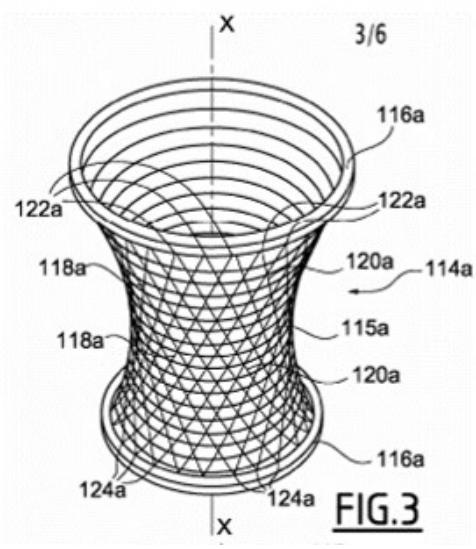

Figure 3.7: Soft foldable pipe concept [11]

Figure 3.8: DCNS foldable pipe pilot test [11]

3.2.2. Thermoplastics

Thermoplastics that are suitable for the cold water pipe are PP, PE, PVC, PU and polychloropeen. All of these plastics are widely used in flexible risers in the offshore industry, which is why a reference case for this is discussed in the following section.

Thermoplastic concepts

1. **Flexible risers in offshore industry**

   Flexible risers are riser systems that enable the oil and gas industry to transport fluids from the subsea bottom to a floating production system. These flexible risers have been applied to shallow water production over four decades because of its flexibility and corrosion resistance. Flexible risers are produced up to around 0.4 m in diameter, having flow velocities up to 30 m/s. It consists of multiple layers of wound metal bands and extruded polymers. The polymetric layers function as sealing, anti-wear and heat-insulators, whereas the metallic layers have to resist the loads (environmental loads, internal pressure, axial loads). The function and most commonly used materials in each layer are summed up in Table 3.3.

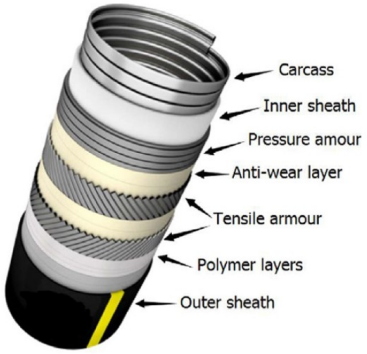

Figure 3.9: Flexible riser design [26]

Layer	Material	Function
Carcass	Duplex steel	External pressure resistance
Pressure armor	Carbon steel	Hoop and radial load resistance
Tensile armor	Carbon steel	Axial and torsional load resistance
Inner sheath	HDPE, XLPE, PA, PVDF	Internal fluid containment
Outer sheath	HDPE, PA, TPE	External fluid barrier
Anti-wear layer	PA, PVDF, HDPE	Abrasion resistance
Insulation layer	PP, PVC, PU	Thermal insulation

Table 3.3: Materials flexible riser design for offshore oil and gas

The anti-collapse capability of offshore flexible risers is often considered as one of the essential factors for deeper water flexible risers [26]. Harsh operating offshore environments in deeper waters may lead to various different failure modes for the flexible risers: collapse, burst, lateral buckling and fatigue. Burst may occur when the internal pressure is larger than the external pressure, whereas collapse may occur when the external pressure is larger than the internal pressure. Radial buckling of the internal carcass can be sub-divided into two failure modes: dry and wet collapse.

- Dry collapse: the outer sheath is non-damaged and all layers within the flexible riser play a role together to resist the collapse. The interlocked carcass together with the pressure armor then form the main layers for the collapse resistance.

- Wet collapse: the outer sheath is breached, meaning the external pressure acts directly on the inner sheath (mainly the carcass).

The outer sheath damage leading to wet collapse remains the most common failure mode [30]. With regard to flexible riser design, API standards 17B and 17J have been developed and are widely accepted specifications. Initial ovalization strongly influences the collapse capacity of the whole cross section.

A summary of the different kind of materials used in the flexible riser design, including some important mechanical properties, are given in Table 3.4 and Table 3.5. The values reported in this table are the average values from CES Edupack.

Mechanical property/Material	Medium C steel	PVC	PE	PP	PET
$\rho\ (kg/m^3)$	7800	1370	949.5	900	1340
$E\ (GPa)$	210	2.205	0.7585	1.223	2.9
$f_y\ (MPa)$	652.5	41.55	23.45	28.95	52.7
elongation $(\%)$	20.5	60	500	350	300
v (-)	0.285	0.4	0.426	0.416	0.39
t_expansion (u_{strain}/C)	12	73.05	162	151	117
t_conductivity $(W/m.C)$	54	0.209	0.435	0.167	0.156
roughness (mm)	0.05	0.0015	0.0015	0.0015	0.0015
salt water durability	limited use	excellent	excellent	excellent	excellent
costs $(€/kg)$	0.655	1.645	1.395	1.49	1.22

Table 3.4: Mechanical properties of the flexible riser design 1

Mechanical property/Material	PU	ABS	PA	PVDF
$\rho\ (kg/m^3)$	1165	1045	1135	1775
$E\ (GPa)$	0.008955	2.415	1.49	2.25
$f_y\ (MPa)$	46.9	42.05	51.5	36.5
elongation $(\%)$	625	32.5	50	306
v (-)	0.48	0.4	0.38	0.42
t_expansion (u_{strain}/C)	163	98.5	130	110
t_conductivity $(W/m.C)$	0.313	0.263	0.28	0.22
roughness (mm)	0.0015	0.0015	0.0015	0.0015
salt water durability	excellent	excellent	acceptable	-
costs $(€/kg)$	1.985	2.545	3.575	-

Table 3.5: Mechanical properties of the flexible riser design 2

2. **Elastomer pipe including rings on the inside**

   An elastomer pipe with rings on the inside of the pipe could provide flexibility and foldability. For instance, by manufacturing a spiral ring within a material such as a synthetic rubber, the system can be unfolded vertically. Since a synthetic rubber is relatively light weight, ballast is needed to keep the cold water pipe straight. A good example of this concept are the airhoses used for washing machines, which can be seen in Figure 3.10.

3. **Flexible fallpipe with rigid buckets and steel catenary lines**

   A flexible fallpipe has been designed and manufactured by vanOord's and is installed onboard of the vessel Stornes. It is a system in which rigid buckets can fold into each other. The system is hanged off by steel catenary lines. With this flexible fallpipe vanOord is able to install rocks on the seabed. Figure 3.11 and Figure 3.12 show the flexible fallpipe.

Figure 3.10: Flexible DUCT air hose concept

Figure 3.11: Flexible fallpipe van Oord 1

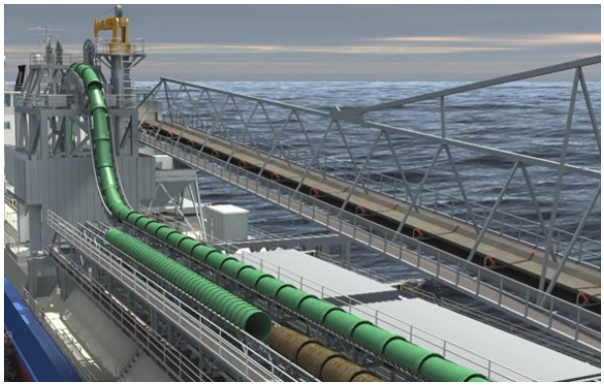

Figure 3.12: Flexible fallpipe van Oord 2

4

Flexible cold water pipe design

In this chapter, the design process for the flexible pipe is discussed. First, the design requirements of the cold water pipe are presented. After this, a design choice regarding the preliminary measurements of the cold water pipe is made. Subsequently, five different cold water pipe concepts are introduced, including three flexible concepts. Finally, a Multi Criteria Analysis of the five different cold water pipe concepts is presented in which a preliminary choice is explained.

4.1. Cold water pipe design requirements

The design requirements of the cold water pipe are of high relevance for the design. The design requirements follow from the design goals as stated in Chapter 1 and from the fact that 10 MW of energy needs to be produced.

Firstly, the design goals of the cold water pipe are repeated:

- Enough strength and stiffness during operation, meaning the cold water pipe does not collapse when water is being pumped through the pipe.
- Easy installation of the cold water pipe by introducing a foldable or flexible concept.
- High flow rates and low pressure losses should be achieved for the upscaling of OTEC.
- Costs of the cold water pipe should be as low as possible.

As a consequence of the fact that 10 MW of electricity needs to be produced, the following design requirements for the cold water pipe are applicable:

- The maximum head loss in the CWP is determined to be 0.6 bar, as discussed in Chapter 2.
- A flow rate of respectively 20.000 kg/s for the cold water pipe.
- A length of the CWP of 1000 m, in order to have a temperature difference of at least 20 °C.

4.2. Cold water pipe design considerations

The two most important preliminary design considerations are the choice of the diameter and the flow speed in the pipe. These two design choices should be carefully chosen such that the pressure drop in the pipe is below 0.6 bar. This is explained in the following section.

4.2.1. Pressure loss

The maximum head loss in the cold water pipe is determined to be 0.6 bar. The head loss in the cold water pipe consists of: the singular head losses, hydrostatic pressure loss and friction loss, which can be seen in equation 4.1. The first term is the friction pressure loss, also known as the Darcy Weissbach term. The second term is the sum of all singular head losses, which can be present due to accelerations, decelerations, curvatures, branches and obstructions. For a straight pipe the only singular head loss that is present is the inlet loss. The third term is called the hydrostatic pressure loss.

$$h_{tot} = f * \frac{L}{D_i} * \frac{u_f^2}{2g} + \sum K * \frac{u_f^2}{2g} + \frac{\Delta\rho}{\rho_c} * y \tag{4.1}$$

in which:

- f is the coefficient of friction [-], which can be determined according to equation C.3
- L is the length of the pipe [m]
- D_i is the internal diameter of the pipe [m]
- u_f is the the flow velocity of the internal seawater [m/s]
- g is the gravitational acceleration, which is 9.81 [m/s^2]
- K is the resistance coefficient, dependent on the shape of the particular design [-]
- ρ_c is the density of the cold water [kg/m^3]
- $\Delta\rho$ is calculated by (ρ_c - $\rho_{average}$)
- y is the length that is reached over the total depth of the pipe [m]

The pressure loss calculations are further explained in Appendix C. The major losses are accomplished by the friction losses, depending on the length, diameter, flow speed and roughness in the pipes. In general, it can be stated that the pressure drop in the pipe is higher for larger values of the length L, the flow speed u_f and the roughness of the pipe. In addition, a relatively larger diameter of the cold water pipe will lead to a lower pressure drop.

4.2.2. Preliminary dimension choice

A mass flow $\dot{m}$ of 20.000 kg/s is achieved through the cold water pipe, assuming a density of 1027 kg/m^3 through the cold water pipe. The density in the cold water pipe is the density corresponding to the cold water that is pumped up from 1000 m. In order to achieve a mass flow of 20.000 kg/s in the cold water pipe there are a few possible combinations of diameters and corresponding flow speed. In Table 4.1, these different dimensions of the cold water pipe are presented.

The mass flow in the cold water pipe is defined as:

$$\dot{m} = \rho_c * u_f * A_i \tag{4.2}$$

in which:

- ρ_c is the density of the cold water [kg/m^3]
- u_f is the the flow velocity of the internal seawater [m/s]
- A_i is the internal cross section of the pipe, calculated by equation 4.3

$$A_i = \frac{1}{4} * \pi * D_i^2 \tag{4.3}$$

in which:

- D_i denotes the internal diameter of the pipe $[m]$

Flow speed u_f (m/s)	**Internal diameter D_i (m)**
1	4.98
2	3.50
3	2.87
4	2.49
5	2.23
6	2.03

Table 4.1: Flow speed in the pipe vs. internal diameter

A relatively low flow speed is favorable such that the head loss is not significant. The range of possible flow velocities in the pipe is from 2 to 6 m/s [33]. However, at flow speeds above 4.53 m/s, there is a high probability of instability occurring. [24]. Therefore, it seems reasonable to focus on flow velocities between 2 and 4 m/s. It must be noted, however, that a larger diameter will lead to higher capital expenditure costs of the pipe.

Since the efficiency is an important parameter for the OTEC system, the lowest possible flow speed of 2 m/s is chosen. This means the diameter that is chosen is 3.5 m, in order to reach the desired 20.000 kg/s. The characteristic values of the cold water pipe are presented in Table 4.2.

Cold Water Pipe	**Value**	**Unit**
$\dot{m}$	20.000	kg/s
u_f	2	m/s
D_i	3.5	m
ρ_c	1027.75	kg/m^3
L	1000	m

Table 4.2: Cold water pipe basis of design values

4.3. MCA cold water pipe concepts

The five pipe concepts that are analysed in the MCA are: a foldable elastomer pipe, a foldable FLEX-hose pipe, a flexible composite pipe, a rigid composite pipe and the reference HDPE pipe. A schematic presentation of the concepts can be seen in Figure 4.1. The concepts are a result of the literature review done in Chapter 3.

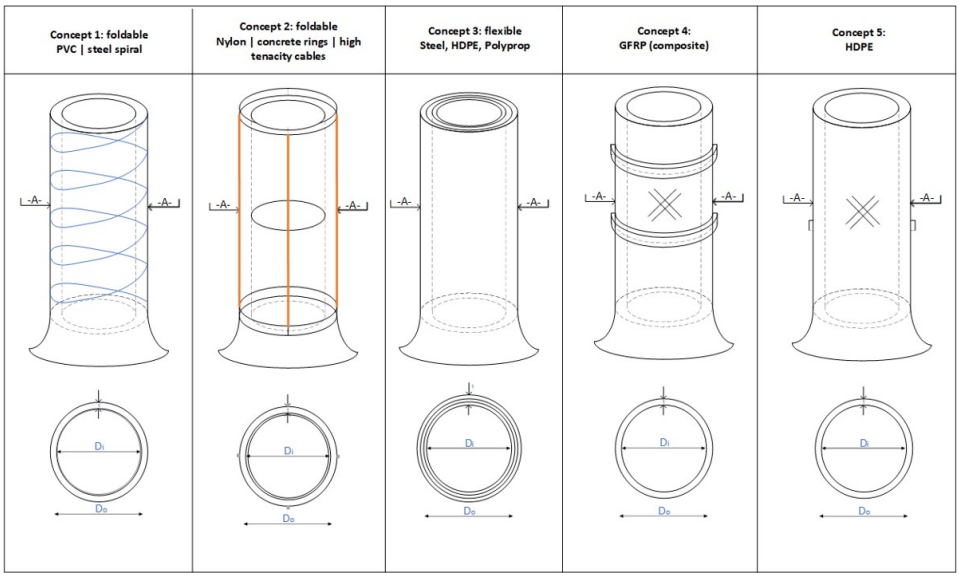

Figure 4.1: Concept drawings foldable and flexible pipes

4.3.1. Criteria definitions

In order to evaluate the most suitable flexible pipe concept a Multi-Criteria Analysis (MCA) is performed on the five different concept designs. The MCA scores the concept designs on five criteria which are defined in such a way that all important characteristics of the concept designs are addressed. For every criteria, the concept is rated on a scale from -2 to 2. The MCA system is provided by Allseas. The description that belongs to the score can be seen in Table 4.3. The scores are then weighed and summed per concept to give the final score. In the section below, the five criteria are explained after which the scores per scenario is given. In Table 4.4, the weight factors are presented, which are determined according to a weigh factor table given by Allseas. The weigh factor table takes into account the given importance with respect to each other and calculates the weight factors accordingly.

Description	Bad	Insufficient	Sufficient	Good	Excellent
Score	-2	-1	0	1	2

Table 4.3: Description score of MCA

Criteria	**Weight factor**
Operational efficiency	0.30
Market readiness	0.13
Costs	0.30
Deployment	0.20
Maintainability	0.07

Table 4.4: Weight factors MCA

1. **Operational efficiency**

   The operational efficiency of the flexible cold water pipe is measured by the flow losses that occur in the pipe, which is measured by the roughness value of the chosen material and the shape of the pipe. The roughness value that belongs to the smooth thermoplastic pipes is equal to 0.0015 mm [31].

   The energy efficiency losses caused by heat transfer from the ambient seawater to the cold water pipe are calculated to be < 0.1 °C, which is why this is considered to be negligible. The heat transfer calculations can be seen in Appendix D.

2. **Market readiness**

   The market readiness of the concepts can be judged on feasibility by pipe material and the associated properties. The parameters used to evaluate the market readiness are the maximum current diameter and size that are available for the concept designs. This is used as a potential implementation time indicator for the design to be produced. The indicator market readiness measures whether the concept would be ready to be produced right now.

3. **Costs**

   The costs of the flexible cold water pipe can be split up into manufacturing costs and installation costs. The manufacturing costs are estimated by material costs that are expected to be needed for the pipe design. The material costs can be estimated by using the price per kg per material type. The installation costs are dependent on the complexity and time needed for the foreseen installation technique offshore. Since it is difficult to make a quantitative estimate of installation costs, this is only done qualitatively by comparing installation techniques in the criteria deployment.

4. **Deployment**

   The deployment of the pipe consists of transportation and installation of the pipe on location. The two deployment methods used in the offshore industry are horizontal and vertical installation. The deployment of the pipe is evaluated by the complexity of the deployment method and the foreseen time of the installation. The joinability of the parts of the pipe is also taken into consideration.

5. **Maintainability**

   The maintenance of the flexible pipe is measured by the probability of corrosion happening or a leak forming in the pipe.

4.3.2. Concept 1: Foldable spiral elastomer pipe

In this concept, a steel spiral is combined into a PVC sheet film. Foldability of the concept is achieved by the ability of the steel spiral to contract and the flexibility of the PVC. The steel spiral's function is to resist the external pressure, whereas the PVC functions for internal fluid containment and flexibility for the foldable pipe design. Currently, this concept is mainly used in ventilation hoses and in irrigation systems. The steel spiral is wrapped into the PVC sheet. The foldable PVC sheet's thickness is expected to be in the order of a few millimeters, in order to be compressionable.

The inner pipe's surface is not entirely smooth since the steel spiral is wrapped into the PVC sheet, meaning the flow is expected to be not entirely in line over the length of the pipe. In-homogeneity's in surface roughness are expected to create vortices leading to significant motions and lowering efficiency. On the other hand, applying enough ballast is expected to straighten the foldable pipe. PVC exists in two forms: hard PVC and flexible PVC. Currently, there are no pipe designs available in large diameters up to 3.5 m. Therefore, it is expected to take some implementation time before this concept could be of use. The costs of this concept are expected to be relatively low, considering the fact that fewer material is expected to be needed in comparison with a HDPE pipe. The costs of flexible PVC is 2.37 €/kg according to CES Edupack. The deployment of the foldable spiral pipe is expected to be easy due to the low density of the material and its foldability in vertical direction. Ballast is needed to lower the pipe during installation. The foldable spiral pipe, however, is expected to be sensitive to corrosion since the steel spiral is wrapped into the PVC sheet.

4.3.3. Concept 2: Foldable FLEX-hose pipe

The foldable FLEX-hose pipe concept consists of a soft inner nylon sheet, concrete rings and vertical tensioners. The soft nylon pipe is held under tension by ballasted weights and supported by longitudinal cables. Prevention of implosion and buckling is achieved by the concrete rings and the cables. The length between the rings should be chosen in such a way that buckling of the material is prevented. The cables could for instance be made of high tenacity poly ethylene and are being inclined in the circumferential direction in both directions to form a mesh.

Previous studies show that membrane contractions induce higher pressure drops due to an inclination angle during pumping which leads to continuous enlargements and contractions in the pipe, lowering the efficiency of the OTEC system. As long as the inclination angle stays below 7 degrees, the pressure losses are not significant [18]. Figure 4.3 confirms this since the only pressure drop that is below 0.6 bar for a flow speed of 2 m/s is the pipe discontinuous pipe with an inclination angle of 5 degrees. The calculation of the pressure drop can be read in Appendix C. In conclusion, the inclination angle is not considered to be a problem as long as the angle does not become larger than 5 degrees. Currently, there are no such pipe designs available in large diameters up to 3.6 m. However, DCNS, an offshore company, is currently doing research into foldable OTEC pipes, which can be seen in Figure 3.8. The total costs of a foldable cold water pipe could be as low as $13.3 M [18]. However, flexible nylon itself is relatively expensive. Flexible nylon costs 10.8 €/kg, according to CES Edupack. The deployment of the foldable pipe is expected to be easy and quick because of its relative low structural weight and the possibility of folding and unfolding the pipe. However, the many pipe joints reduce the robustness of the concept. In addition, nylon needs a thin layer of continuous material called microns in order to make it completely water resistant. These might be more subjected to cracks and failures if loaded for a longer time. The corrosion resistance of nylon, poly-ethylene and concrete is considered to be sufficient. However, when the cables are chosen to be made of steel, coating is required. Lastly, since the nylon sheet is in the order of millimeters, there is also the risk of a leak forming in the pipe which should be taken into account.

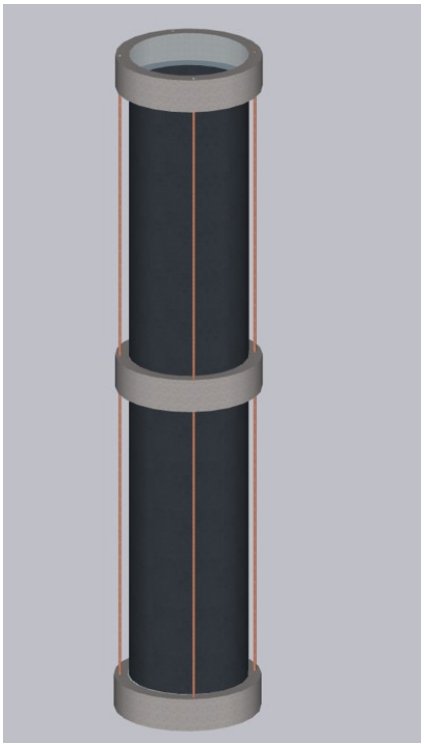

Figure 4.2: Soft foldable pipe concept with cables and rings

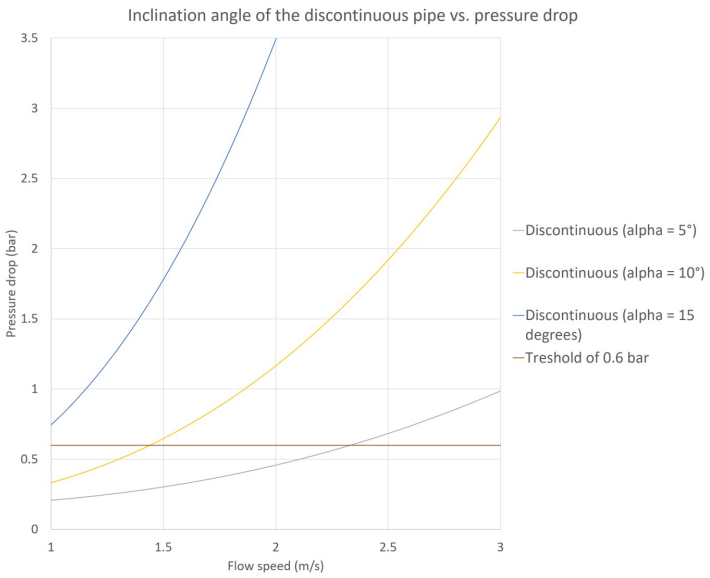

Figure 4.3: Inclination angle of the foldable discontinuous pipe

4.3.4. Concept 3: Flexible composite pipe

In this concept, a laminated composite comprising different layers of materials is suggested. Materials that are expected to be incorporated in this concept are steel in carcass form in combination with thermoplastics. Within the offshore industry, this flexible composite pipe is used more frequently lately as a riser system to transport fluids such as petroleum.

The operational efficiency is expected to be excellent due to the smooth roughness of the inner carcass. However, the current maximum diameter of a flexible composite pipe is 0.4 m, meaning upscaling is expected to be difficult (Source). Since this concept consists of multiple materials wrapped into each other, the costs are expected to be higher. In addition, deployment of the pipe is expected to be difficult, since a large reel is expected to be needed in order to install a 1000 m long flexible pipe (Source) . Lastly, maintainability of the pipe is expected to be sufficient with proper internal coating preventing corrosion and relatively thick layers on top of each other.

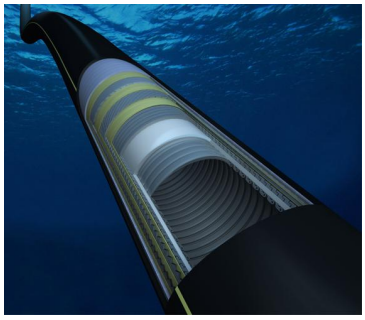

Figure 4.4: Flexible riser in offshore environment [26]

4.3.5. Concept 4: Rigid composite pipe

The rigid composite concept comprises a FRP pipe, which is a corrosion resistant pipe system. A typical glass fibre reinforced pipe is shown in Figure 4.5.The composite is manufactured in lengths up to 12 m. In addition, there is no no need for costly pipe coating, wrapping, lining, painting, or use of polyethylene wraps.

The operational efficiency is expected to be excellent due to the smooth roughness of the composite pipe. Composite pipes are available up to 4 m, meaning the possible implementation time could be relatively soon. However, the costs of this concept are expected to be relatively high since the price of composites is estimated to be 23.3 €/kg. Also, the deployment is expected to be more difficult due to poor join-ability of the composite parts, thereby making the installation procedure more complex and possibly having to do a large part of the installation operation offshore. Lastly, since composite pipes are known to be corrosion resistant the maintainability of the pipe is expected to be excellent.

Figure 4.5: Glass Fibre Reinforced Polymer pipe

4.3.6. Concept 5: Reference HDPE pipe

Concept 5 comprises the reference HDPE pipe. HDPE is often mentioned as the best material choice due to high flexibility, lightness, stability, long life-time in both fatigue and corrosion and cheap to average material prices. In offshore environment, HDPE is mostly used for the transmission of water over longer distance and it is most well known for it high strength-to-density ratio. A picture of a typical HDPE pipe can be seen in Figure 4.6.

Figure 4.6: Typical HDPE pipe

The operational efficiency is determined to be excellent, due to the smooth inner surface in the HDPE pipe. The market readiness is determined to be excellent as well due to the fact that current diameters go as high as 3.5 m in diameter. The expected costs are determined to be acceptable as well since HDPE's price is only 1.40 €/kg according to CES Edupack. However, installation is expected to be relatively difficult with longer HDPE pipes up to 500 m that have to be joined together and installed offshore [31]. Lastly, maintainability is determined to be excellent due to excellent corrosion resistance of the HDPE material.

4.4. Results of MCA

The results of the MCA are shown in Table 4.5.

Concept name	Foldable spiral	FLEX-hose	Flexible composite	Rigid composite	HDPE
Operational efficiency WF = 0.30	-2	-2	2	2	2
Market readiness WF = 0.13	-2	-1	-1	2	2
Costs WF = 0.30	2	2	-1	-2	0
Deployment WF = 0.23	2	2	0	-2	-1
Maintainability WF = 0.07	-2	2	0	-2	2
Total Score	0.00	0.41	0.17	-0.28	0.80

Table 4.5: Results Multi Criteria Analysis flexible pipe designs

From the MCA that has been performed it can be concluded that concept 2 and 5 are considered to be the best cold water pipe designs. Secondly, concept 1 and 4 are not sufficient enough for the cold water pipe design.

The foldable spiral concept is expected to generate large motions due to the spiral that is present in the pipe, which is unfavorable. The inner pipe's surface is not entirely smooth, meaning the flow is expected to be not entirely in line over the length of the pipe. In-homogeneity's in surface roughness are expected to create vortices leading to significant motions and lowering efficiency. In addition, no designs are available on the market currently. This means that a long time will be needed before implementation is possible, considering this concept needs to start from scratch.

The foldable FLEX-hose concept is expected to be a good concept due to easy deployment with the foldable concept and fewer material costs that are expected to be needed. However, the inclination angle while pumping may not become significant, meaning above 5 degrees, since this will lead to lower energy efficiency. In addition, no current design is available on the market, meaning research and development is needed. However, the foldable pilot tests performed by DCNS show promising developments as shown in Figure 3.8.

The flexible composite concept performs average in the MCA. Especially the low maximum current diameter of 0.4 m in combination with non-foldability are the main reason that this concept is not further analysed.

The rigid composite concept is interesting due to the fact that large diameters are currently available for composite pipes. The main disadvantage, however, is that the material costs of composites are very high.

Te reference HDPE pipe also performs well in the MCA. The current market that is focused on HDPE, as well as the relatively low material costs are considered to be the main advantages. Installation is expected to be relatively difficult, since large parts will have to be joined together offshore.

4.4.1. Choice of design

The chosen concept is concept 2 due to the possibility of foldability and the expected lower costs that are associated with the concept. In addition, the market readiness is expected to improve in the future as tests are done for foldable concepts by DCNS.

5

Literature review thin walled flexible concept design

In this chapter, the chosen thin walled flexible concept is reviewed through literature research about thin walled pressure vessel theory and creep. First, the thin walled pressure vessel theory is discussed, including the theory of buckling of vessels under external pressure. Subsequently, a collapse pressure analysis is performed for some preliminary design values of the flexible concept. Lastly, the risk of creep occurring for plastics is discussed including some recommendations on the prevention of creep.

5.1. Thin walled pressure vessel theory

Pressure vessels are commonly seen in the form of spheres, cylinders, ellipsoids or some composite of these materials. In principal, the pressures exerted on a circular cylinder generate three possible stresses: axial stresses, hoop stresses and radial stresses. Axial stresses arise from pressures that are exerted by closures. Hoop stresses are generated by the pressure exerted on the inner and outer cylindrical surfaces. Radial stresses, which are by definition always negative because it is compressive, arise as a result of the external and internal pressure, given the wall thickness of the pipe is sufficiently large. For a thin-walled cylinder the hoop stress is generally approximately twice the longitudinal stress, and the absolute value of the radial stress is fewer than $\frac{1}{20}$ of the hoop stress [35]. A schematic picture of the three principal stresses can be seen in Figure 5.1. When the thickness of a pipe is small in comparison with the other dimensions, a pipe can be modelled as a membrane and the corresponding stresses are calculated by neglecting the bending moments.

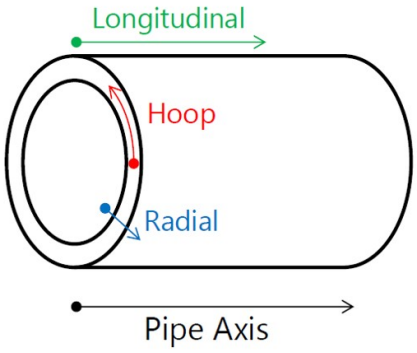

Figure 5.1: Three principal pipe stress directions: axial stress, hoop stress and longitudinal stress

5.1.1. Axial stress

The axial stress in a thin walled cylinder can be calculated as a result of hydrostatic pressure, ballast and pre-tension for the thin walled FLEX-hose foldable concept. The resultant force causes a normal stress in the sheet, according to equation 5.1. Elongation in the axial direction also leads to lateral contraction at the same time. The ratio of the unit lateral contraction to the unit axial elongation is constant within the elastic limit for a given material, and this is what describes the so called poisson ratio.

$$\sigma_a = \frac{F_s}{A_s} \tag{5.1}$$

in which:

- F_s denotes the axial force in the sheet calculated along the length of the pipe [N]
- A_s denotes the cross section of the sheet, calculated by equation 5.2 [m^2]

$$A_s = \frac{1}{4} * \pi * (D_o^2 - D_i^2) \tag{5.2}$$

in which:

- D_o denotes the outer diameter of the pipe [m]
- D_i denotes the inner diameter of the pipe [m]

5.1.2. Hoop stress

If a thin circular ring is subjected to the action of radial forces uniformly distributed along its circumference by internal and external pressure, hoop forces will be produced throughout its thickness which act in tangential direction. A uniform enlargement of the ring will take place if the acting forces are radial outward, or contraction will occur if the acting forces are radial inward. The hoop stress through a thin walled circular cylinder is described by equation 6.15, which is a widely used formula in industrial standards. A clarification of the hoop stress formula is given in Figure 5.2. The difference in pressure between the inside and the outside of the pipe is accounted for in this formula. The formula provides reasonably accurate results for large $\frac{D}{t}$ ratios [25].

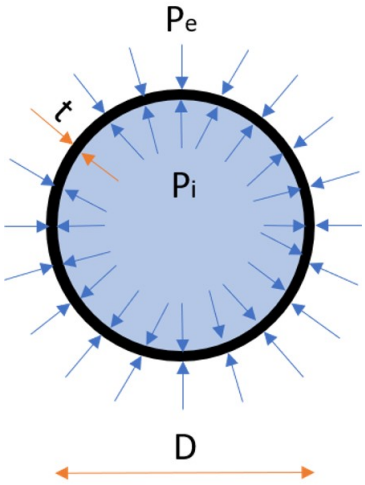

Figure 5.2: Hoop stress formula explanation

$$\sigma_h = \frac{(p_i - p_e) * \bar{D}}{2 * t} \tag{5.3}$$

in which:

- p_i denotes the internal pressure $[N/m^2]$
- p_e denotes the external pressure $[N/m^2]$
- $\bar{D}$ denotes the average diameter $[m]$
- t denotes the thickness of the pipe $[m]$

5.1.3. Radial stress

The presence of internal and external pressure compresses the shell radially, thereby generating radial stresses. The radial stress formula for the inner radius and outer radius are given by equation 5.4 and 5.5. However, for thin-walled circular cylinders where $\frac{D}{t}$ > 20 the radial stress can be neglected since the thickness is relatively too small in comparison to the diameter.

$$\sigma_{r,i} = -p_i \tag{5.4}$$

$$\sigma_{r,e} = -p_e \tag{5.5}$$

in which:

- p_i denotes the internal pressure $[N/m^2]$
- p_e denotes the external pressure $[N/m^2]$

5.2. Buckling of cylindrical cylinders under external pressure

Rings or cylindrical bodies are liable to collapse as a result of combined uniform compression and bending due to an external pressure alone if their flexural rigidity is insufficient. When a circular cylinder is subjected to external pressure and the primary stresses become compressive ($p_e > p_i$) buckling instability can occur at stresses below the elastic limit or yield strength of the material. The pressure at which the annular shape becomes unstable and begins to buckle, and the deflections increase indefinitely, is called the critical collapse pressure. Primary stresses become compressive for the case that the external pressure is larger than the internal pressure. This type of failure gives little warning leading to a rapid increase in radial deflection is also called implosion. [19]

5.2.1. Buckling shapes

A thin walled cylinder buckles in a definite pattern depending on its relative dimensions and the restraint conditions at the ends. They are described by the number of lobes with the smallest number giving the lowest collapsing pressure. The number of lobes for a cylinder of given dimensions is largely dependent the type of restraint at the circumference or edge of the ends of the cylinder and the distance between the restraints. A thin walled cylinder whose length is large in comparison to its diameter will buckle elastically in the form of two lobes when subject to uniform external pressure. The ring is assumed to be perfectly circular before the application of external pressure. Each cross section of the thickness of the arc is subjected to a straight slender column under a central axial load for which the buckling load is given by Euler's formula [19]. Different buckling mode shapes (n=2, n=3 and n=4) in which the thin-walled structure could deform are shown in Figure 5.3. It is the most probable the thin walled foldable FLEX-hose pipe will deform in its first mode forming an ellipse as shown in Figure H.3.

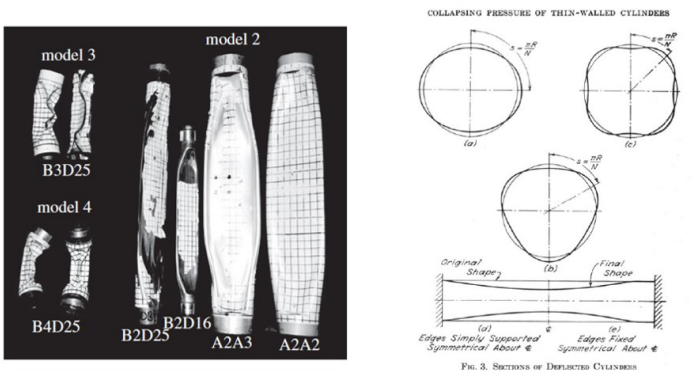

Figure 5.3: Implosion with different failure shapes [35]

Description of buckling ellipse shape at n=2

The buckling ellipse for n=2 is shown in Figure H.3. It is important to note that the circular ring compresses more in the vertical plane in comparison to the horizontal plane due to the ellipse shape. Further explanation and the derivation of the ellipse shape and geometries is provided in Appendix H. The relation between the horizontal compression u_o and vertical compression u is given by equation 5.6.

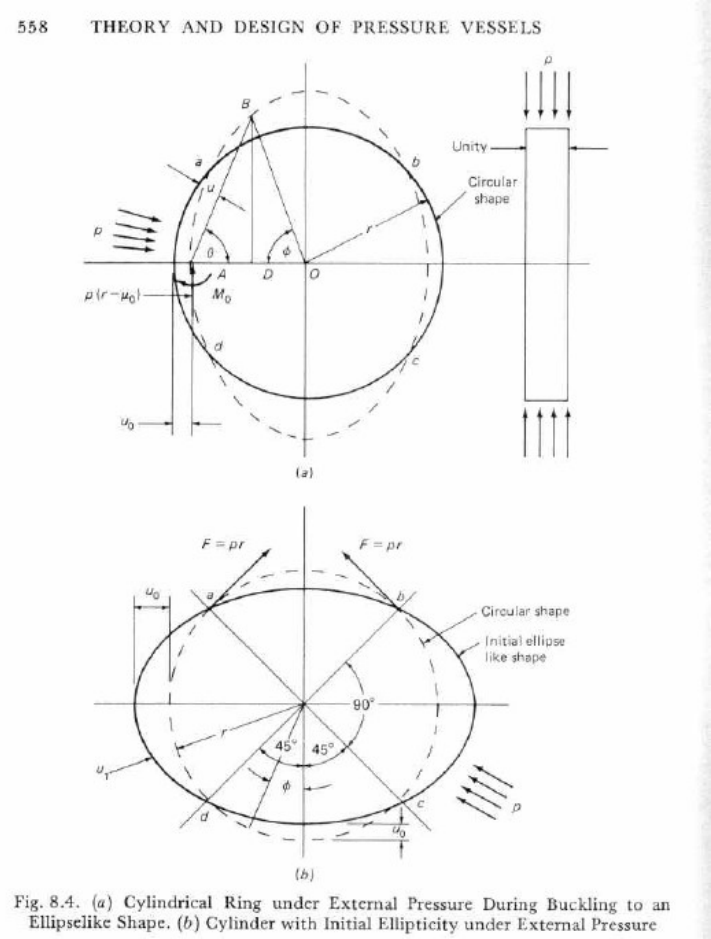

Fig. 8.4. (a) Cylindrical Ring under External Pressure During Buckling to an Ellipselike Shape. (b) Cylinder with Initial Ellipticity under External Pressure

Figure 5.4: Cylindrical ring under external pressure ellipse shape [19]

$$\frac{\overline{AB}^2}{2} - \overline{AO} \cdot \overline{AD} = r\,(u_0 - u) \tag{5.6}$$

in which:

- $\overline{AB}$ denotes the length from A to B, as shown in Figure H.3 $[m]$
- $\overline{AO}$ denotes the length from A to O, as shown in Figure H.3 $[m]$
- $\overline{AD}$ denotes the length from A to D, as shown in Figure H.3 $[m]$
- r denotes the radius r of the thin walled cylinder $[m]$
- u_0 denotes the horizontal compression at the right and left edge $[m]$
- u denotes the compression along the circle as a function of the angle $[m]$

5.2.2. Critical collapse pressure

The critical collapse pressure is defined as the pressure at which the annular shape becomes unstable and begins to buckle. The derivation of general differential equations that are applicable is described by Sturm [35]. The axial tension is not included. According to these equations the collapsing pressure per unit of area, W_c, under a uniform external pressure is equal to the product of the collapsing stiffness and the cube of the $\frac{t}{D}$ ratio of the cylinder. The collapse pressure is defined by equation 5.7.

$$W_c = KE(\frac{t}{D})^3 \tag{5.7}$$

in which:

- W_c is the collapse pressure in due to uniform external pressure [MPa]
- E is for the linear elastic modulus of elasticity [MPa]
- t and D are the thickness and the diameter of the thin walled pipe [m]
- K is a constant, dependent on the boundary conditions and the forcing applied to the thin walled pipe, determined by Figures 5.5 and 5.6

5.3. Preliminary design: collapse pressure analysis

The preliminary FLEX-hose foldable concept design comprises a vertical pipe from nylon with a determined diameter of 3.5 m and a preliminary thickness of 0.01 m, supported by vertical tensioners and concrete rings on a distance of 10 m between each other. The thickness of the design of the nylon sheet is relatively very small to the diameter, meaning it is important that the structural integrity of the design is tested. Thus, the concept is subject to an external and internal pressure and since the internal pressure is lower due to pressure losses, there is a possibility of instability due to buckling.

5.3.1. Determination of the K-value

The determination of the constant K depends on the boundary conditions and the forcing applied. The collapsing pressure is dependent on whether the boundaries can be modelled fixed or simply supported and whether the pressure is applied to the sides only or to the sides and the edges. The different graphs for these situations are shown in Figure 5.5 and 5.6 [35]. The graph to be used for the FLEX-hose foldable concept is chosen to be simply supported and to have pressures on both the sides and the ends.

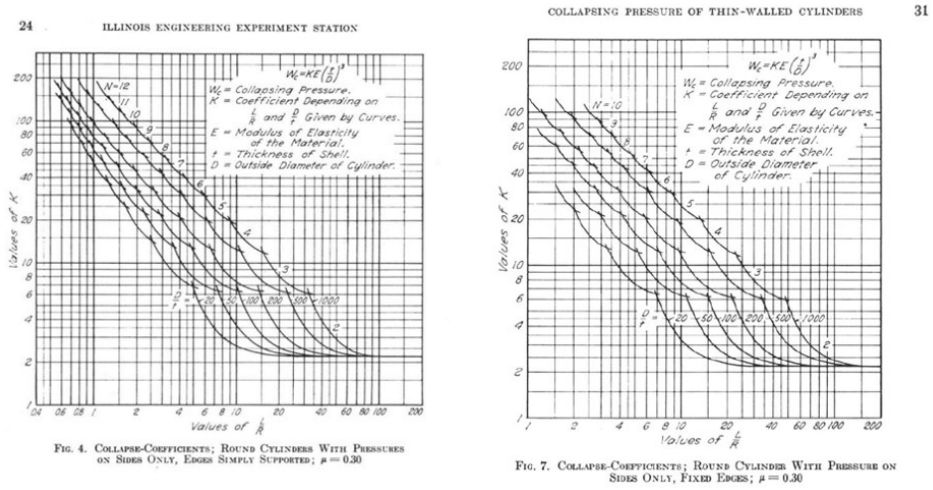

Fig. 4. Collapse-Coefficients; Round Cylinders With Pressures on Sides Only, Edges Simply Supported; $\mu = 0.30$

Fig. 7. Collapse-Coefficients; Round Cylinder With Pressure on Sides Only, Fixed Edges; $\mu = 0.30$

Figure 5.5: K-values for pressure on sides only [35]

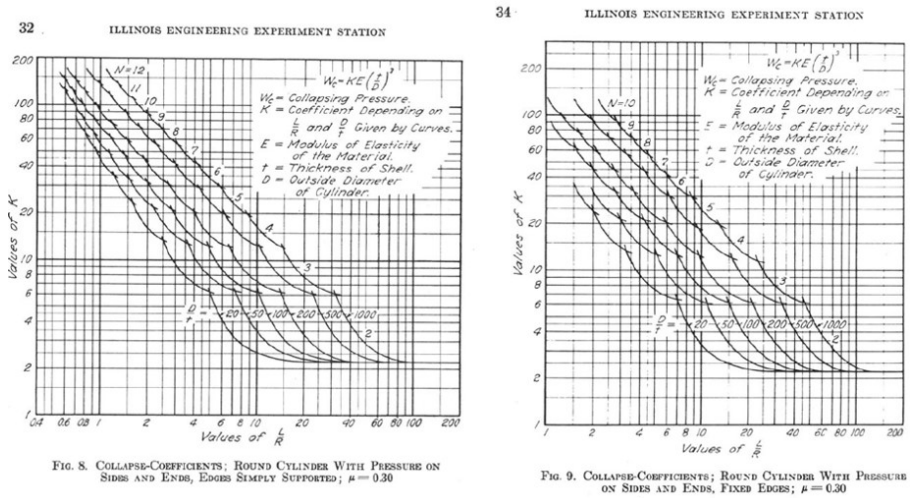

Fig. 8. Collapse-Coefficients; Round Cylinder With Pressure on Sides and Ends, Edges Simply Supported; $\mu = 0.30$

Fig. 9. Collapse-Coefficients; Round Cylinder With Pressure on Sides and Ends, Fixed Edges; $\mu = 0.30$

Figure 5.6: K-values for pressure on sides and ends [35]

5.3.2. Preliminary results collapse pressure

For the preliminary design the design values are listed in Table 5.1. $L_{concrete}$ denotes the distance between every concrete ring and R_i denotes the radius of the internal diameter of the pipe.

Design parameter	Value	Unit
D_i	3.50	m
t	0.01	m
$L_{concrete}$	10	m
R_i	1.75	m
E	495	MPa

Table 5.1: Preliminary design values with FLEX-hose foldable design

Sensitivity analysis in thickness and length

A sensitivity analysis has been performed for the collapse pressure, according to equation 5.7. The thickness and the length between the rings has been varied in the sensitivity analysis. The results of the sensitivity analysis are shown in Table 5.2. The graphs corresponding to the determination of the different K-values are presented in Appendix H.

$t(m)$	$L_{concrete}(m)$	$L_{concrete}/R_i$	D_i/t	$K-value$	$W_c(MPa)$	$W_c(kN/m^2)$
0.01	10	6	350	16	0.00018	0.18
0.01	7.5	4	350	25	0.00029	0.29
0,01	5	3	350	35	0.00040	0.40
0.05	10	6	70	8	0.01155	11.55
0.05	7.5	4	70	9	0.01299	12.99
0.05	5	3	70	12.5	0.01804	18.04
0.1	10	6	35	5.5	0.06350	63.50
0.1	7.5	4	35	9	0.10391	103.91
0.1	5	3	35	12.5	0.14431	144.31

Table 5.2: Sensitivities for collapse pressure

Conclusion collapse pressure preliminary results

The calculated collapse pressure for a thin walled flexible nylon sheet without axial tension varies between 0.13 kN/m^2 and 103.50 kN/m^2, depending on the thickness t and length L between the rings. In general, it can be stated that the ratio of $\frac{D}{t}$ and $\frac{L}{R}$ have a large impact on the collapse pressure. The collapse pressure of cylindrical structures can be increased when the distance L becomes smaller between the stiffener rings and when the thickness becomes larger in comparison to the diameter of the pipe. In addition, the chosen material and its corresponding Young's Modulus also has an impact on the collapse pressure of a structure. A relatively large $\frac{D}{t}$ ratio is undesirable as this leads to a lower structural integrity. Also, a relatively lower value of $\frac{L}{R}$ is desirable, meaning it is favorable to choose the distance L between the rings as small as possible. Moreover, a higher stiffness, meaning a larger modulus of elasticity, leads to a larger collapse pressure of the system. Lastly, in order to increase the resistance against collapse in the thin walled nylon sheet, it is beneficial to have tension in the sheet to prevent collapse from happening. This is introduced in Chapter 6.

5.4. Creep

In this sub-chapter, problems that could arise from creep are discussed. A reference case for a HDPE design case is used to be able to investigate the negative influences of plastics experiencing creep over time.

5.4.1. Reference case: HDPE

Creep is the tendency of a solid material to deform permanently under the influence of constant stress. It occurs as a function of time through extended exposure of stress levels that are smaller than the yield strength of the material. Since the sheet in the flexible pipe is made of plastic, creep is an important phenomena to investigate. The lifetime of polymers like HDPE is restricted by 3 failure mechanisms: ductile or creep failure, brittle failure due to cracks caused by cycling loading and brittle failure due to molecular decomposition. A schematic representation of these three failure mechanisms is shown in Figure 5.7 [8].

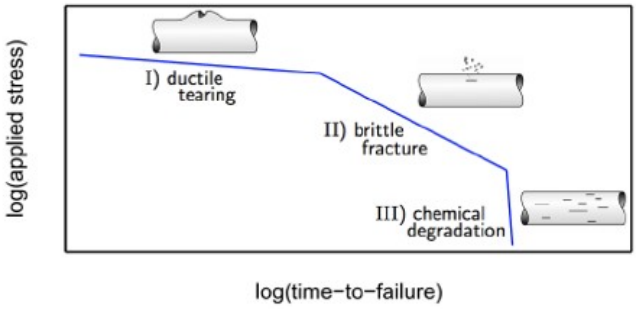

Figure 5.7: Failure mechanisms HDPE over time [8]

As time passes by, creep could lead to failure of the material. The strain rate of plastics is highly dependent on temperature and the applied stress. As a result of creep, the Young's Modulus of a plastic material changes over time. A relatively lower Young's Modulus leads to relaxation of the material. For example, the Young's Modulus of HDPE reduces from around 1125 MPa to 260 MPa after 30 years, as is shown in Figure 5.8.

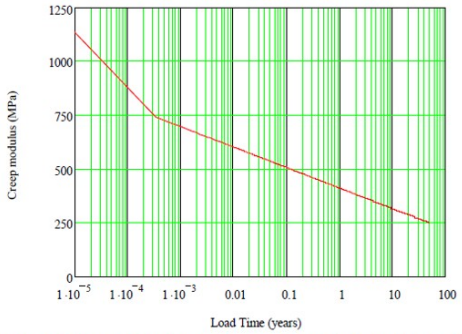

FIGURE 12: CREEP MODULUS OF HDPE PIPE MATERIAL (AT 23°C)

Figure 5.8: Creep modulus of HDPE material [8]

Conclusion creep

In order to mitigate creep as much as possible, it is beneficial to choose a material that has similar strength properties but is lower in density, creating lower tensions. Next to this, locally increasing the strength of the pipe by means of reinforcements also reduces the maximum stress in the pipe, which could be beneficial for the mitigation of creep.

II

Model

6

Modelling of FLEX-hose concept

In this chapter, the model that is implemented including the calculations is described. First, the main goal of the model is described. After this, the preliminary design values of the pipe design are described. Lastly, the model is described including important calculations and limitations.

6.1. Scope of modelling

The main goal of the model is to assess the feasibility of the FLEX-hose foldable pipe concept design. The feasibility is assessed by calculating the tension that is necessary in the sheet to resist collapse, as well as by calculating the associated pressure drop in the FLEX-hose foldable pipe concept. In addition, the amount and weight of the concrete rings is also taken into consideration to asses the feasibility of the concept. In the case of large radial displacement of the sheet, a larger pressure drop is present in the pipe due to contraction and enlargement losses. In the end, this may lead to an energy loss in the cold water pipe which is significant. The main loads that are exerted on the pipe are being caused by the movements of the platform, the dynamic wave forces, the current and the flow running through the pipe while in operation. In this model, only the flow running through the pipe while in operation is examined.

6.2. Preliminary design values

A preliminary concept design is used as start input for the model. The FLEX-hose concept consists of a thin sheet of nylon, supported by concrete rings and steel cables. The nylon sheet is attached to the concrete rings and the cables are attached to the concrete rings. The attachment of the concrete rings to the nylon sheet is a challenge on its own. In general, a plastic such as a nylon is not joined to a concrete ring. An idea could be to manufacture small systems in the sheet on which the concrete ring could be hung up upon. Another solution could be some kind of epoxy or other joining material. The cables run through the concrete rings and can be used during installation to lower the pipe. The force distribution in the cables and the sheet respectively is determined by the axial stiffness of the nylon sheet and the cables. A 3D visualization can be seen below in Figure 6.1.

The preliminary design values are listed in Table 6.1 and Table 6.2. Flexible nylon properties as stated in Table 5.1 are used for the sheet properties. The concrete rings are determined to have a height of 0.5 m and a thickness of 0.4 m [18]. A concrete ring of a maximum height of 0.5 m is seen as feasible. This has been decided in consultation with Allseas. The submerged weight of one concrete ring is calculated to be 33.04 kN. An illustration of two cross sections of the preliminary design are given in Figure 6.1 and Figure 6.2. The distance between the cable and the sheet is 2/3 of the length of the concrete ring, which is 0.34 m. This length has been determined by the requirement that the sheet may not touch the cables.

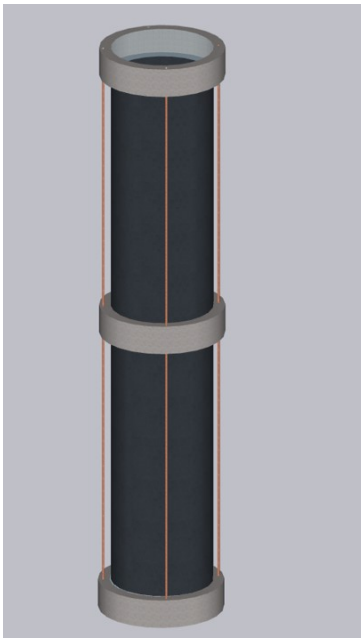

Figure 6.1: FLEX-hose Foldable pipe concept drawing with nylon sheet, concrete rings and steel cables

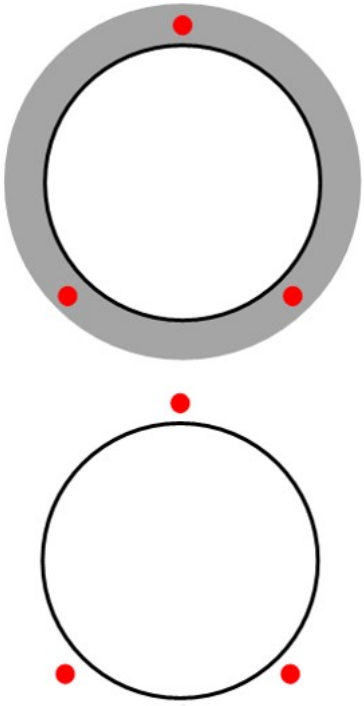

Figure 6.2: Cross sections of pipe at concrete ring and in between span

Design parameter	Value	Unit
$D_{o,nylon}$	3.50	m
$D_{i,nylon}$	3.48	m
t_{nylon}	0.01	m
E_{nylon}	355	MPa
cables	3	-
D_{cable}	0.04	m

Table 6.1: Design parameters sheet and cables

Design parameter	Value	Unit
$L_{concrete}$	10	m
$h_{concrete}$	0.5	m
$D_{i,concrete}$	3.50	m
$D_{o,concrete}$	4.30	m

Table 6.2: Design parameters concrete rings

6.3. Model description

The process of modelling the pipe design consists of coming up with pipe design parameters, running the model and its calculations, analysing the output, comparing the results to the design requirements and finally changing the pipe design parameters accordingly to satisfy the design requirements. In order to satisfy the design requirements, many iterations in the modelling calculations have been done. This process is illustrated by Figure 6.3. Figure 6.4 presents the complete model description, including the steps that are taken in order to calculate the desired design configuration. In the following section, all the calculation steps that are done in the model are discussed.

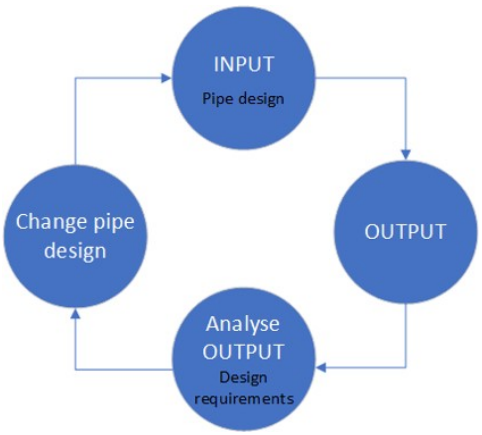

Figure 6.3: Design iteration procedure of modelling

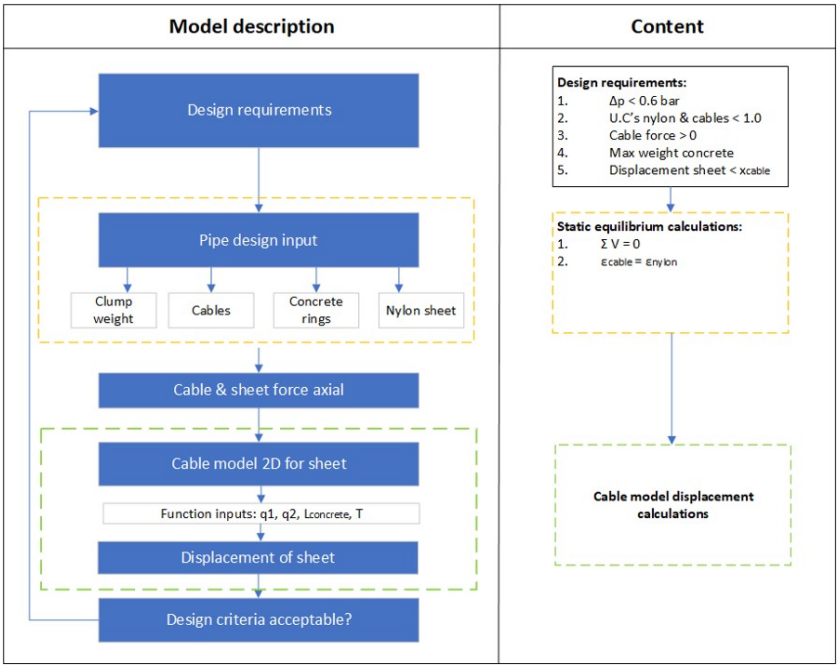

Figure 6.4: Model description flow diagram

6.3.1. Design requirements

The design requirements are used to asses whether the pipe design input parameters are acceptable. The design requirements for the FLEX-hose foldable concept design are:

1. Δp needs to be below 0.6 bar, as explained in Chapter 2. The pressure drop calculations are done by using the diffusor analogy and are explained in section C.2 in Appendix C.
2. The unity checks for the nylon sheet and the cables for the stresses should be < 1.0.

   For the cable, equation 6.1 should be satisfied.

   $$\sigma_c = \frac{F_c}{A_c} < 1.0 \tag{6.1}$$

   in which:

   - F_c denotes the cable force [N]
   - A_c denotes the cross section of one cable, calculated by equation 6.2 [m^2].

   $$A_{cable} = \frac{1}{4} * \pi * D_{cable}^2 \tag{6.2}$$

   in which:

   - D_{cable} denotes the diameter of the cable [m]

   For the sheet, equation 6.3 should be satisfied.

   $$\sigma_{VM} = \sqrt{\sigma_h^2 + \sigma_a^2 - \sigma_h * \sigma_a} < 1.0 \tag{6.3}$$

   in which:

   - σ_h denotes the hoop stress, as calculated in equation 6.15 [N/m^2]
   - σ_a denotes the axial stress, as calculated in equation 5.1 [N/m^2]
3. The cable force should be positive (>0)

   In order for the pipe to be hanging straight and for the cable not to buckle, the cable force should always be positive during operation. For the cable this means that the equilibrium at the bottom of the pipe should satisfy equation 6.4. An illustration of the vertical equilibrium is given in Figure 6.5. Locally, tension is introduced into the concrete. This means it is advise-able to include reinforcement into the concrete.

   $$F_{clump} - F_{hydro,clump} - T_{pre-tension,sheet} > 0 \tag{6.4}$$

   in which:

   - F_{clump} is the clump weight at the bottom of the pipe [N]
   - $F_{hydro,clump}$ is the hydrostatic force acting upon the clump weight [N]
   - $T_{pre-tension,sheet}$ is the pre-tension in the sheet by making the sheet shorter [N]
4. The sheet should not be in contact with the cables.

   The radial displacement of the sheet as a result of the pressure difference, is not allowed to touch the cables that run through the concrete rings. In case the sheet touches the cable, it is expected there is a high probability that the sheet will fail locally and the streamline of the flow will change direction influencing the pressure drop negatively.
5. The maximum weight of the structure should be < 2000 mT

   In order to be able to make the installation of the foldable structure feasible, the total structure including the concrete rings should not be too heavy. A limit of 2000 mT has been determined, since two reference projects of foldable pipes have masses of respectively 1521 mT and 1601 mT, as can be seen in Table 6.3.

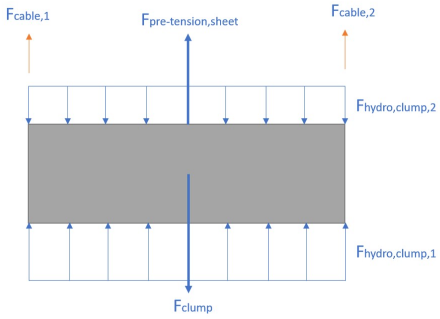

Figure 6.5: Clarification vertical equilibrium at bottom of pipe

Concept	Total mass (mT)
Steel Concept - Kleute	4228
Composite concept - Kleute	1028
Bundle concept - Kleute	2043
Soft concept - Kleute	1521
HDPE concept - Brakel	1601
Steel concept - Adiputra	15000
Aluminium - Adiputra	6200
FRP - Adiputra	941

Table 6.3: Previous cold water pipe projects masses

6.3.2. Static equilibrium calculations

The goal of static equilibrium calculations is to calculate the stresses and the strains in the materials while the cold water pipe is in operation. The temperature at the surface and the temperature at the bottom of the pipe are used as input for the determination of the density of the ambient seawater. Next to this, the material weights of the nylon sheet, the concrete rings and the cables are used as an input to determine the stresses and the strains.

The model assumptions that are used to calculate the forces in the static equilibrium are:

- Vertical equilibrium of forces at the location of each concrete ring.
- Strains are equal on the interface ε_{nylon} = ε_{steel}.
- Sheet stress governed by axial tension (σ_a) and hoop stress (σ_h).
- Cable stress governed by axial tension.
- Pressure losses governed by pumping loss, inlet loss, wall friction loss, contraction losses and enlargement losses.

Temperature profile

The temperature profile for the years 2016, 2017 and 2018 at an offshore location near Bonaire are used as input. The temperature at the surface at the location is therefore determined to be 27.4 °C, and the temperature at 1000 m deep is 5.1 °C. Further explanation is provided in Appendix F.

Water density profile

The water density profile offshore is dependent on the temperature of the water, as well as the salinity of the water. In this study, only the influence of the temperature is used in the model. The density of the ambient seawater is modelled as a linear function. Using a surface water temperature of 27.4 °C, and a bottom temperature of 5.1 °C, the water density is determined to be 1022.7 kg/m^3 and 1027.7 kg/m^3

respectively at the surface and at the bottom. The water density profile is approximated by equation 6.5, which is a linear interpolation of the two values calculated at the surface and the bottom of the pipe using the temperature plot as input. The positive z-coordinate is in upward direction and the function starts at 1000 m depth. The water density of the cold water flowing through the pipe is determined to be 1022.7 kg/m^3. The average ambient seawater is calculated to be 1025.2 kg/m^3. Further explanation is provided in Appendix F.

$$\rho_a(z) = 1022.7 + (\frac{\rho_c - \rho_s}{L}) * z \tag{6.5}$$

in which:

- ρ_c is the density of the cold seawater [kg/m^3]
- ρ_s is the density of the surface seawater [kg/m^3]
- L is the length of the cold water pipe [m]
- z is the depth in the water, in which the z-axis is positive downwards and starts at the surface of the water

Submerged weight

The submerged weight of materials that are used in the modelling are given in Table 6.4. The submerged weight is calculated by equation 6.6. Flexible nylon is a material that is just heavier than the ambient seawater, meaning a larger ballast will probably be needed.

Material	Dry weight	Submerged weight	Unit
Concrete	2400	1375	kg/m^3
Flexible nylon	1045	20	kg/m^3
Polyester	1380	356	kg/m^3
Rigid nylon	1140	116	kg/m^3
Steel	7800	6775	kg/m^3
Dyneema	980	-45	kg/m^3

Table 6.4: Dry weight and submerged weight of materials

$$\rho_{submerged} = \rho_{m,dry} - \rho_{a,average} \tag{6.6}$$

in which:

- $\rho_{m,dry}$ is the dry weight of the material [kg/m^3]
- $\rho_{a,average}$ is the average ambient seawater density, which is calculated to be 1025.25 kg/m^3

Static force calculations

In order to be able to calculate the tension in the sheet and the cables, a model for the force distribution in the cables as well as the sheet is necessary. For this, the static vertical equilibrium is considered. By using a static model, it is possible to calculate the stresses and strains in the vertical direction. The forces that are used in the model are forces as a result of the submerged weight, hydrostatic pressure and the concrete rings, which are shown in Figure 6.7. The axial forces in the sheet and the cable are calculated by respectively equation 6.7 and equation 6.8. The first and the second term in equation 6.7 respectively represent the force due to the pre-tension that is a applied and due to the submerged weight. The last term in the equation describes the effect of the concrete ballast stations. N is the amount of ballast stations determined by the distance between the concrete rings and can be calculated using equation 6.9. The positive z-coordinate is in upward direction and the function starts at 1000 m depth, which is illustrated in Figure 6.6.

$$F_s = T_{pre-tension} + (\rho_{submerged,nylon} * g * A_s * z) + \sum_{n=1}^{n=N} F_{s,ballast,n} \tag{6.7}$$

$$F_c = (\rho_{submerged,cable} * g * A * z) + \sum_{n=1}^{n=N} F_{c,ballast,n} \tag{6.8}$$

$$N = \frac{L_{total}}{L_{concrete}} \tag{6.9}$$

in which:

- $F_{s,ballast,n}$ is the percentage of the concrete ring weight that is transferred to the sheet $[N]$
- $F_{c,ballast,n}$ is the percentage of the concrete ring weight that is transferred to the cable $[N]$
- L_{total} denotes the total length of the cold water pipe, which is 1000 m
- $L_{concrete}$ denotes the length between every concrete ring $[m]$

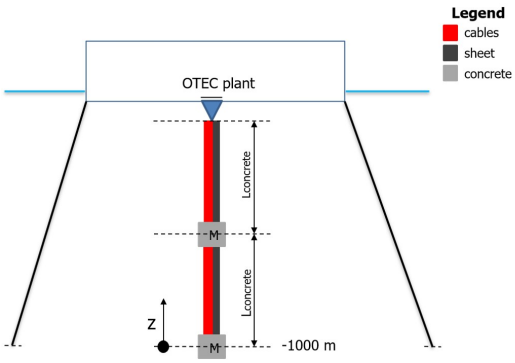

Figure 6.6: Positive z-axis in model

At the location of the concrete rings, the sum of the vertical forces is set to zero, which is illustrated by respectively equations 6.14 and 6.13. Equation 6.13 represents the vertical equilibrium at the bottom of the pipe, whereas equation 6.14 represents the calculation performed at every concrete ring. Effectively, this means that the weight of the concrete is transferred to the cables and the sheet, denoted by the $F_{s,ballast,n}$ and $F_{c,ballast,n}$ in equations 6.7 and 6.8. Both the cables and the sheet take a part of the additional load, which is determined according to the axial stiffness of the sheet and the cable as demonstrated by equation 6.12 and in Table 7.2 for the materials polyester, rigid nylon, steel and dyneema. The pre-strain in the material $\epsilon_{pre-strain}$ at every location is defined by equation 6.10, which is the same at every location on the sheet. The pre-strain in the material is separate from the additional strain since the pre-strain is applied beforehand. The pre-strain is achieved by making the sheet shorter between every concrete ring. The length that the sheet should be made shorter to achieve the pre-tension is calculated by equation 6.11. The pre-stress is therefore applied at every part of the sheet separately.

$$\epsilon_{s,pre-strain} = \frac{T_{pre,tension}}{E_s * A_s} \tag{6.10}$$

$$\Delta l = \epsilon_{s,pre-strain} * L_{concrete} \tag{6.11}$$

$$\epsilon_{s,additional} = \frac{F_s}{E_s * A_s} = \frac{F_c}{E_c * A_c} = \epsilon_{c,additional} \tag{6.12}$$

in which:

- $\epsilon_{s,pre-strain}$ is the pre-strain in the sheet [%]
- ϵ_c and ϵ_s are the additional strain in the cable and the sheet respectively [%]
- E_s and E_c are the Young's Modulus of the sheet material and the cable material [MPa]

E_s (MPa)	A_s (m^2)	E_c (MPa)	A_c (m^2)	% sheet	% cable
495	0.11	5500	0.12	72.35	9.21
495	0.11	9000	0.12	61.53	12.82
495	0.11	200000	0.12	6.71	31.09
495	0.11	65000	0.12	18.13	27.29

Table 6.5: Force distribution as a result of different materials for cables

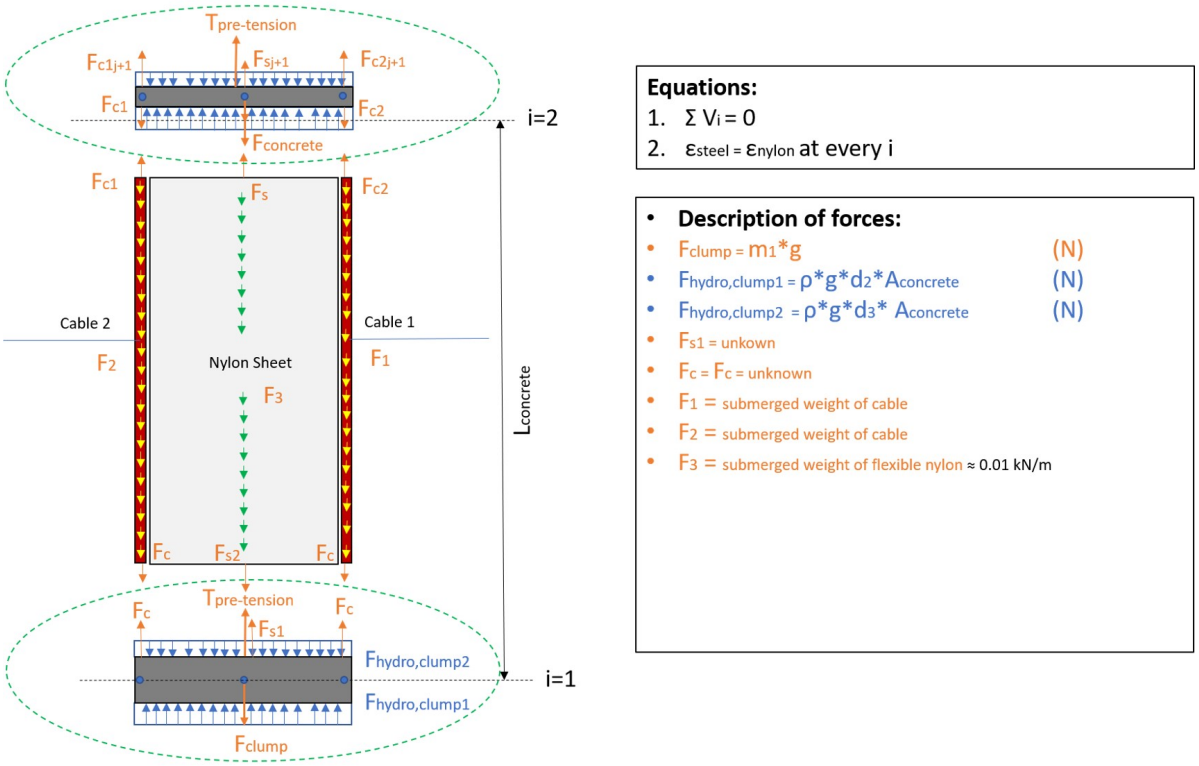

Figure 6.7: Static equilibrium calculations

$$\sum V = F_{clump} - F_{hydro,clump} - T_{pre-tension} - F_c * n - F_s = 0 \tag{6.13}$$

$$\sum V = F_{c1,j} + F_{c2,j} + F_{c3,j} + F_{s,j} + F_{concrete} - F_{hydro,concrete} - T_{pre-tension} - F_{c1,j+1} - F_{c2,j+1} + F_{s,j+1} = 0 \tag{6.14}$$

in which:

- $F_{c1,j}$, $F_{c2,j}$ and $F_{c3,j}$ denote the cable forces for cable 1,2 and 3 at location j, which is the location 1 before the concrete ring's weight is added [N]
- $F_{c1,j+1}$, $F_{c2,j+1}$ and $F_{c3,j+1}$ denote the cable forces for cable 1,2 and 3 at location j+1, which is the location at which the the concrete ring's weight is added [N]
- $F_{s,j}$ denotes the sheet force at location j [N]

- $F_{concrete}$ is the weight of a concrete ring, which is calculated to be 33.04 kN, resulting from the design parameters in Table 6.2 [N]
- $F_{hydro,concrete}$ is the hydrostatic pressure working upon one concrete ring, having a height of 0.5 m [N]

Pressure difference during operation

There is a pressure difference present between the inside and the outside of the cold water pipe. This pressure induced difference is a consequence of the OTEC pumps that need to maintain the flow in vertical direction by suction. The suction leads to a relatively lower pressure in the pipe. Also, the pressure losses in the pipe result in a lower pressure in the pipe. This pressure difference results in a hoop stress in the thin walled cylinder, according to equation 6.15. The smaller the thickness of the sheet, the higher the expected hoop stress in the sheet. A uniform enlargement of the ring will take place if the acting forces are radial outward, or contraction will occur if the acting forces are radial inward. The situation in which contraction occurs is shown in Figure 6.8. These deformations only occur in the situation when the net external pressure is below the critical collapse pressure. Buckling instability can occur at stresses below the elastic limit or yield strength of the material when the primary stresses become compressive ($p_e > p_i$) .

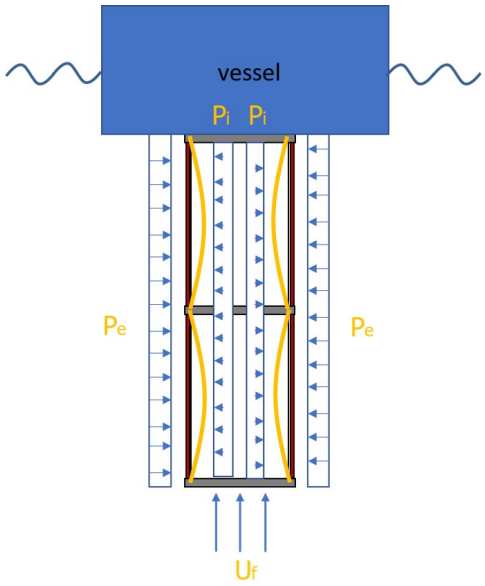

Figure 6.8: Expected deformation while pumping without buckling occuring

$$\sigma_{hoop} = \frac{(p_i - p_e) * \bar{D}}{2 * t} \tag{6.15}$$

The external pressure is governed by the hydrostatic pressure on the outside of the pipe due to the ambient seawater. The ambient seawater function (in kg/m^3) as described in section of Appendix F is used. The ambient seawater function is a linear interpolation between the cold water and the warm water density. Equation 6.16 describes the external pressure acting upon the pipe. The hydrostatic pressure increases over depth.

$$p_e = \rho_{ambient} * g * z \tag{6.16}$$

The internal pressure consists of the hydrostatic pressure and the friction losses as a consequence of pumping. The friction losses consist of the the inlet friction, hydrostatic head loss, wall friction, and the friction caused by deformation of the membrane. Equation 6.17 describes the internal pressure upon the pipe. The internal pressure reduces when closer to the water surface, since more pressure drop is accumulated for. Also, a larger radial deformation of the sheet, leads to a higher pressure drop. This is shown in Figure 6.9. At a flow speed of 2 m/s , the maximum inclination angle to stay below 0.6 bar is 7.5 degrees. This means the inclination angle has a value of 7.5 degrees at every location along the pipe length. The positive z-coordinate of equation 6.17 is in upward direction and the function starts

at 1000 m depth, which is illustrated in Figure 6.6. z_1 is the location, starting at the value of 1000 and counting back to 0. A more in depth explanation of the pressure losses is given in Appendix C.

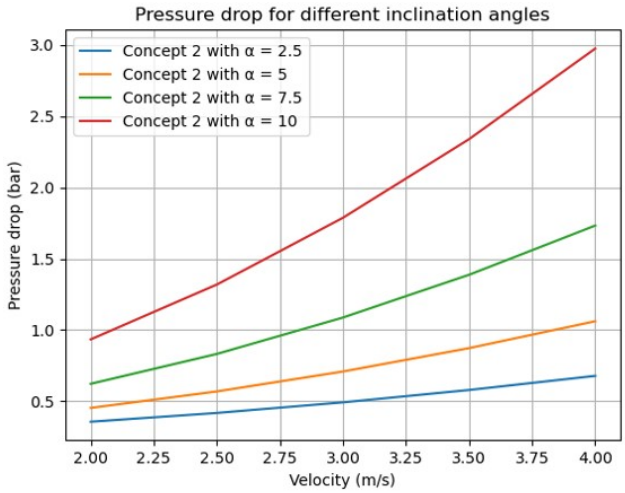

Figure 6.9: Pressure drop for different inclination angles

$$p_i = \rho_{cold} * g * z_1 - dP_{inlet} - \frac{(dP_{hydrostatic} + dP_{wallfriction} + dP_{contraction} + dP_{enlargement})}{L_{total}} * z \quad (6.17)$$

in which:

- dP_{inlet} is the pressure drop at the inlet of the pipe, as calculated by equation C.6 [bar]
- $dP_{hydrostatic}$ denotes the hydrostatic pressure drop, as calculated by equation C.7 [bar]
- $dP_{wallfriction}$ denotes the wall friction pressure drop, as calculated by equation C.2 [bar]
- $dP_{contraction}$ denotes the contraction pressure drop, as calculated by equation C.9 [bar]
- $dP_{enlargement}$ denotes the enlargement pressure drop, as calculated by equation C.10 [bar]

6.3.3. 2D sheet model displacement

The goal of modelling the displacement of the sheet is to keep the angles of inclination of the sheet within acceptable limits, meaning below 5 to 7.5 degrees. The importance of keeping the angle of inclination angle within these limits, is to prevent the pressure drop in the FLEX-hose foldable pipe from becoming too significant. In the 2D sheet model, the tension and the pressure difference are used as input to calculate the displacement of the sheet. An illustration of the sheet model is given in Figure J.1. The thin walled sheet is divided into two zones in order to calculate the deformed sheet. In this sheet model the assumption is made the sheet contracts uniformly inwards as a results of uniform loading along the length. However, it should be noted it might be possible for the thin walled sheet to form an ellipse shape as a result of buckling instability as discussed in section 5.2.1.

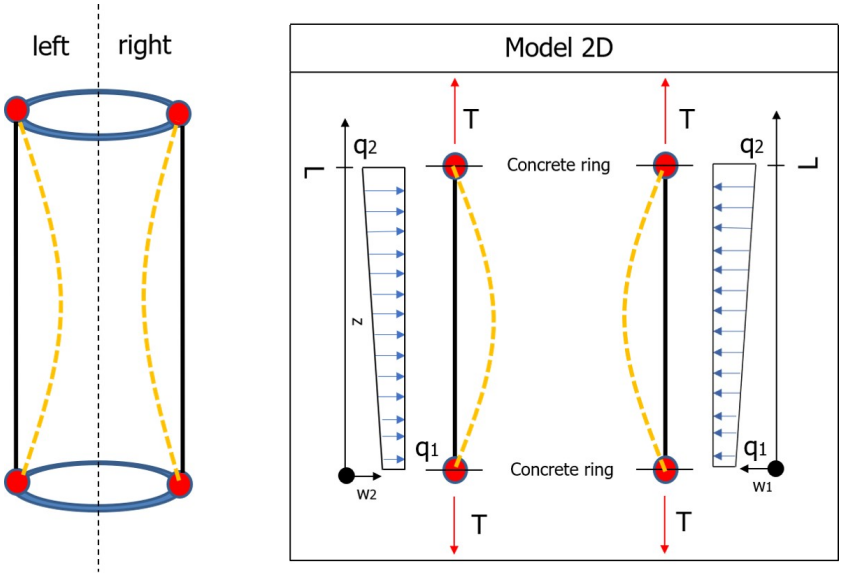

Figure 6.10: 2D sheet model of the thin walled sheet

Sheet model assumptions

The model assumptions for the 2D sheet model are:

- Plastic nylon sheet is modelled as two 2D cables on tension, implying there is no bending stiffness, constant tension and small deformations occur.

  By using the 2D sheet model, the effect of the circular shape of the thin sheet is neglected. In order to check whether the deformation as a result of buckling could become an issue, an ellipse calculation for the thin walled sheet is performed. An elaborate explanation of the ellipse shape and calculation is presented in Appendix H.

- At the concrete rings the displacement is 0, meaning w(0) = 0 and w(L) = 0
- The q-load is modelled by the pressure difference p_e - p_i $[N/m^2]$

The equation of motion for the left and right part of the sheet is given by equation 6.18.

$$\ddot{w} - \frac{T}{\rho A} w'' = \frac{q_1}{\rho A} + \frac{q_2 - q_1}{L \rho A} \tag{6.18}$$

Since dynamics is disregarded in this thesis, the equation of motion becomes equation J.3.

$$-c^2 w'' = \frac{q_1}{\rho A} + \frac{q_2 - q_1}{L \rho A} \tag{6.19}$$

The displacement of the 2D sheet, thereby solving the differential equation, is given by equation 6.20. A complete derivation of the solution of the equation of motion is given in Appendix J.

$$w(x) = -\frac{1}{6}\frac{q_2 - q_1}{2T} * x^3 - \frac{1}{2}\frac{q_1}{T} * x^2 + \frac{L(2q_1 + q_2)}{6T} * x \tag{6.20}$$

in which:

- T is the tension in the sheet [N]
- L is the span between the concrete rings [m]
- q_1 is the pressure difference p_e - p_i at the location of the lower concrete ring [N/m^2]
- q_2 is the pressure difference p_e - p_i at the location of the upper concrete ring [N/m^2]

7

Model results

In this chapter, the model results of the FLEX-hose foldable concept design are presented. First, the model approach is discussed. Then, the results of the sensitivity study are presented, including comparing a span width of 5 m and 10 m between the concrete rings. After this, the outputs for two model configurations of the model are discussed. Finally, the two possible design configurations are presented and discussed.

7.1. Model approach

Throughout the optimization of the model many parameters have been varied. The number of cables has been varied between 3 and 5. Through running the model numerous times, it is concluded that three cables are sufficient to resist the axial forces in the material. This was checked by making sure the unity checks of the cable stresses stay below the yield criterion. In addition, the span between the concrete rings has also been varied between 5 m and 10 m to investigate the effect on the results, which is presented in section 7.2.1 [18].

7.2. Sensitivity study

For the sensitivity study, the material choice of the cables and the pre-tension in the sheet has been varied. The materials that have been analysed can be seen in Table 7.1. In Table 7.2, the corresponding force division per material is shown. The pre-tension has been varied between 500 kN to 15000 kN. In order to optimize the results and meet the design criteria, the thickness of the sheet may also be altered. The weight of the concrete rings is 33.04 kN in submerged weight. Due to feasibility considerations, the weight of the concrete rings has not been varied.

Material	**Density (kg/m^3)**	**Young's Modulus (MPa)**	**Yield strength (MPa)**
Steel	7860	200000	2160
Polyester	1380	5500	850
Rigid nylon	1140	9000	1050
Dyneema	980	65000	3300

Table 7.1: Materials used for cables in model

E_s **(MPa)**	A_s **(m^2)**	E_c **(MPa)**	A_c **(m^2)**	**% sheet**	**% cable**
495	0.11	5500	0.12	72.35	9.21
495	0.11	9000	0.12	61.53	12.82
495	0.11	200000	0.12	6.71	31.09
495	0.11	65000	0.12	18.13	27.29

Table 7.2: Force distribution as a result of different materials for cables

7.2.1. Span between concrete rings

In Figure 7.1 and Figure 7.2, the result of varying the pre-tension is shown for a span width of 5 m and 10 m. From these two figures, it can be concluded that for a span width of 10 m, the calculated pressure drops are significantly higher. With a pre-tension of 15 MN, the calculated pressure drop is above 2 bar. Since the design requirement of staying below 0.6 bar is not met by far, this design configuration is not sufficient. However, by using a length of 5 m between the concrete rings, the calculated pressure drop at 15 MN is 0.87 bar. Since this value is close to 0.6 bar, more model runs were examined, which is discussed in the next section.

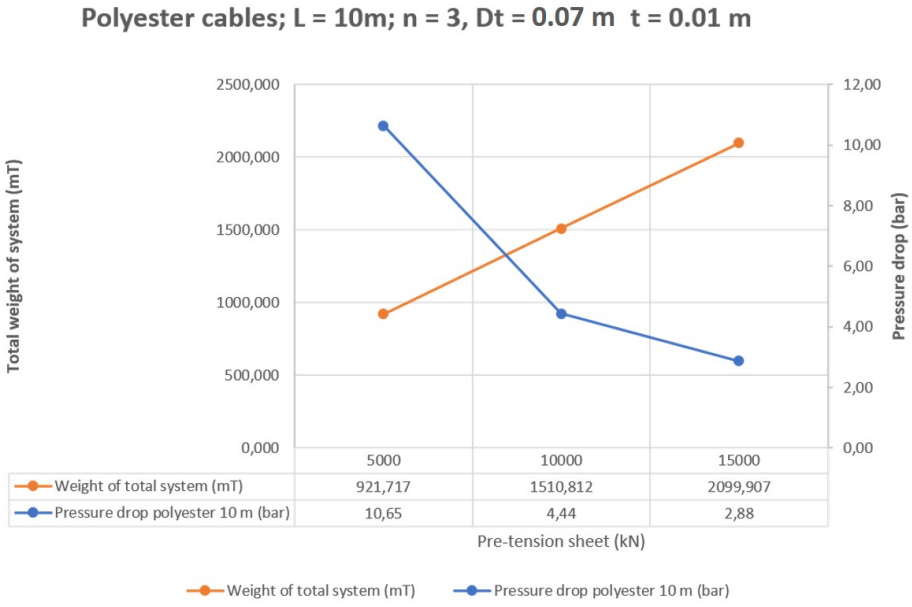

Figure 7.1: Model runs with a concrete ring span of 10 m

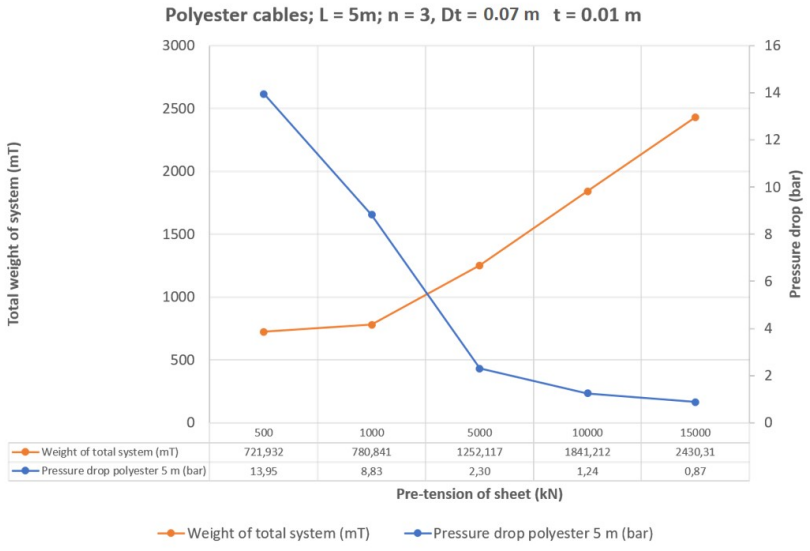

Figure 7.2: Model runs with a concrete ring span of 5 m

Design input parameters

The design configurations of the runs in the next section are shown in Table 7.8 and Table 7.3. Both runs are done with polyester cables.

Design parameter	Value	Unit
1) Cables		
ρ_{cable}	1380	kg/m^3
E_{cable}	5500	MPa
$f_{y,cable}$	850	MPa
nr of cables	3	-
D_{cable}	0.07	m
2) Sheet		
ρ_{sheet}	1025	kg/m^3
E_{sheet}	495	MPa
$f_{y,sheet}$	29	MPa
T_{pre}	15000	kN
t	0.06	m
Do_{nylon}	3.5	m
u_f	2	m/s
Allowed angle	7.5	$degrees$
Pressure drop input	0.63	bar
3) Concrete rings		
$Di_{concrete}$	3.5	m
$Do_{concrete}$	4.3	m
$h_{concrete}$	0.5	m
Submerged weight	33.04	kN

Table 7.3: Design polyester cables 15 MN

Design parameter	Value	Unit
1) Cables		
ρ_{cable}	1380	kg/m^3
E_{cable}	5500	MPa
$f_{y,cable}$	850	MPa
nr of cables	3	-
D_{cable}	0.07	m
2) Sheet		
ρ_{sheet}	1025	kg/m^3
E_{sheet}	495	MPa
$f_{y,sheet}$	29	MPa
T_{pre}	10000	kN
t	0.04	m
Do_{nylon}	3.5	m
u_f	2	m/s
Allowed angle	7.5	$degrees$
Pressure drop input	0.63	bar
3) Concrete rings		
$Di_{concrete}$	3.5	m
$Do_{concrete}$	4.3	m
$h_{concrete}$	0.5	m
Submerged weight	33.04	kN

Table 7.4: Design polyester cables 10 MN

7.2.2. Force distribution

In the following section, model runs are presented for a pre-tension of 10 MN and 15 MN. The force distribution as a consequence of the sheet being attached to the concrete rings is shown in Table 7.5. The largest percentage of weight (77.2 %) is transferred to the sheet for a design in which polyester is chosen as the cable material. The two plots differ in thickness in order to satisfy the design requirements.

Run	Sheet %	Cable %
Run 1 - Rigid nylon	67.44	10.85
Run 2 - Polyester	77.2	7.6
Run 3 - Steel	8.52	30.5
Run 4 - Dyneema	22.24	25.90

Table 7.5: Force distributions of run 1 and 2

7.2.3. Pressure difference

As discussed in Chapter 5, a pressure difference is present during pumping water through the cold water pipe. The pressure difference is the largest in the upper section of the pipe, as can be seen in Figures 7.3 7.4. The shape of the pressure difference graph can be explained by the fact that more pressure is lost once the water gets closer to the surface. Also, the difference in water density between the ambient seawater and the cold seawater explains the shape of the graph. The maximum pressure difference is calculated to be 40 kN/m^2. A positive net external pressure on the pipe, means a negative pressure is present inside the pipe, leading to compression of the pipe. This is also shown in Figure 7.5, since the hoop stress is negative. Buckling instability could occur as a consequence of this negative hoop stress. This has not been quantitatively calculated, but is a significant risk which should be taken into account.

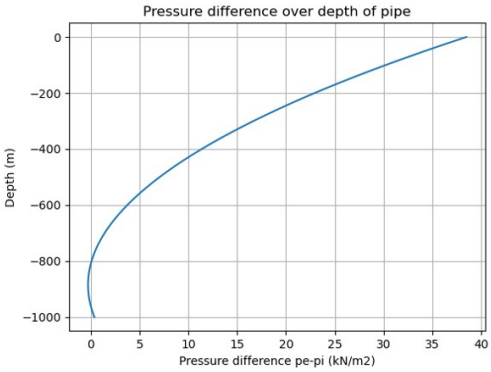

Figure 7.3: Pressure difference due to pumping exerted on the outside of the pipe, T = 10 MN, t = 0.04 m

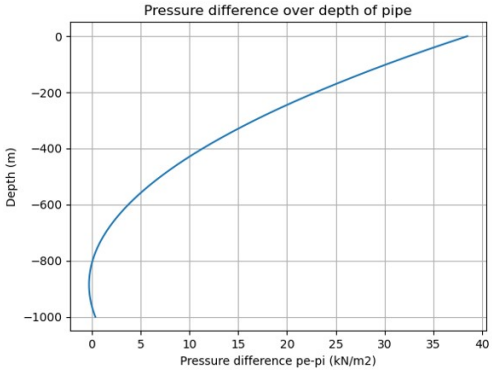

Figure 7.4: Pressure difference due to pumping exerted on the outside of the pipe, T = 15 MN, t = 0.06 m

7.2.4. Axial tension and hoop stress sheet

As a result of the pre-tension, concrete ballasts and the pressure difference axial stresses and hoop stresses occur in the thin walled sheet. Due to the high pre-tension, the axial stress in the sheet is governing and the hoop stress is relatively low. Two plots for the axial tension, hoop stress and von Mises stress are shown in Figures 7.5 and 7.6. The hoop stress is negative due to the compression while pumping. The maximum stress in the nylon is calculated to be 26 MPa, where the yield criterion is at 29 MPa. This means the nylon sheet is axially loaded almost to its full potential to resist the deformation that happens while pumping.

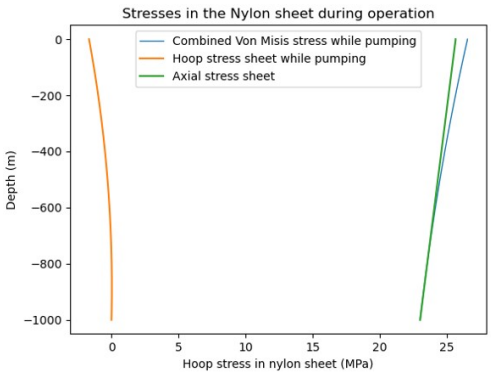

Figure 7.5: Hoop stress and combined von misis stress nylon sheet, T = 10 MN, t = 0.04 m

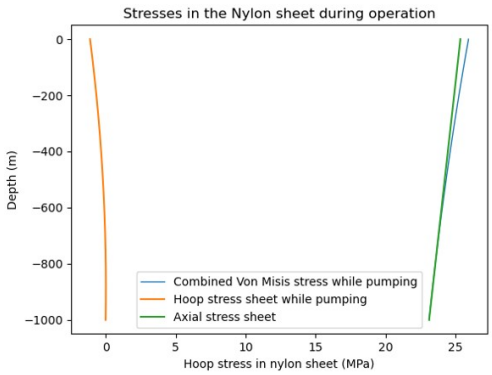

Figure 7.6: fig.Hoop stress and combined von misis stress nylon sheet, T = 15 MN, t = 0.06 m

7.2.5. Axial tension cables

The axial tension in the cables is shown in Figure 7.7 and 7.8. Since the polyester cables take only 7.6 % of the concrete load per section, the cable forces are relatively much smaller compared to the nylon sheet forces.

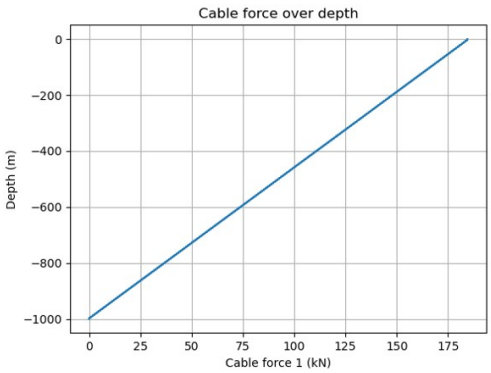

Figure 7.7: Cable force over depth, T = 10 MN, t = 0.04 m

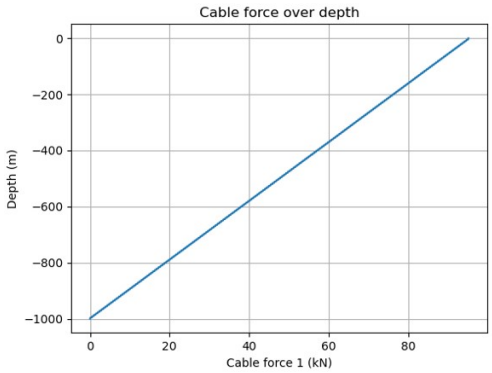

Figure 7.8: Cable force over depth, T = 15 MN, t = 0.06 m

7.2.6. Displacement of sheet

The large pre-tension of 10 MN causes the thin walled sheet not to have a pressure drop above 0.6 bar. In addition, this means the deformation of the sheet is influenced by the pre-tension applied. The deformation of the sheet is shown in Figure 7.9 and 7.9. It is clear to see that a larger pre-tension of 15 MN leads to a smaller deformation. In Figure 7.10, it can also be seen that in the upper region more deformation takes place due to the fact that the pressure difference is larger.

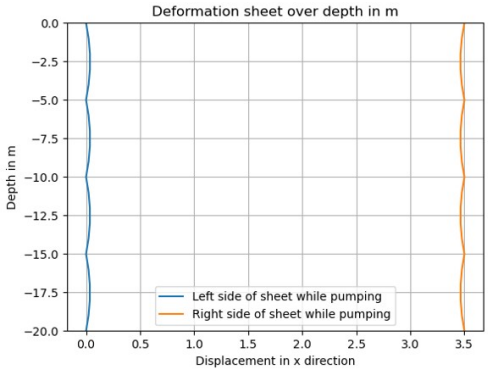

Figure 7.9: Deformation sheet first 20 m, T = 10 MN, t = 0.04 m

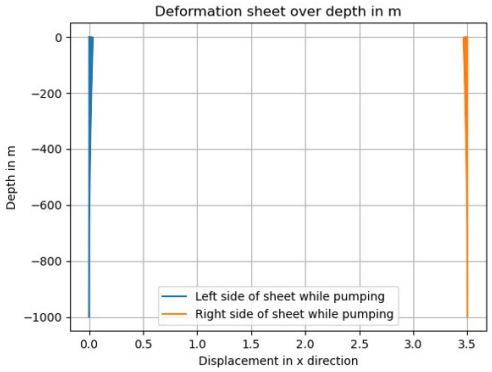

Figure 7.10: Deformation sheet total, T = 10 MN, t = 0.04 m

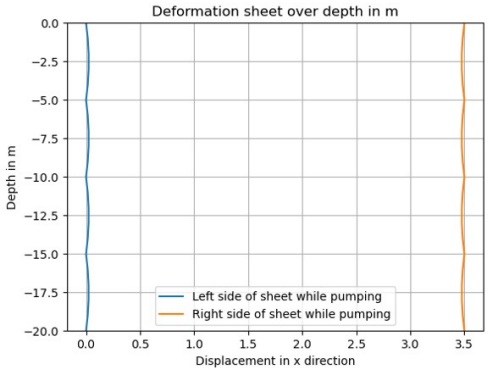

Figure 7.11: Deformation sheet first 20 m, T = 15 MN, t = 0.04 m

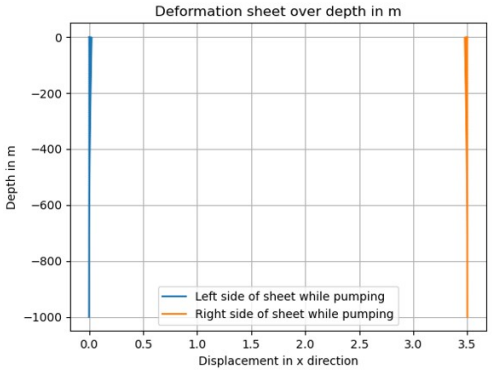

Figure 7.12: Deformation sheet total, T = 15 MN, t = 0.06 m

7.2.7. Inclination angle

The inclination angle of the sheet is the angle halfway between the concrete rings. For a design with a pre-tension of 10 MN, the maximum inclination angle is 10.2 degrees at the top. By applying a higher pre-tension of 15 MN, the maximum angle of inclination angle is 7.6 degrees at the top. Both inclination angles have a mean value below 7.5 degrees which is why it is acceptable.

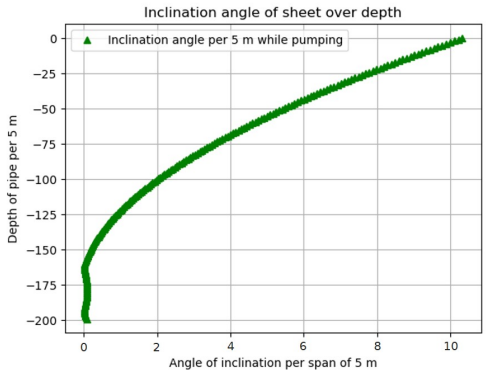

Figure 7.13: Inclination angle over depth, T = 10 MN

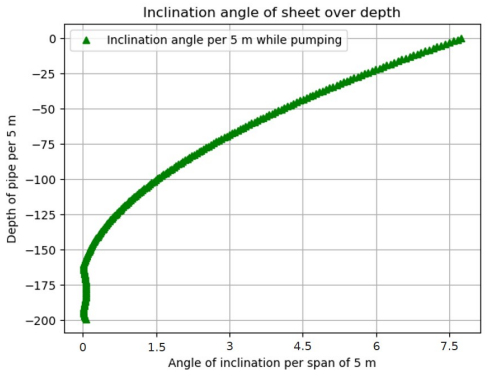

Figure 7.14: Inclination angle over depth, T = 15 MN

7.3. Summary of results

In the following section, a summary of all the model results is given.

7.3.1. Material choice

Steel is concluded to be too heavy for the FLEX-hose foldable concept design. The weight of steel adds up quickly over a length of 1000 m. In addition, in the steel concept only 8.52 % of the concrete ring's load is transferred to the sheet. Dyneema could be an interesting material choice due to its high strength. However, dyneema is expensive as its costs up to 100 €/kg, according to CES Edupack. Using polyester for the cables is the regarded to be a good choice due to the fact that a larger percentage of the load is transferred to the sheet.

7.3.2. Discussion of results

The results of the design parameters as summarized in Table 7.8 and Table 7.3 are given in Table 7.7 and Table 7.3 respectively. For both design parameters, the calculated pressure drop is acceptable as it is smaller than 0.6 bar. However, the thickness needed to keep the unity check of the stresses within acceptable limits is at least 0.04 m. Foldability is questionable for a thickness of 0.04 m. Prevention of the sheet touching the cables is achieved by placing the cables on a distance of 0.34 m from the sheet. The prevention of the sheet touching the cables is calculated by the ellipse form as shown in Figure H.3. Lastly, the system weight of the total FLEX-hose concept is calculated to be 1843 mT and 2423 mT respectively. The FLEX-hose foldable pipe concept could be installed by the Oceanic vessel of Allseas. The Oceanic is able to lift 300 mT. A calculation of the lift of the foldable pipe is given in Appendix G.

Design parameter	Value	Unit
Collapse	No	
Calculated pressure drop	0.48	bar
Gross energy left	14.09	MW
Mean angle	2.5	°
Maximum angle	7.6	°
U.C cable stress	0.29	-
U.C sheet stress	0.89	-
Total weight of concrete	6608.00	kN
Total weight of system (sub)	24323.00	kN
Vertical displacement	48.72	m
Clump weight force	17672.84	kN
h_{clump}	54.38	m
Sheet touches cable	No	

Table 7.6: Design polyester cables results for T = 15 MN

Design parameter	Value	Unit
Collapse	No	
Calculated pressure drop	0.59	bar
Gross energy left	13.77	MW
Mean angle	3.1	°
Maximum angle	10.2	°
U.C cable stress	0.26	-
U.C sheet stress	0.96	-
Total weight of concrete	6608.00	kN
Total weight of system (sub)	18433.30	kN
Vertical displacement	32.26	m
Clump weight force	11781.90	kN
h_{clump}	36.25	m
Sheet touches cable	No	

Table 7.7: Design polyester cables results for T = 10 MN

7.4. Final design

The final design which satisfies the design requirements is the design summarized in Table 7.8. The reason for choosing a pre-tension of 10 MN instead of 15 MN is the total system weight. The total system weight of 1843 mT as stated in Table 7.7 is considered to be feasible since it is lower than 2000 mT. A picture of the final design which satisfies all design requirements is shown in Figure 7.15.

Design parameter	**Value**	**Unit**
1) Cables		
ρ_{cable}	1380	kg/m^3
E_{cable}	5500	MPa
$f_{y,cable}$	850	MPa
nr of cables	3	-
D_{cable}	0.07	m
2) Sheet		
ρ_{sheet}	1025	kg/m^3
E_{sheet}	495	MPa
$f_{y,sheet}$	29	MPa
T_{pre}	10000	kN
t	0.04	m
Do_{nylon}	3.5	m
u_f	2	m/s
Allowed angle	7.5	$degrees$
Pressure drop input	0.63	bar
3) Concrete rings		
$Di_{concrete}$	3.5	m
$Do_{concrete}$	4.3	m
$h_{concrete}$	0.5	m
Submerged weight	33.04	kN

Table 7.8: Design polyester cables 10 MN

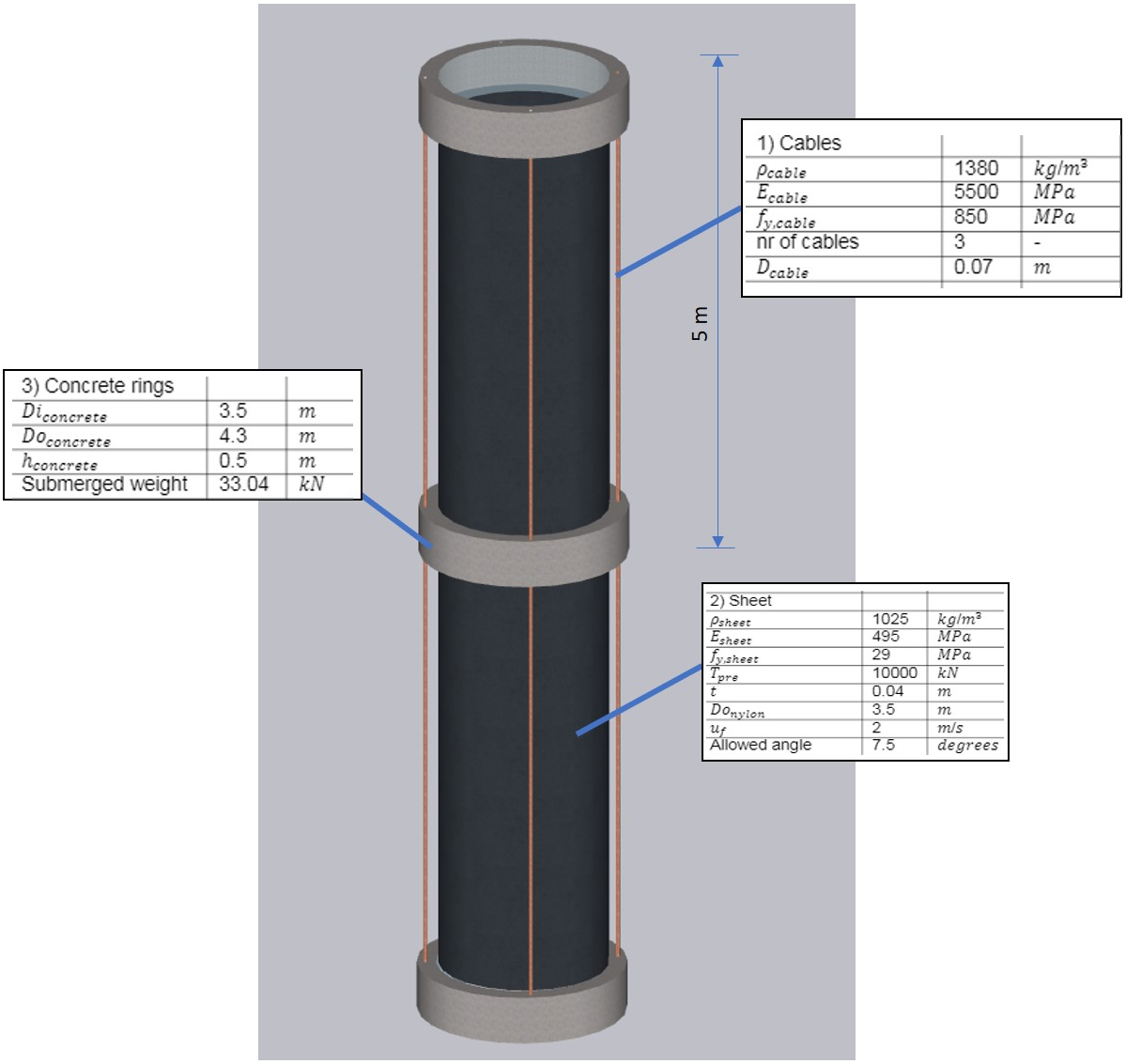

Figure 7.15: Final design picture foldable concept design

III

Conclusions

8

Conclusions

In this chapter, the conclusions of this thesis are presented. The conclusions of the thesis are presented by reflecting upon the research question and the sub-questions. First, the key design requirements of a 10 MW OTEC cold water pipe are discussed. Subsequently, the foldable FLEX-hose concept is discussed in comparison with other cold water pipe concepts. After this, the technical risks of the foldable FLEX-hose concept during operation that influence the technical feasibility are discussed.

8.1. Key design requirements

The key design requirements of the cold water pipe OTEC pipe that have been established in this thesis are a consequence of the criteria of generating 10 MW and are concluded to be:

- The maximum head loss in the CWP is determined to be 0.6 bar. The reason for the value of 0.6 bar, is that in the OTEC system itself energy is lost during pumping the water through the system. The pressure drop in the cold water pipe, warm water pipe, heat exchangers and other pipes add up to a net OTEC efficiency of 70 %.
- A flow rate of respectively 20.000 kg/s for the cold water pipe. This has been established to be a good flow rate for the cold water pipe by previous research in order to generate 10 MW.
- A length of the CWP of 1000 m, in order to have a temperature difference of at least 20 °C.

8.2. Foldable concept compared to other cold water pipe concepts

The foldable FLEX-hose concept is concluded to be attractive in comparison to other current cold water pipe concepts due to easy deployment with the foldable concept and fewer material costs that are expected to be needed. However, the inclination angle while pumping may not become significant, meaning above 7.5 degrees, since this will lead to lower OTEC energy efficiency below 70%. In addition, no current design is available on the market, meaning research and development is needed. The other foldable concept, in which a spiral is wrapped into a sheet, is concluded to be less attractive. The main reason is that the foldable spiral concept is expected to generate large motions due to the spiral that is present in the pipe. In-homogeneity's in surface roughness are expected to create vortices in the flow leading to significant motions and lowering efficiency.

Non-flexible cold water pipe concepts such as a composite pipe and a HDPE pipe have also been assessed. The rigid composite concept is interesting due to the fact that large diameters are currently available for composite pipes and the high strengths that can be achieved with composite structures. However, a composite pipe structure is concluded to be less susceptible due to the expectation of very high material costs. Secondly, the current HDPE pipe is concluded to be the most attractive currently for the OTEC cold water pipe. The main reasons for this are the fact that the current market is focused on HDPE and the relatively low material costs. However, installation is expected to be relatively difficult, since large parts will have to be joined together offshore.

8.3. Technical risks of foldable FLEX-hose concept

In the following section, the conclusions about the technical risks in relation to the feasibility are discussed. The final foldable concept design consists of a total of 200 concrete rings over 1000 m, a nylon sheet thickness of 0.04 m and three polyester cables of 0.07 m. The total system weight of the foldable pipe with concrete rings is 1840 mT, which could be installed with an offshore installation vessel. The main challenges regarding technical risks of the FLEX-hose concept that have been established in this thesis are: pressure drop becoming too large, buckling instability leading to collapse, creep, foldability of the plastic material and the attachment of the concrete and the nylon.

8.3.1. Pressure drop

The pressure drop in the FLEX-hose foldable cold water pipe due to the displacement of the sheet is concluded to be governing for the design. In order to have a pressure drop below 0.6 bar and have a FLEX-hose foldable design which is below 2000 mT in weight, a high pre-tension of at least 10 MN is needed. The high pre-tension is achieved by making every 5 m of sheet 0.16 m shorter. Using a span distance of 5 m between the concrete rings is concluded to be needed to keep the pressure drop below 0.6 bar. This would mean a total of 200 rings over 1000 m. However, a large pre-tension of 10 MN is still needed, leading to a large clump weight of approximately 12 MN. This could for instance be done by a clump weight made from steel. In addition, the pressure drop in the cold water pipe increases significantly when the sheet contracts in the upper region from the sea surface until -200 m. This can be explained by the fact that the pressure difference is the largest in the upper region. It is therefore recommended to locally increase the strength of the pipe in the upper region, for instance by a transition piece.

8.3.2. Collapse

Since the hoop stress becomes negative during pumping of the water, buckling instability could occur at stresses below the elastic limit or yield strength of the material. In this case, the thin walled sheet will deform in an ellipse shape. The calculated collapse pressure for a thin walled flexible nylon sheet without axial tension varies between 0.13 kN/m^2 and 103.50 kN/m^2, depending on the thickness t and length L between the rings. This is relatively low since the maximum pressure difference during pumping is calculated to be 40 kN/m^2. In order to prevent instabilities from occurring, a pre-tension should be introduced into the sheet. However, since the thin walled structure has a very high D/t ratio, there is still a probability of instabilities occurring.

8.3.3. Creep

The foldable FLEX-hose pipe is operational for 30 years and is therefore subjected to creep when loaded for a longer period of time. As time passes by, the creep of the nylon could lead to failure of the material. It could therefore be beneficial to locally increase the strength of the pipe by means of reinforcements such as fibers thereby reducing the maximum stress in the pipe. It is recommended for future research to investigate the behaviour of a nylon plastic when loaded for a longer period of time.

8.3.4. Foldability

To meet the design criteria of the cables and sheet not exceeding their unity checks, the needed wall thickness of the nylon sheet has been calculated to be 0.04 m. The question is, whether this would still be foldable. The thicker the wall thickness gets, the more difficult it will be to fold the material. The foldability of a nylon sheet of 0.04 m is an uncertainty which should be investigated by future research. From my own opinion and expertise, I would say a maximum thickness of 0.01 m is foldable.

8.3.5. Attachment concrete and nylon

The attachment of the concrete rings to the nylon sheet is a challenge on its own. In general, a plastic such as a nylon is not joined to a concrete ring. An idea could be to manufacture small systems in the sheet on which the concrete ring could be hung up upon. Another solution could be some kind of epoxy or other joining material. Future research is needed to investigate whether this could be possible.

9

Recommendations

In this chapter, the recommendations following from the conclusions are presented. First, the recommendations regarding the design of the flexible cold water pipe are discussed. Subsequently, possible future work for a foldable OTEC pipes is discussed.

9.1. Design of the FLEX-hose cold water pipe

As stated in the conclusions in the previous chapter, the main challenges and technical risks have been concluded to be:

1. The pressure drop due to the inclination angle in the pipe (< 0.6 bar)
2. The possibility of instability occurring in a thin walled pipe (< 0.05 m) structure due to buckling collapse
3. The possibility of creep in the nylon sheet (over a life-time of 30 years)
4. Foldability of a nylon sheet of 0.04 m
5. The attachment of concrete blocks to a nylon sheet

Regarding these technical risks, certain recommendations can be made. Firstly, since the pressure difference is the largest in the upper section of the pipe and the environmental loads have the most impact in the upper section, it is recommended to design a transition piece from the vessel or platform to the flexible pipe with stiffer elements. Also, it is recommended to look into the effects of waves, current and the movement of the vessel on the pipe design. Especially in the upper part of the foldable pipe, this is expected to have a large influence. It is therefore recommended this should be further researched. Secondly, the shape of the thin walled sheet will deform into once the water flows through the pipe, is an uncertainty. The shape the cold water pipe during pumping will therefore have to be validated with an experimental set-up. The non-occurrence of buckling also has to be validated for smaller thicknesses < 0.05 m of pipes. Thirdly, it could be interesting to investigate the use of fibers in flexible materials in order to locally increase the strength of the material. In the long term, this will lead to lower stresses in the material. Regarding the foldability of nylon materials, future research should be done regarding the thickness at which nylon material can be folded. Lastly, further research should be done on how to attach a concrete block and a sheet in a good way.

9.2. Future work for foldable OTEC pipe concepts

Regarding the modelling done in this thesis, it would be scientifically interesting to make a new model in which the sheet is modelled in 3D by using the shell equations. This could be good work for the future in order to understand the deformation of the thin walled sheet better. Secondly, a concept in which the cables are attached to the sheet through a sleeve could be interesting for future research. In this way more stability is provided meaning the possibility of instability occurring becomes a lot smaller.

IV

Appendices

A

New energy concepts for a vessel

As discussed in Chapter 1, the energy transition is changing the maritime industry. In this Appendix, the Multi Criteria Analysis for different energy concepts on a vessel is explained. The application of the Multi Criteria Analysis is for a stationary vessel offshore which has to produce energy for a longer period of time (e.g. for deep sea mining, see Appendix E). The energy resource should meet the regulations for NO_x, SO_x and CO_2, it should therefore be a sustainable form of energy production.

The following forms of energy production on a vessel have been identified:

- Conventional diesel generators (on board)
- Dual fuel diesel generators (ICE) (on board)
- Fuel cells using hydrogen (PEMFC) (on board)
- Solar energy (on deck)
- Wind energy with high masts (on deck)
- LNG tanks (on board)
- Nuclear energy (on board)
- OTEC (on deck)

Solar energy is not incorporated in the MCA because it requires too much space on a vessel. Large spaces are required on the offshore vessel (262 m x 262 m), which are needed for other activities offshore making it a less favorable option. Wind energy is also not incorporated since high masts on a vessel require much space as well. As a logical consequence, it would also be difficult to operate cranes and other offshore equipment. Also, the capacity factors of

A.1. Current developments energy concepts vessels

In the following section, the current developments for new forms of energy production on board of a vessel are discussed.

A.1.1. Conventional diesel generators

Conventionally, diesel generators are used on board of a vessel which run on MDO (marine diesel oil) or HFO (heavy fuel oil). However, HFO and MDO heavily produce the gasses NO_x, SO_x and CO_2 when being burned which is disadvantageous for air quality and the greenhouse effect, which can be seen in Figure A.1. Conventional diesel generators do not pass the requirement of *IMO2020* since heavy fuel oils and marine diesel oil heavily emit NO_x, SO_x and CO_2.

With the legal obligation of *IMO 2020*, vessels are obligated to comply to the limit for sulphur in fuel oil used on board of vessels. Current vessels using heavy fuel oils, have to install a so called ”scrubber”.

Table 34 – *Emissions factors for top-down emissions from combustion of fuels*

Emissions substance	Marine HFO emissions factor (g/g fuel)	Marine MDO emissions factor (g/g fuel)	Marine LNG emissions factor (g/g fuel)
CO_2	3.11400	3.20600	2.75000
CH_4	0.00006	0.00006	0.05120
N_2O	0.00016	0.00015	0.00011
NO_x	0.09300	0.08725	0.00783
CO	0.00277	0.00277	0.00783
NMVOC	0.00308	0.00308	0.00301

Figure A.1: Greenhouse gas intensities shipping sector [14]

According to a study performed by Bluerise B.V, offshore diesel costs only 0.168 €/kWh [6]. However, offshore diesel heavily produces CO_2, NO_2 and SO_2. Another disadvantage of conventional diesel generators is that the fuel for the offshore vessel needs to be transported to the vessel, or the vessel needs to go to the shore to re-fuel. Taking into account the plans of IMO conventional diesel generators are not advised to be a good primary source of energy for future offshore vessels, which is why conventional diesel generators are not assessed in the MCA.

A.2. Multi Criteria Analysis

The energy concepts for an offshore vessel are compared to one another on the criteria market readiness, refuelling necessity, capital expenditure (CAPEX), capacity factor and CO_2 produced. Each criteria is given a weight factor according to the importance. Sustainability and costs are seen as criteria which are vital for new technologies, which is why these are weighed accordingly. The energy sources are scored according to an interval from -2 to 2, in which -2 means bad and +2 means excellent. The scores of -1, 0 and 1 respectively mean insufficient, sufficient and good.

Description	Weight factor	Criteria
Desirable	1	Market readiness
Important	2	Refuelling, CAPEX, capacity factor
Crucial	3	$CO_2 produced$

Table A.1: Weight factors of MCA energy concepts

A.2.1. Criteria

In the following section, the criteria that are used in the MCA are explained.

Market readiness: The criteria market readiness is aimed at scoring the energy technology on the level of readiness for using the technology in the future. The following argumentation is used for this:

- If the technology has been implemented on a ship yet, the score in the MCA is positive, meaning a 1 or a 2. The score of 2 is given when the technology or energy source already exists for a longer period of time.
- If the technology has not been implemented on a ship yet, but is seen as promising for the future, the score of 0 is given.

Refuelling: The criteria refuelling is aimed at making an estimation of the variable operational costs of the energy production. Strictly speaking, this depends on the costs of the fuel used. However, for simplicity it is only assessed whether or not refuelling is needed when the vessel stays offshore for a few years. The difference between -2 and 2 is rather substantial, but this has been chosen since the operating costs of fuel over the lifetime can be substantial. Fuel costs represent as much as 50-60 % of the total operating costs This depends on the type of ship and service. The following argumentation is used for this:

- If a tanker is expected to have to sail to the vessel for refuelling within 2 years, it is a score of -2.
- If the vessel does not need an external supply to refuel, it is rated as 2.

CAPEX: The criteria CAPEX is aimed to score the energy source on the capital expenditure it is expected to cost. The most expensive option is rated as -2 and the cheapest option as 2. Although the costs are hard to predict, a reasonable estimate has been made by using some reference projects.

Capacity factor: The criteria capacity factor is aimed to score the energy source on its reliability. The capacity factor is a ratio of the actual energy output over a given period of time to the maximum possible electrical energy output over that period. Since renewable sources such as solar power and wind energy are dependent on the actual weather the capacity factors are lower. Though the difference in capacity factor is only very small, it is incorporated in the MCA.

CO2 produced: The criteria CO2 produced is aimed to score the energy source on impact on the environment. The reference case as worst for this criteria, is the CO2 emitted with conventional diesel, which is 3.2 g CO2/g fuel. If the energy source produces no CO2, a maximum score of 2 is assigned. If the energy source produces CO2, a score of 1, 0, -1 or -2 is assigned, according to how much CO2 is produced. The intervals are listed below:

- 0.00 - 0.63 g/g fuel is a score of 2

- 0.64 - 1.27 g/g fuel is a score of 1
- 1.28 - 1.91 g/g fuel is a score of 0
- 1.92 - 2.55 g/g fuel is a score of -1
- 2.56 - 3.20 g/g fuel is a score of -2

A.2.2. Dual fuel diesel generator (ICE CI)

A new energy development to lower harmful emissions in the maritime emissions, uses ammonia or methanol for power generation in combination with an Internal Combustion Engine. A small percentage of diesel is still used, however, mainly ammonia is used to generate energy in the combustion engine. The costs of this concept are estimated to be around €10.000.000 for 10 MW, which is relatively cheap and therefore economically attractive. The capacity factor is high (90 %) as long as the fuel is available on the vessel. With this combination of ammonia and diesel, 80 % of CO2 can be reduced, which makes it an attractive renewable fuel for shipping. The vessel needs refuelling since ammonia or methanol needs to be stored in the vessel. The market has not seen the implementation of ammonia into engines yet. However, DNVGL predicts the usage of ammonia in shipping to rise in the coming decade, which is why it is seen as a promising new concept.

A.2.3. Fuel cells with hydrogen (PEMFC)

Fuel cells are a new kind of energy supply for offshore vessels. For marine vessel, fuel cells are the only viable, true zero-emission option. A fuel cell functions like a battery; it produces electricity with high efficiencies up to 55 % through an electro-chemical process. The difference is that with a fuel cell, the energy is stored separately in the form of a hydrogen fuel. As long as the hydrogen fuel is available, the fuel cell produces electricity. Additionally, hydrogen fuel can be produced from renewable sources, including solar, wind, hydroelectric, and geothermal energy. For a vessel, this would mean that hydrogen tanks in the vessel have to be filled in a place like a port or at some place offshore with hydrogen supply. The costs of this concept are estimated to be around €30.000.000 for 10 MW. The capacity factor is high (90 %) as long as the fuel is available on the vessel. The vessel needs refuelling since hydrogen needs to be stored in the vessel. The market has not seen the implementation of fuel cells into shipping yet. However, fuel cells are already used in products like cars and can be a good integrated energy system on board of a vessel. In Figure A.2, a diagram is shown how a fuel cell works.

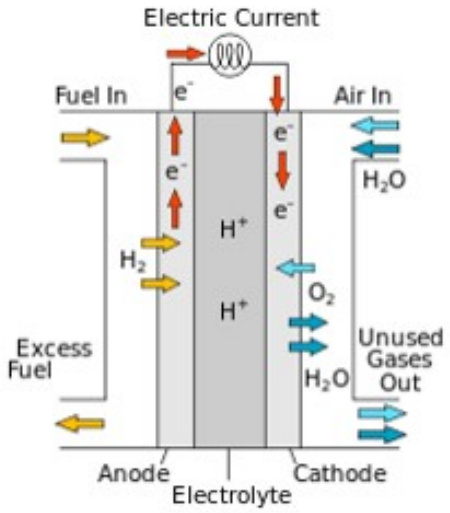

Figure A.2: Diagram of fuel cell

A.2.4. LNG tanks

LNG, also known as Liquid Natural Gas, is compressed natural gas stored in liquid form which can be used for power generation. LNG complies with the requirements of *IMO 2020*, meaning it produces only very little NO_2 and almost no environmentally damaging SO_2 emissions. Compared to conventional heavy fuel oils, LNG represents a 25 % reduction in CO_2, a 90 % reduction in NO_2 and a 100 % reduction in SO_2 emissions [15]. CO_2 emissions for LNG are still as substantial as 2.75 g/g fuel, meaning it is not sustainable and renewable. As stated before, this is only a 25 % reduction in CO_2 emissions. The costs of this concept are estimated to be around €32.000.000 for 10 MW. LNG has existed for quite some time now, though only recently it has been incorporated in more energy systems. The capacity factor is high (87 %) as long as the fuel is available on the vessel. The vessel needs refuelling since LNG needs to be stored in the vessel.

A.2.5. Nuclear energy vessel

Nuclear energy vessels are used in the military, for instance in submarine ships. Also, the Russian governments has produced the Akademik Lomonosov, a nuclear vessel able to produce 70 MW. There is quite much knowledge about nuclear energy, though only one large commercial vessel has been built at the moment. Also, safety is a big issue with nuclear power plants. The waste of the energy has to be stored on the vessel as well. With a large nuclear energy vessel, the probability of refuelling is rather low since the nuclear energy does not have to be stored. The costs of this concept are estimated to be around €62.000.000 for 10 MW, which is relatively expensive. The largest plant of OTEC right now is a 1 MW plant in Japan, meaning much research and development still needs to be done.

A.2.6. OTEC vessel/installation

Ocean Thermal Energy Conversion (OTEC) can be used to produce clean and base-load electricity without emitting CO_2. OTEC installations offshore (such as a TLP) or on a vessel could be used for power generation. An advantage of OTEC is that it does not need storage, meaning it is not needed to refuel. The costs of OTEC are estimated to be around €63.000.0000 for 10 MW, which is relatively expensive. The capacity factor of OTEC is high (90 %), since all year round the temperature difference is larger than 20 degrees Celsius.

A.2.7. Results of Multi Criteria Analysis

Energy concept for vessel	Market	Refuelling	CAPEX	Cap. factor	CO2 produced	Score
Dual fuel diesel generator	0	-2	2	2	1	7
Fuel cells with hydrogen	0	-2	0	2	2	6
LNG tanks	2	-2	0	1	-1	-3
Nuclear energy vessel	1	2	-2	2	2	11
OTEC on a vessel	0	2	-2	2	2	10

Table A.2: MCA table energy concepts on a vessel

From the results of the MCA it can be concluded that according to the criteria listed, OTEC on a vessel and nuclear energy on a vessel are the winners for the future of renewable energy concepts on vessels. Also dual fuel diesel generators and fuel cells are promising due to low emissions and high capacity factors. However, the final scores are still quite close to one another, meaning the conclusions are sensitive. In

B

IMO 2020 regulations

IMO 2020

Taking bold action to clean up shipping emissions by reducing the sulphur content in ships' fuel oil

HOW?

0.50% reduced from 3.50%
– significantly less sulphur permitted in ships' fuel oil

77% drop in overall SOx emissions from ships
– annual reduction of approximately 8.5 million metric tonnes of SOx

WHEN?

- From **1 January 2020**

AIR POLLUTION & HEALTH

- Premature deaths avoided
- **Significant** reduction in shipping's negative effect on human health through air pollution

Reductions in:

- stroke
- asthma
- cardiovascular disease
- lung cancer
- pulmonary disease

Cutting sulphur emissions helps prevent acid rain, which means:

- **less** harm to crops, forests and aquatic species
- **tackling** ocean acidification

WHERE?

- Health benefits felt globally
- Strongest in coastal communities
- Major impact in vulnerable areas

#IMOSulphurLimit **#BreatheLife** **#BeatAirPollution**

(Sources: University of Delaware study, February 2018; "Health Impacts Associated with Delay of MARPOL Global Sulphur Standards" presented by Finland to IMO, August 2016)

IMO INTERNATIONAL MARITIME ORGANIZATION

SUSTAINABLE DEVELOPMENT GOALS

IMO 2020 - FAQs

What is the sulphur 2020 limit?

From 1 January 2020, the limit for sulphur in fuel oil used on board ships operating outside designated emission control areas will be reduced to 0.50% m/m (mass by mass), from 3.50% m/m.

This limit is set in Annex VI of the International Maritime Organization (IMO) International convention for the Prevention of Pollution from Ships (MARPOL).

How can ships comply?

i) Use a compliant fuel oil with a sulphur content that does not exceed 0.50%
ii) If exceeding 0.50%, use an equivalent e.g. an Exhaust Gas Cleaning System ("scrubber")
iii) Use an alternative fuel e.g. LNG, methanol
iv) Use onshore power supply when at berth

What must ships do before 1 January 2020?

Ship operators and owners must plan ahead. IMO has issued guidance, including ship implementation and planning guidance.

Who is responsible for enforcement?

Monitoring and enforcement of the new limit falls to Governments and national authorities of Member States that are Parties to MARPOL Annex VI.

Flag States (the State of registry of a ship) and port States have rights and responsibilities to enforce compliance.

What is IMO doing to help implementation?

IMO has been working with Member States as well as the shipping industry, bunker suppliers and refiners to identify and mitigate transitional issues so that ships may meet the new requirement.

A range of guidance has been developed, including specific port State control guidelines and guidelines on consistent implementation.

Are there any exemptions?

If a ship simply cannot obtain compliant fuel oil, they can complete a Fuel Oil Non-Availability Report (FONAR). This can be taken into account by port State control, but is not an exemption.

Where can I find out more?

A list of IMO measures to support implementation of the 0.50% limit can be found opposite.

Please visit www.imo.org for further information.

IMO Instruments

Relevant (non-exhaustive) list of IMO instruments:

TREATY

- MARPOL Annex VI regulation 14, including the 0.50% sulphur limit from 1 January 2020
- Amendments to MARPOL Annex VI (Prohibition on the carriage of non-compliant fuel oil for combustion purposes for propulsion or operation on board a ship), enter into force from 1 March 2020 (MEPC.305(73))

IMPLEMENTATION

- 2019 Guidelines for consistent implementation of 0.50% sulphur limit under MARPOL Annex VI (MEPC.320(74))
- Guidance on the development of a ship implementation plan for the consistent implementation of the 0.50% sulphur limit under MARPOL Annex VI (MEPC.1/Circ.878)

BEST PRACTICE

- Guidance on best practice for fuel oil purchasers/users for assuring the quality of fuel oil used on board ships (MEPC.1/Circ.875)
- Guidance on best practice for fuel oil suppliers for assuring the quality of fuel oil delivered to ships (MEPC.1/Circ.875/Add.1)
- Guidance for best practice for Member State/coastal State (MEPC.1/Circ.884)
- Delivery of compliant fuel oil by suppliers (MSC-MEPC.5/Circ.15)
- Interim recommendations to enhance the safety of ships relating to the use of oil fuel (MSC.465(101))

PORT STATE CONTROL / SAMPLING

- 2019 Guidelines for port State control under MARPOL Annex VI Chapter 3 (2019 PSC Guidelines) (MEPC.321(74))
- Guidance for port State control on contingency measures for addressing non-compliant fuel oil (MEPC.1/Circ.881)
- 2019 Guidelines for on board sampling for the verification of the sulphur content of the fuel oil used on board ships (MEPC.1/Circ.864/Rev.1)

OTHER CIRCULARS

- Early application of the approved amendments to the verification procedures for a MARPOL Annex VI fuel oil sample (MEPC.1/Circ.882)
- Guidance on indication of ongoing compliance in the case of the failure of a single monitoring instrument, and recommended actions to take if the Exhaust Gas Cleaning System (EGCS) fails to meet the provisions of the 2015 EGCS Guidelines (MEPC.259(68)) (MEPC.1/Circ.883)
- Reporting of availability of compliant fuel oils in accordance with regulation 18.1 of MARPOL Annex VI (MEPC.1/Circ.880)
- Reporting of data related to fuel oil availability and quality in GISIS to promote greater understanding of the consistent implementation of the 0.50% m/m Sulphur limit under MARPOL Annex VI (MEPC.1/Circ.887)

C

Hydraulic pressure losses in the pipe

In this Appendix, the formulas which are used for the hydraulic pressure losses in the cold water pipe are shown [31].

The pressure drop in a pipeline (head loss in m) can generally be described by equation C.1:

$$h_{tot} = f * \frac{L}{D} * \frac{u_f^2}{2g} + \sum K * \frac{u_f^2}{2g} + \frac{\Delta\rho}{\rho_{inside}} * y \quad \text{(C.1)}$$

The first term is called the friction pressure loss (also known as the Darcy Weissbach term), and can be determined with figure C.1. The second term is the sum of all singular head losses. Singular head losses can be present due due to accelerations, decelerations, curvatures, branches and obstructions. It is assumed that the pipe inlet loss is the main singular head loss, since there are no curvatures, branches or obstructions in the cold water pipe. The third term is called the hydrostatic pressure loss.

C.1. Continuous pipe concepts

In this section, the relevant calculations for the pressure drop for the continuous pipe concepts are presented. The pressure drop in the continuous pipe consists of the inlet loss, the friction loss and the hydrostatic loss.

C.1.1. Assumptions

- u_f is assumed to be constant throughout the pipe
- $\rho_{average}$ is calculated by assuming a linear density water profile

C.1.2. Friction pressure loss

The friction pressure loss is calculated according to the Darcy Weissbach formula (equation C.2), in which:

- f is the coefficient of friction [-], which can be determined according to equation C.3
- L is the length of the pipe [m]
- D is the internal diameter of the pipe [m]
- u_f is the the flow velocity of the internal seawater [m/s]
- g is the gravitational acceleration, which is 9.81 [m/s^2]

$$h_{friction} = f * \frac{L}{D} * \frac{u_f^2}{2g} \tag{C.2}$$

The coefficient of friction can be calculated according to equation C.3, in which:

- ϵ is the roughness of the pipe [m]
- D is the internal diameter of the pipe [m]
- Re is the Reynolds number, which is calculated by equation C.4.

$$f = \frac{1}{\sqrt{f_D}} = -1.8 \log\left[\left(\frac{\frac{\epsilon}{D}}{3.7}\right)^{1.11} + \frac{6.9}{Re}\right] \tag{C.3}$$

The Reynolds number can be calculated by equation C.4, in which:

- u_f is the the average flow velocity of the internal seawater [m/s]
- D is the internal diameter of the pipe [m]
- ν is the kinematic viscosity [m^2/s], which is calculated by equation C.5

$$Re = \frac{u_f * D}{\nu} \tag{C.4}$$

The kinematic viscosity can be calculated by equation C.5, in which:

- η is the dynamic viscosity [$Pa.s$], dependent on the temperature
- ρ_{cold} is the density of the cold water inside the pipe [kg/m^3]

$$\nu = \frac{\eta}{\rho_{cold}} \tag{C.5}$$

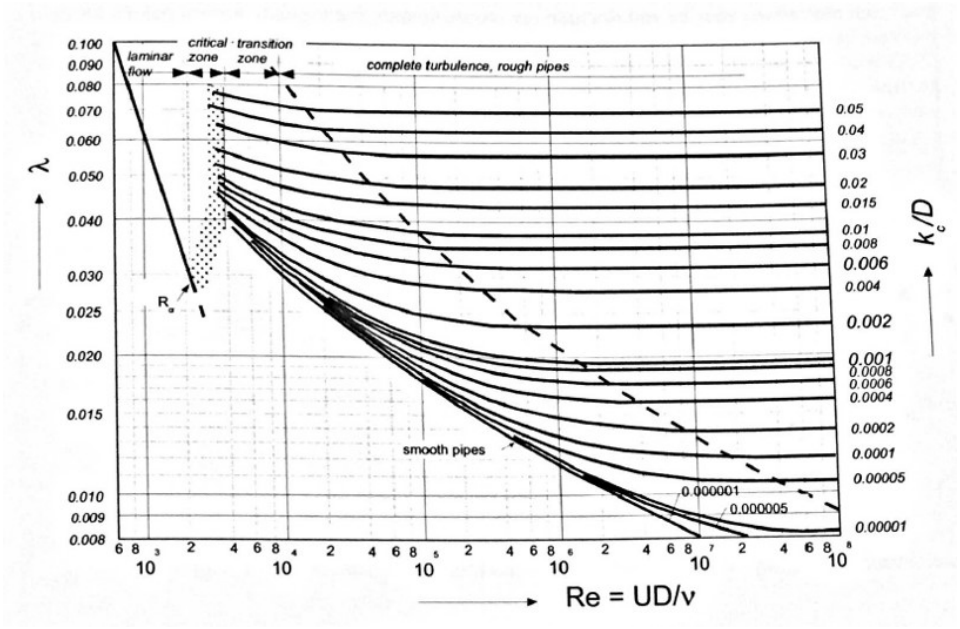

Figure C.1: Moody diagram for coefficient of friction [31]

C.1.3. Singular head losses

The sum of the head losses is assumed to consist of the pipe inlet pressure loss and the pipe outlet pressure loss. The K value is assumed to be 0.2, which is the K-value for a curved entrance with a bell shape. The maximum value of K, when no curved entrance is used, is 0.5.

The sum of these losses is calculated according to equation C.6, in which:

- h_{in} is the pipe inlet pressure loss $[m]$
- K is the inlet/outlet K value, also known as the pipe entry loss coefficient [-]
- u_f is the the flow velocity of the internal seawater $[m/s]$
- g is the gravitational acceleration, which is 9.81 $[m/s^2]$

$$h_{inlet} = K * \frac{u_f^2}{2g} \tag{C.6}$$

C.1.4. Hydrostatic pressure loss

The hydrostatic pressure loss is calculated according to equation C.7, in which:

- ρ_{cold} is the density of the cold water $[kg/m^3]$
- $\rho_{average}$ is calculated by equation C.8
- y is the total depth $[m]$

$$h_{hydro} = \frac{\rho_{cold} - \rho_{average}}{\rho_{cold}} * y \tag{C.7}$$

$$\rho_{average} = \frac{\rho_{cold} - \rho_{warm}}{2} \tag{C.8}$$

C.2. Discontinuous pipe concept

In this section, the relevant calculations for the pressure drop in the discontinuous pipe concepts are presented. The pressure drop in the continuous pipe consists of the inlet loss, the friction loss, the hydrostatic loss, the contraction losses and the enlargements losses. The inlet loss, hydrostatic loss and the friction loss are calculated according to respectively equation C.6, C.7 and C.2. A curved shape of the inlet with a K-value of 0.2 is assumed.

C.2.1. Assumptions

- The discontinuous pipe is modelled as having straight linear boundaries.
- Conservation of mass and volume is applied.
- The velocity is assumed to accelerate in the contraction part, reaching a higher velocity. This velocity is used for the estimation of the new ”enlargement” part. The velocity profile is assumed to be as shown in Figure C.2.

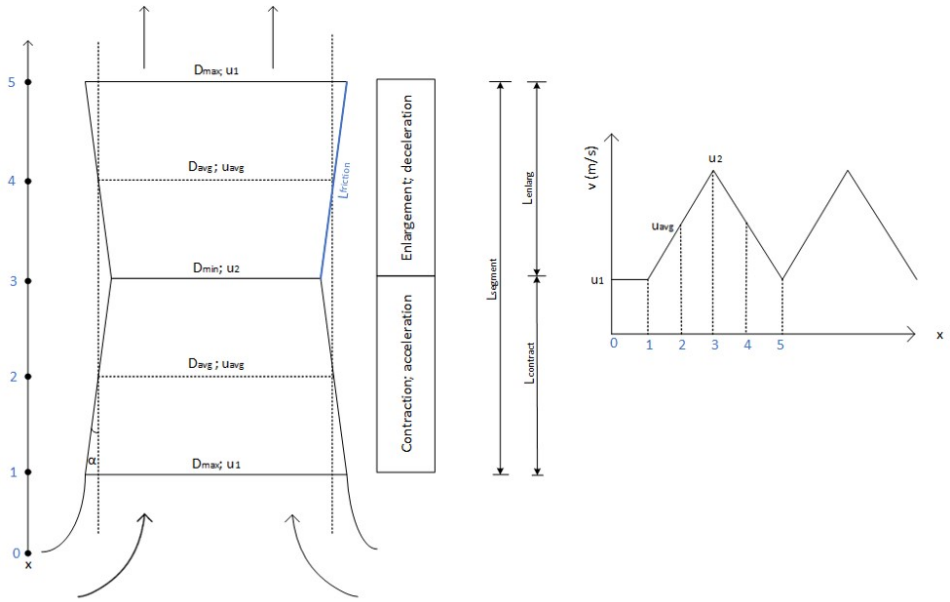

Figure C.2: Pressure losses in discontinuous pipe

C.2.2. Contraction and enlargement losses

The contraction and enlargement losses are calculated by respectively equation C.9 and C.10. The diffusor analogy is used to calculate the pressure losses in the foldable pipe.

$$h_{contraction} = K_c * \frac{u_2^2}{2g} \tag{C.9}$$

in which:

- u_2 denotes the flow speed after the contraction $[m/s]$

The value of K_c and K_e are determined by respectively Figure C.3 and C.4.

$$h_{enlargement} = K_e * \frac{(u_1 - u_2)^2}{2g} \tag{C.10}$$

in which:

- u_1 denotes the flow speed before the enlargement $[m/s]$
- u_2 denotes the flow speed after the enlargement $[m/s]$

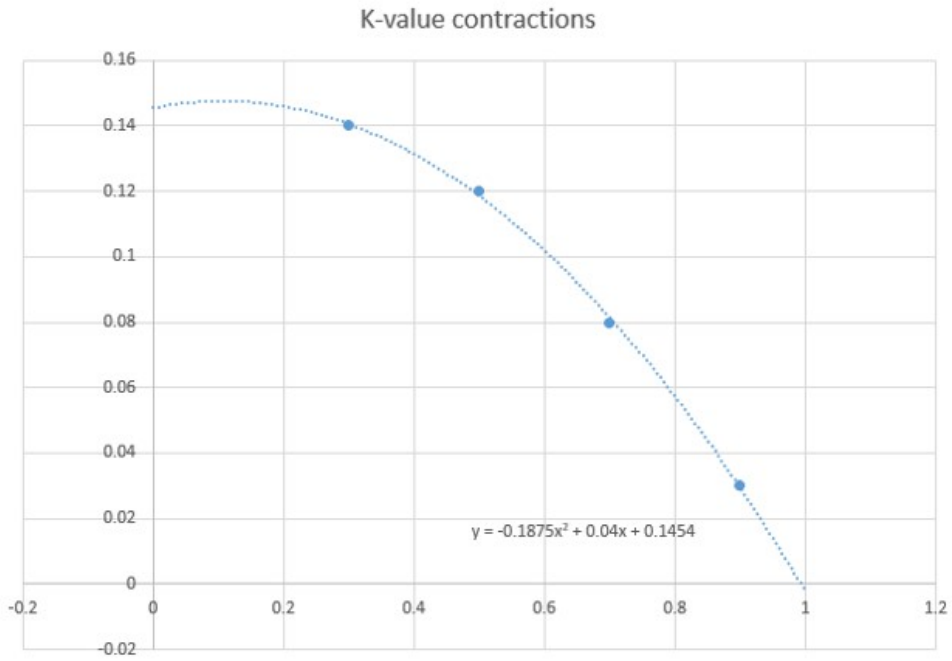

Figure C.3: K value contractions

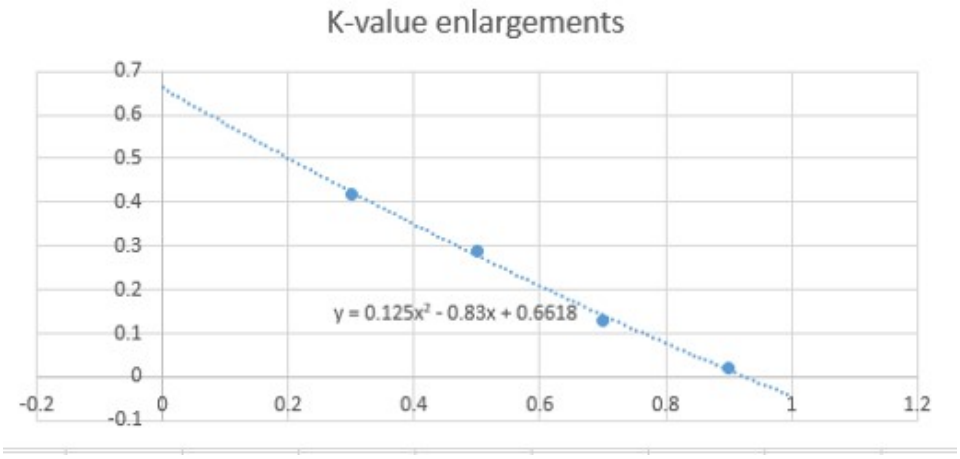

Figure C.4: K value enlargements

C.2.3. Pressure loss in the pipe for the different concepts

The operational efficiency of the flexible cold water pipe is measured by the flow losses that occur in the pipe. In order to have the highest efficiency of the overall OTEC system, it is favorable to have a low head loss. The parameters that influence the head loss are the flow speed, the diameter and the smoothness value of the pipe. Plastic pipe refers to respectively concept 3,PVC and HDPE. The pressure drop of the cold water pipe should stay below 0.6 bar as a threshold. This is chosen as a threshold to optimize the energy efficiency. The results of the pressure drop comparison can be seen in Figure C.5.

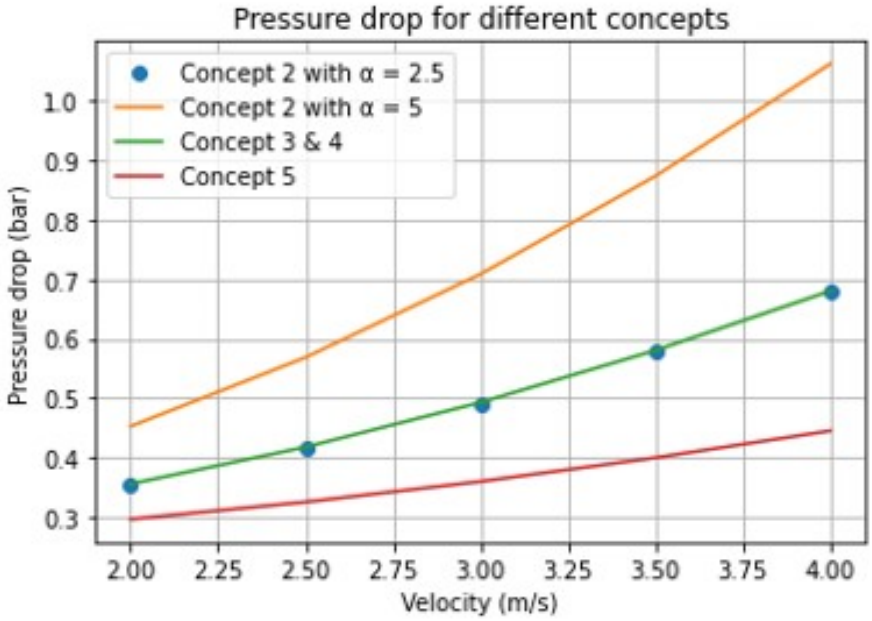

Figure C.5: Pressure drop for different concepts with different roughness values

From this graph, it can be concluded that the HDPE pipe causes the lowest pressure drop in the pipe. Due to very similar roughness values for the coated steel carcass and the FRP of concept 3 and 4, these two pipes are plotted in the same category. The foldable concept can be concluded to be feasible with the requirement that the average inclination angle should stay below 5 degrees. The roughness values used are stated in Table C.1. Concept 1 is not shown in the graph since the roughness value including a steel spiral on the inside of the pipe is expected to cause a significant pressure drop above 1 bar.

Concept	Inner pipe material	Roughness value (mm)
1	PVC with steel spiral	0.15
2	Nylon	0.0015
3	Coated steel carcass	0.003
4	FRP	0.005
5	HDPE	0.0015

Table C.1: Roughness values for different materials

D

Heat losses through the cold water pipe

In this Appendix, the heat that is transferred from the water outside the pipe into the water inside the thin pipe film is calculated. The heat transfer that is calculated is the heat transfer through the wall of the pipe. Previous studies calculated the heat transfer through an OTEC pipe, which is what is used as a guideline for this calculation [22]. The most important equations are equation D.8 and equation D.9. In section D.0.1, the heat transfer for the different concepts is presented.

The cold water pipe exchanges heat as a consequence of the temperature difference. For the Bonaire profile, the average water temperature on the outside is 11.7 degrees. The temperature profile can be seen in Appendix F. It is a plot of the average temperature profile in 2017, 2018 and 2019.

The process of heat losses in the pipe consists of three steps:

- convection from the pipe wall to the internal cold seawater
- conduction through the pipe wall
- convection from the ambient seawater to the pipe wall

For each step, the heat transfer coefficient should be determined.

The internal heat transfer coefficient is determined by the Dittus-Boelter correlation applicable for fully developed flows, which can be seen in equation D.1. Since the Reynolds number of the flow inside the pipe is relatively high ($> 1\mathrm{E}6$), this is a valid correlation to use. The correlation gives a Nusselt number (Nu) as output, which is a dimensionless number for the heat transfer coefficient.

$$Nu = 0.023 Re^{0.8} Pr^{0.3} \tag{D.1}$$

The Prandtl and Reynolds number are calculated taking the seawater dynamic viscosity of the average seawater temperature outside of the pipe. The Prandtl number accounts for the physical properties of the fluid and can be interpreted as the ratio of momentum diffusivity to thermal diffusivity and is calculated as:

$$Pr = \frac{\mu c_p}{k} \tag{D.2}$$

With the Nusselt number, the heat transfer coefficient of the convection from the pipe wall to the ambient seawater can be calculated by equation D.3.

$$h_o = \frac{kNu}{d_o} \tag{D.3}$$

The heat transfer through the pipe wall itself is determined by the thermal resistance R, which can be calculated by equation D.4

$$R_{wall} = \frac{\ln \frac{D_0}{D_i}}{2\pi\lambda_w dL} \tag{D.4}$$

The external convection is more difficult to predict because flow separation happens across the pipe. A turbulent area will form. Due to this phenomena, the empirical relation developed by Churchill and Bernstein is used for the determination of the Nusselt number:

$$Nu = 0.3 + \frac{0.62Re^{1/2}Pr^{1/3}}{\left[1 + (0.4/Pr)^{2/3}\right]^{1/4}} \cdot \left[1 + \left(\frac{Re^{5/8}}{282000}\right)\right]^{4/5} \tag{D.5}$$

Based on these three individual heat transfer coefficients, the (outside) overall heat transfer coefficient and heat loss per meter pipe can be determined applying, respectively, equation D.6 and D.7.

$$U_o = \left(\frac{D_o}{D_i h_i} + \frac{\ln \frac{D_0}{D_i}}{2\lambda_w} + \frac{1}{h_0}\right)^{-1} \tag{D.6}$$

$$dQ = dA_o U_o \left(T_i - T_o\right) \tag{D.7}$$

The difference in temperature over dL can now be calculated by equation D.8.

$$dT = \frac{dQ}{cp_{water} * m} * dL \tag{D.8}$$

in which:

- dQ is the total heat that is transferred through the pipe over per meter [W/m]
- cp_{water} is the specific heat capacity [$J/kg.K$], which is 3985 $J/kg.K$ for seawater
- m is the mass flow of the cold water in the pipe [kg/s]

By discretization of the pipe into small segments of dL, it is possible to calculate the internal seawater in the cold water pipe by applying an Euler forward scheme. This can be done by using the fact that at the boundary condition at the inlet pipe, the internal seawater is equal to the outside ambient seawater. The total heat balance of the convection along the three processes can be described by equation D.9.

$$dQ = dA_i h_i \left(T_i - T_{wi}\right) = \frac{\left(T_{wi} - T_{wo}\right)}{R_{wall}} = dA_o h_o \left(T_{wo} - T_o\right) \tag{D.9}$$

in which:

- A_i is the internal diameter [m]
- A_o is the outer diameter [m]
- h_i is the internal surface resistance coefficient
- h_o is the outer external resistance coefficient
- T_i is the internal temperature in the pipe [°C]
- T_{wi} is the temperature on the inside of the wall [°C]
- T_{wo} is the temperature on the outside of the wall [°C]
- T_o is the outer temperature on the outside of the pipe [°C]

D.0.1. Heat transfer for the different concepts

Since the concepts are thin walled and there exists an average temperature difference of approximately 6.4 degrees, thermal energy is transferred from the ambient seawater to the inside of the pipe. Every material has its own thermal conductivity k value, and this can be seen in Figure D.1. Clearly, polypropylene has the lowest thermal conductivity, whereas composite has the highest thermal conductivity.

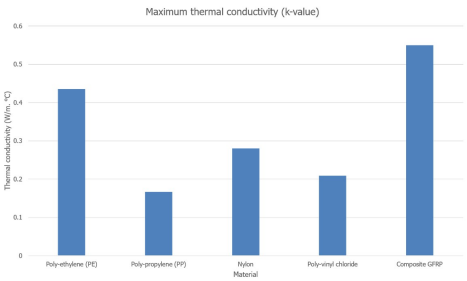

Figure D.1: Thermal conductivity values for several materials

In general, plastics have a relatively low thermal conductivity below 1 $W/m.C$, whereas conductors such as aluminium and steel have high thermal conductivity's above 50 $W/m.C$. The results for concept 1,2,4 and 5 are discussed and can be seen in Figure D.2. Concept 3 is not incorporated in the results since this concept is expected not to have large heat transfer happening, due to more than one layer being present, including plastic materials.

It can be concluded that the composite concept has the highest temperature loss, and this can be explained by having the highest value of thermal conductivity. However, the temperature loss in the pipe is negligible as for a pipe with a thickness of 5 mm, the temperature loss is only 0.087 degrees. In conclusion, for plastics such as PE, PP, nylon, PVC and composite GFRP the temperature loss due to heat transfer is not significant, which is why it is not incorporated in the MCA.

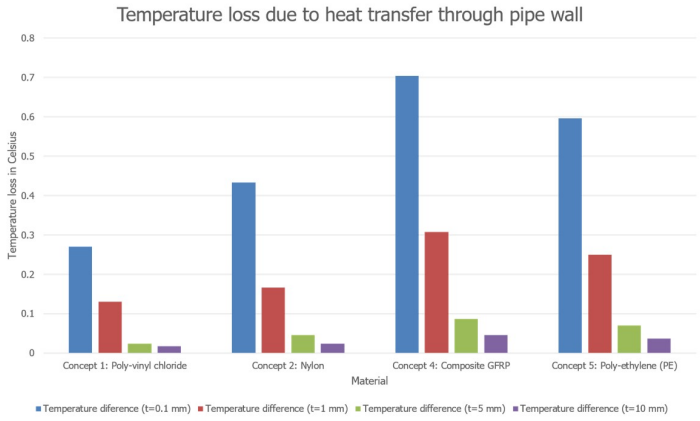

Figure D.2: Temperature loss heat transfer

E

Deep Sea Mining application for OTEC

In this Appendix, the deep sea mining market is discussed. Deep sea mining requires high energy capacities for a longer period of time offshore in stationary vessel mode, implying an OTEC installation could be the answer. Having an OTEC installation on a vessel which goes offshore for a longer period of time could provide the energy needed for the deep sea mining activities.

E.1. Background deep sea mining

Deep sea mining is a technology that started in 1960 when companies such as West Germany, Japan and Canada became interested. In order to be able to fund the capital expensive deep sea mining, companies formed consortia and used subsidies from the government. Falling commodity prices, changes in international maritime law and politic law tensions between North and South eventually led to the end of the deep sea mining industry around 1980 [34].

Due to rising demand in scarce metals and minerals that are possible to be mined at deeper seas, the urge and interest is there to start deep sea mining. Minerals that are possible to be mined include manganese nodules, copper, nickel, gold, zinc and cobalt. Manganese nodules are also referred to as poly-metallic nodules. Manganese nodules are potato like shaped mineral rocks with a diameter of 0.01 m - 0.12 m. Although the deep sea mining industry is a very promising market, it is also a capital intensive market [34].

Exploration contracts for particular zones are given by the ISA (international seabed authority). In collaboration with the UN, the ISA can award exploration contracts to do research for certain areas. The Clarion Clipperton Zone (CCZ) has been investigated and contains many poly-metallic nodules. Other areas that are interesting for the deep sea mining industry are the Peru basin, near the Cook island and in the Central Indian ocean basin. On the environmental impact of deep sea mining at the bottom of the seabed has not been done much research yet. Habitats of rare species and plants live at the bottom of the sea and might be impacted by the deep sea mining industry. In total there are considered to be three different main types of mineral deposits [28], which can be seen in Figure E.1:

- Massive sulphides in the neighborhood of hydro-thermal vents
- Poly-metallic nodules on flat areas of the sea bottom (abyssal plains)
- Cobalt rich crusts present on slopes and summits

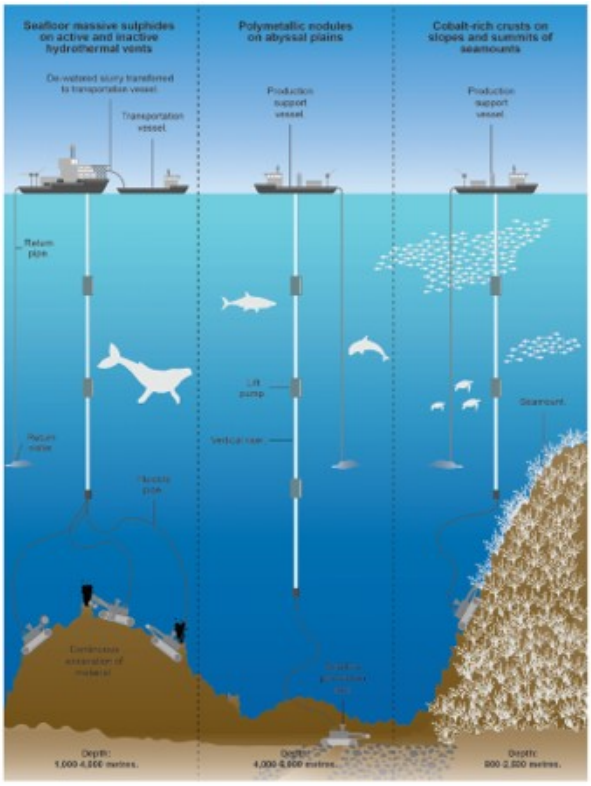

Figure E.1: Processes in deep sea mining [16]

E.2. Relevance for OTEC technology

Two possible concepts for combining OTEC with DSM are shown in Figure E.2 and E.3 [17] [6].

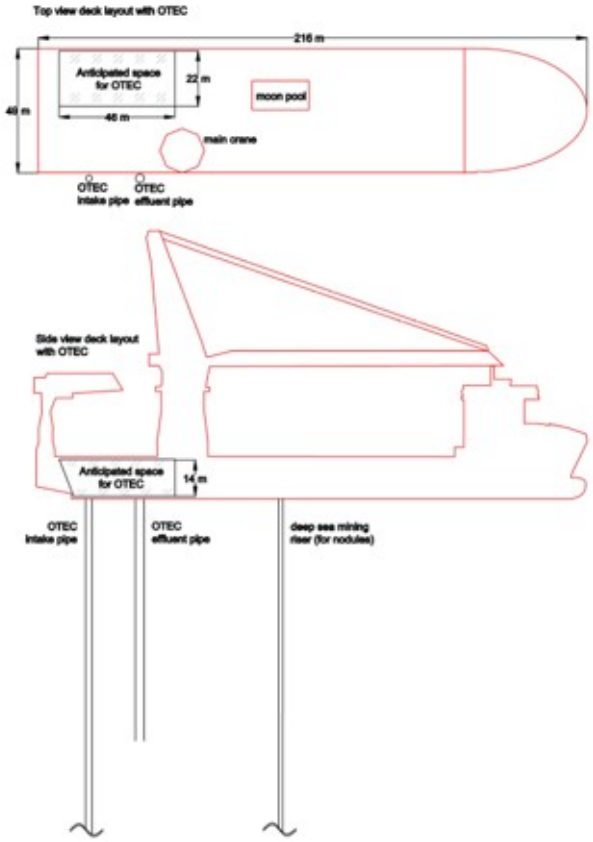

Figure E.2: OTEC onboard of a vessel for DSM [6]

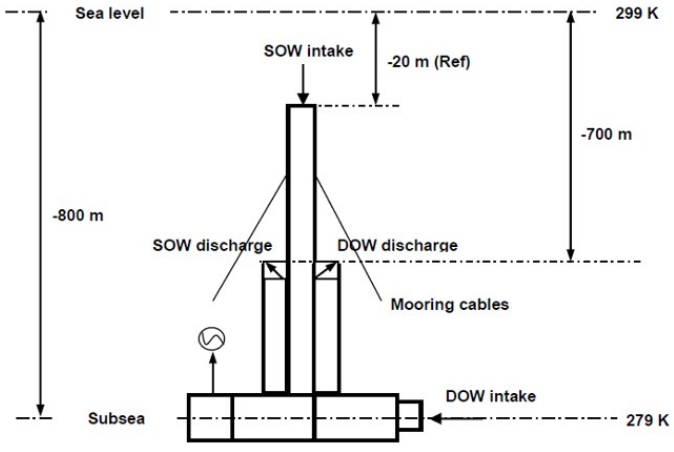

Figure E.3: OTEC subsea concept [6]

F

Conditions on Bonaire

F.1. Current over depth in years 2016, 2017 and 2018

The current profile data has been retrieved from Copernicus data. The location used for this data is (12.250; -68.500).

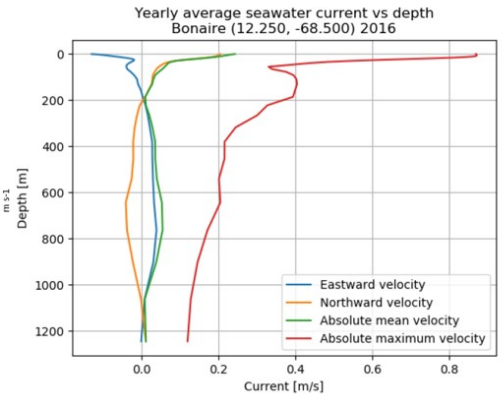

Figure F.1: Current over depth profile 2016

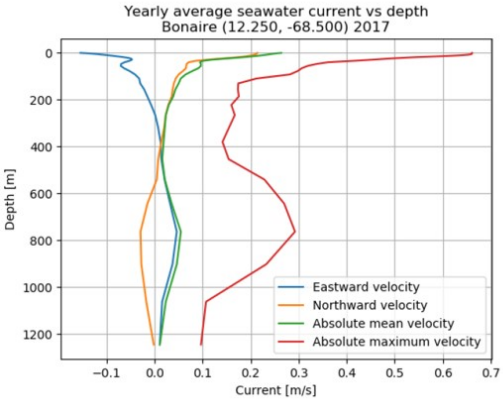

Figure F.2: Current over depth profile 2017 [10]

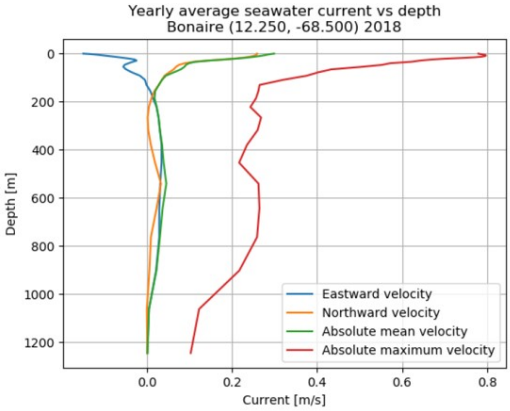

Figure F.3: Current over depth profile 2018 [10]

F.2. Bathymetry

In Figure F.4, the rough bathymetry of the island of Bonaire is shown. The website Navionics is used for the retrieval of the bathymetry data. It is clea to see the bathymetry is steepest around location 1 and location 2. This is favorable since in this way, the shortest distance for the electricity cables to the shore is achieved.

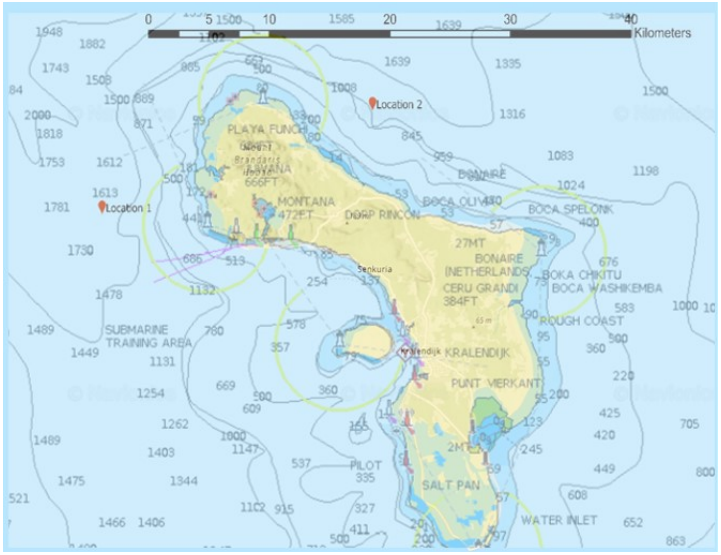

Figure F.4: Bathymetry location 1 and 2

F.3. Map of the island

In Figure F.5, the grid connections at the island of Bonaire are shown. It is clear to see that most grid connections are located at the west side of the island.

Figure F.5: Energy grid Bonaire

F.4. Water density at the location

The temperature dependency of the water density is shown in Figure F.6. The density function of water as a function is plotted in Figure F.8.

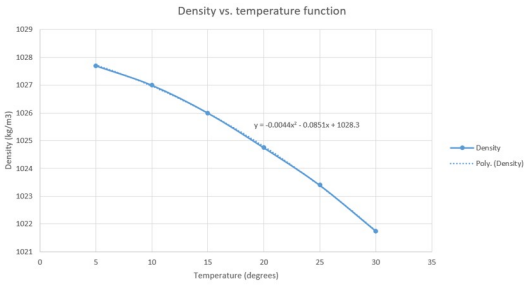

Figure F.6: Water density as a function of temperature

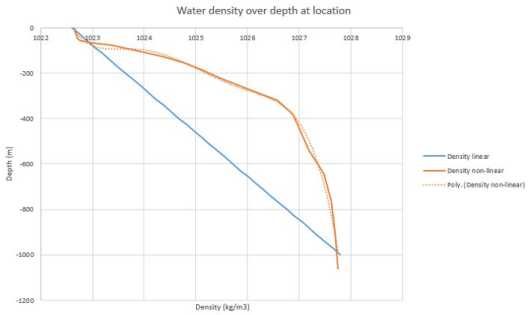

Figure F.7: Linear vs theoretical density function over depth

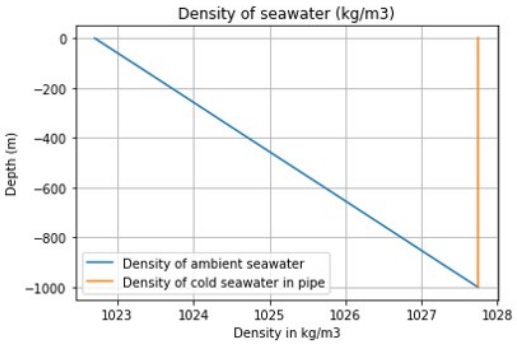

Figure F.8: Density ambient seawater

F.4.1. Salinity in the water

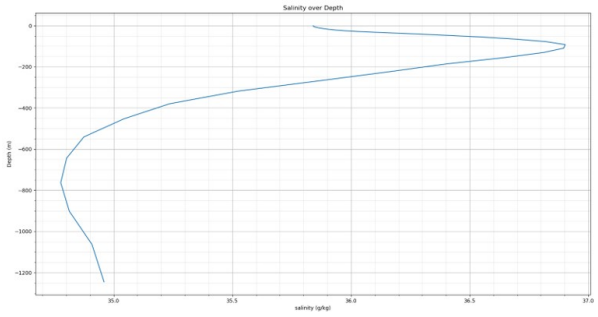

Figure F.9: Water salinity over depth at location for years 2017-2019 [10]

F.4.2. Temperature profile Bonaire

The inlet temperature differs from approximately 4.7 degrees to 5.7 degrees and the temperature at the surface differs from 26.0 degrees to 30.3 degrees in the years 2016, 2017 and 2018. However, the difference in ocean temperature (between 0 and 1000 m) is always above 20 degrees, as can be seen in Figure F.12. A minimum temperature difference of 20 degrees is guaranteed throughout the years, with the exception of one year which is negligible. In the year 2018, a few days in February the temperature difference was below 20 degrees.

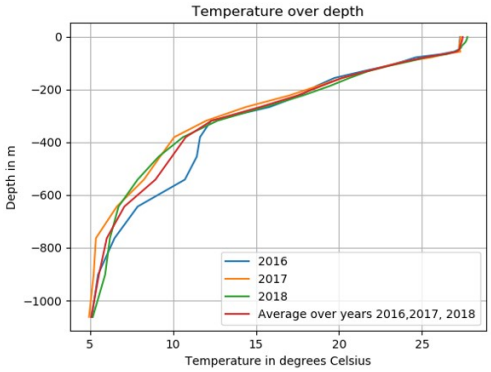

Figure F.10: Temperature over depth in 2016, 2017 and 2018

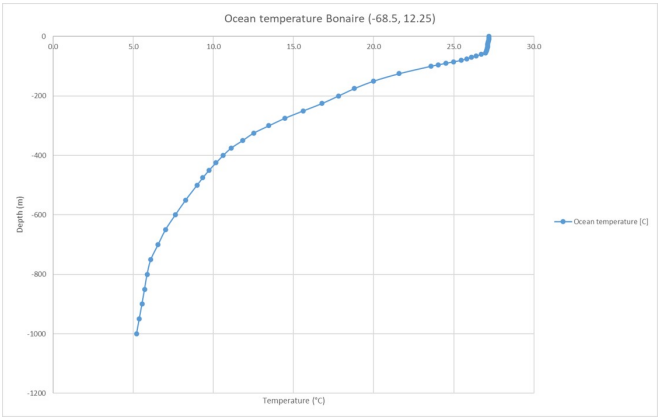

Figure F.11: Temperature profile Bonaire

F.5. Environmental conditions on Bonaire

The environmental conditions that are assessed at the chosen location for the OTEC deployment are current, waves (mainly driven by wind) and temperature. Copernicus data has been retrieved for the significant wave height, wave direction and current profile [10]. The significant wave height and current have been calculated for a return period of 100 years as input for the forces working upon the cold water pipe. The return period of 100 years has been chosen as an input for the design loads. Even though there is no public design standard for OTEC pipes yet, the design criterion of withstanding a weather condition with a return period of 100 years is chosen. This is assumed to be reasonable and on the safe side.

Figure F.12: Difference in temperature between inlet and surface water

F.6. Location

The chosen location for the Ocean Thermal Energy Conversion plant is Bonaire. The island of Bonaire is of commercial interest to Allseas. In addition, Bonaire is located in the Caribbean meaning favorable conditions of at least 20 degrees temperature difference are present for OTEC.

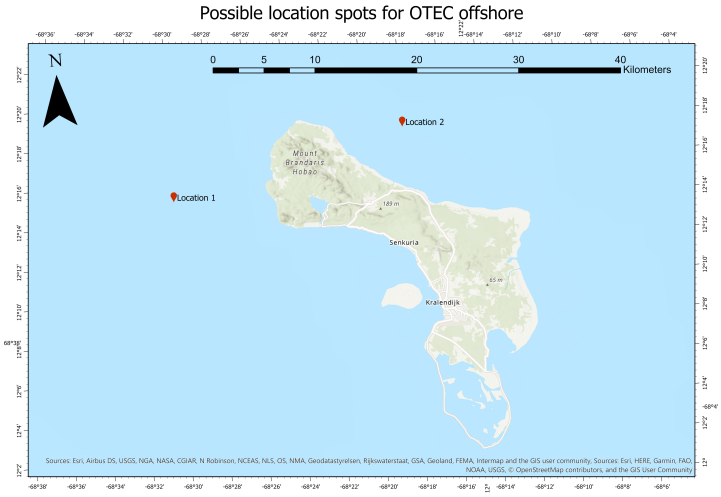

Figure F.13: Location spots for OTEC offshore

Three possible spots for the location of the OTEC plant have been selected and can be seen in Figure F.13. Location 1 has coordinates (12.25, -68.5) and Location 2 has coordinates (12.30, -68.3).

Location 1 is selected to be the most suitable location for an offshore OTEC plant due to the the relative short distance to the shore and an easy grid connection to the power station of BOPEC, which is located at the shore next to location 1 (see Appendix F). Also, location 1 is located in a more sheltered are compared to location 2 since the dominant wave direction is from the east and flows along the east coast in north direction meaning location 2 is more subjected to environmental conditions.

The depth at the chosen location is of importance to the design of the OTEC installation. A depth of at least 1000 m is needed in order to make sure the temperature difference is large enough. The specific water depth is mainly of importance for the mooring system. A water depth of at least 1100 m is chosen to be a reasonable estimate for the water depth since the inlet of the cold water pipe should not be too close to the seabed, else the seabed will be influenced. Location 1 is approximately 1750 m deep, meaning it meets the requirement of at least 1100 m.

However, it is favorable to have the shortest distance to shore since a cable has to transport the generated electricity to shore. For this reason, Location 1 has been moved slightly to the east and south direction. The final coordinates are: (12.20; -68.45). The environmental conditions for this location are assumed to be the same. The depth at this location is 1200 m.

F.6.1. Current conditions

The current conditions at the chosen location vary over time and over depth. Copernicus data has been retrieved and is used as input for the current conditions. The current profile for 3 years (2016,2017 and 2018) was used for this analysis. The main current direction around the area of Bonaire is in direction north west, which can be explained by the Caribbean current which flows through the Caribbean from the east along the coast of South America into the Gulf of Mexico. In Figure F.14, the Caribbean current can clearly be seen moving the water in west direction.

The maximum current velocities measured at the surface of the water have been summed up in Table F.1. The current profiles over depth can be found in Appendix F. Using the maximum current velocity at the surface a current profile can be determined using equation F.1 [18]. A maximum current velocity at 1000 m depth of 0.2 m/s is assumed in this current profile, which is a conservative estimate of the current velocity at 1000 m deep.

$$V_c = V_{max} * exp(-0.0043z) + 0.2 \tag{F.1}$$

in which:

- V_{max} is the maximum current speed at the surface measured [m/s]
- z is the location coordinate, in which the origin of the axis is at the water surface and the positive coordinate is downwards [m]

Table F.1: Maximum current velocity at the surface

Year	Maximum current velocity (z=0)	Maximum current velocity (z=-1000m)
2016	0.85 m/s	0.14 m/s
2017	0.66 m/s	0.16 m/s
2018	0.77 m/s	0.16 m/s

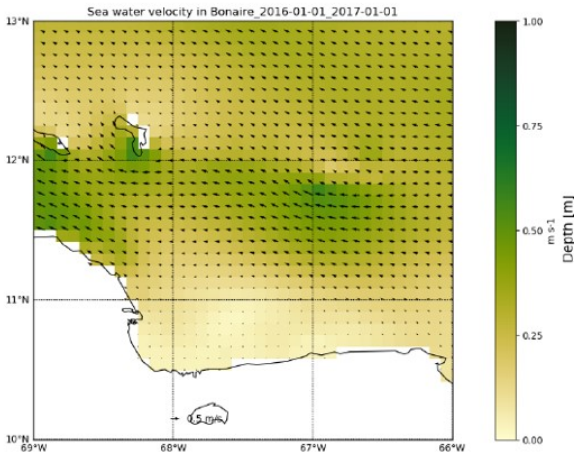

Figure F.14: Caribbean current profile

A current profile distribution for the design life of the OTEC plant should be determined in order to give a correct estimate for the forces that act upon the structure. Since only 3 years of current data was

available, a Gumbel extrapolation was not used since the estimation gives too much of incorrectness. Instead, other OTEC works have been used as input to determine a realistic maximum current acting upon the pipe. Previous OTEC installation designs were mainly focused on the location of Curacao. However, since Curacao lies in the same area as Bonaire in the Caribbean the current conditions can be assumed to be similar. A maximum current velocity at the surface of 2.2 m/s for a return period of 100 years was used for Curacao [8]. A conservative estimate of 2.0 m/s was chosen for the maximum current velocity at the surface, which is more than double the maximum current velocity measured in the years 2016, 2017 and 2018.

F.6.2. Wave conditions

The main wave direction at the chosen location spot is from the east and is dominated by the wind. In Figure F.15 , the direction of the waves is plotted for the years 2016, 2017 and 2018. It can clearly be seen that the dominant wave direction is from the east (90 degrees). By analysing the wave direction graph, it can be concluded the mean value of wave direction is 90 degrees and it is clear that the wave direction spectrum represents a normal distribution with a mean of 90.7 degrees and a standard deviation of 21.6 degrees.

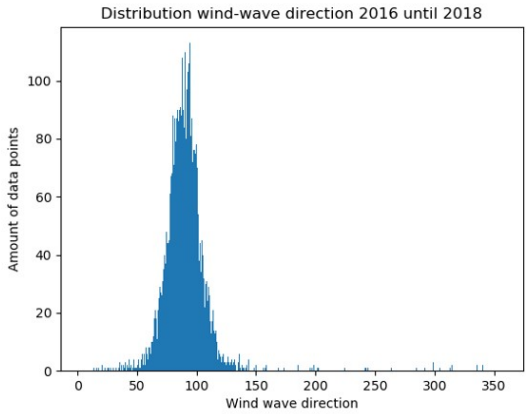

Figure F.15: Wave direction histogram for 3 years

F.6.3. Determination of extreme wave height

In order to determine the extreme wave height at the chosen location, a Gumbel extrapolation to the significant wave height in 100 years is done. After this, the significant wave height is converted into an extreme wave height representable for 100 years. With the value of the extreme wave height, the peak period corresponding to these conditions can be determined. Finally, by using linear wave theory, the corresponding wave length and wave frequency can be calculated.

For a total of 10 years (2008 - 2017), the significant wave height from Copernicus has been used as input for the significant wave height. The data contains 8 data points per day. The significant wave height has been plotted for the years 2014 and 2017 as can be seen in Figure F.16. This has been done since these two years have caused the highest and lowest significant wave height.

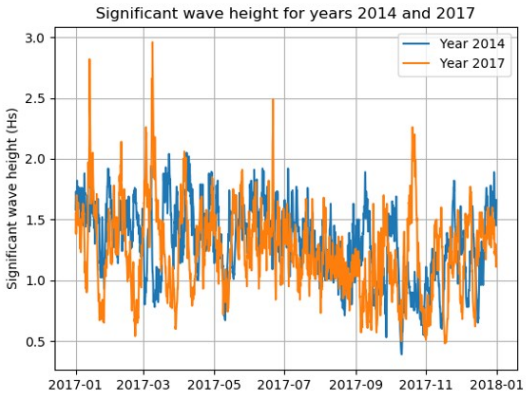

Figure F.16: Significant wave height in 2014 and in 2017

For each year, the extreme value of the significant wave height has been reported and this can be seen in Table F.2. By using the maximum values per year for 10 years (n=10) including the rank of each significant wave height, a Gumbel extrapolation can be used to estimate the maximum significant wave height with a return period of 100 years. The Gumbel cumulative density function (CDF) is represented by equation F.2.

Year	$H_{s,max}$ **(m)**	**Rank (#)**
2014	2.05	10
2012	2.12	9
2013	2.18	8
2008	2.3	7
2010	2.34	7
2015	2.45	5
2011	2.5	4
2016	2.62	3
2009	2.71	2
2017	2.96	1

Table F.2: Significant wave height per year

$$F_x = \exp(-\exp(-(\frac{x-u}{\alpha}))) \tag{F.2}$$

In this distribution x, u and α are used and can be calculated by the equations below.

$$\bar{x} = \sum_{i=1}^{n} \frac{x_i}{n}$$

$$s_x^2 = \frac{1}{(n-1)} \sum_{i=1}^{n} (x_i - \bar{x})^2$$

$$u = \bar{x} - 0.5772\alpha$$
$$\alpha = \frac{\sqrt{6} s_x}{\pi}$$

The results of the Gumbel extrapolation can be seen in Figure F.17. Equation F.3 describes the function of the significant wave height. Inserting the desired return period, gives the corresponding significant wave height. For 30 years, H_s is equal to 3.13 m. For 100 years, H_s is equal to 3.48 m.

$$H_s(t) = 0.2953ln(t) + 2.1268 \tag{F.3}$$

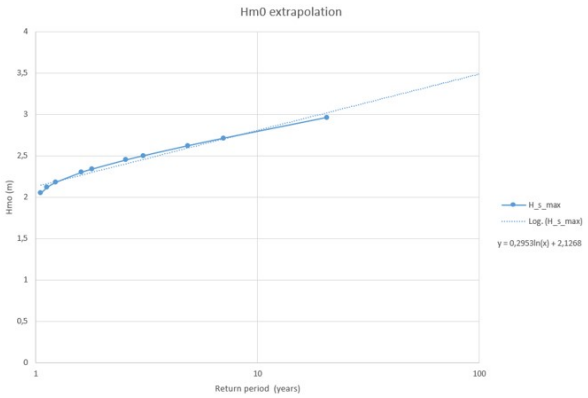

Figure F.17: Gumbel extrapolation significant wave height

In order to get a maximum wave height for 100 years, the significant wave height for 100 years needs to be converted to the extreme wave height. An easy rule of thumb, is that in many storms the maximum wave height is approximately equal to twice the significant wave height (equation F.4). In this conversion factor, it is assumed that the crest heights and wave heights are Rayleigh distributed and a duration of a 6 hour storm with a zero crossing period of 10 seconds.

$$H_{max} = 1.96 * H_s \tag{F.4}$$

in which:

- H_s is the significant wave height [m]

The maximum wave height for 100 year return period, according to equation F.4 is equal to 6.84 m. This is a value for the wave height in a severe storm. By assuming we have regular waves, the amplitude of the corresponding wave can be estimated to be half of the value of H_{max}, meaning a_{max} for 100 years is 3.42 m.

The corresponding period, wave frequency and wave length can be calculated using the dispersion relation for deep water. The results are listed in Table F.3.

Parameter	Value	Unit	Parameter	Value	Unit
H_s	3.49	m	H_{max}	6.84	m
T_s	7.47	s	T_{max}	10.46	s
w_s	0.85	rad/s	w_{max}	0.60	rad/s
L_s	87.18	m	L_{max}	170.87	m

Table F.3: Results 100 year environmental values

G

Installation of foldable pipe

The idea of the installation sequence of the foldable FLEX-hose is shown in Figure G.1 and Figure G.2. The folded pipe can be transported on the vessel, as shown in Figure G.1. Once the vessel is at the desired location, the foldable pipe can be installed as shown in Figure G.2.

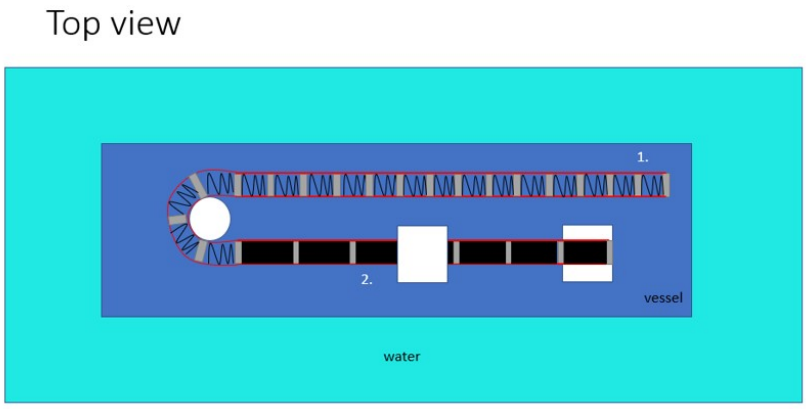

Figure G.1: Top view installation

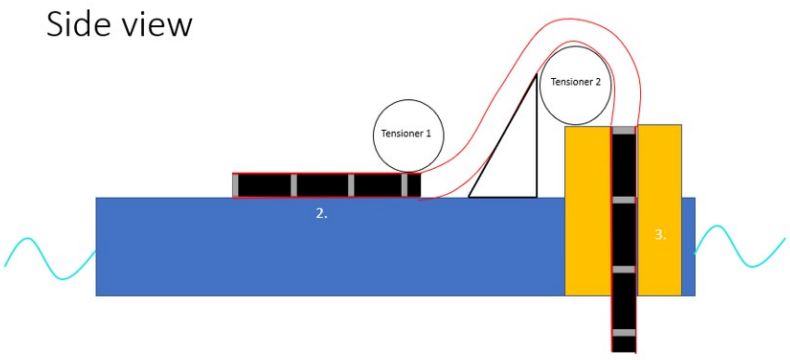

Figure G.2: Side view installation

G.1. Foldable pipe design during lifting calculation

In order to be able to check whether an offshore installation vessel could be able to lift the total foldable concept design, a rough calculation is provided by the lifting operation shown in Figure G.3.
The assumptions of the lifting case are:

- F_{cwp} = 1840 mT
- F_{crane} = 250 mT (Oceanic)
- F_{vessel} = 3719 mT (Oceanic)
- ρ_w = 1027.75 kg/m^3
- A_{vessel} = 129 x 25 = 3225 m^2 (Oceanic)

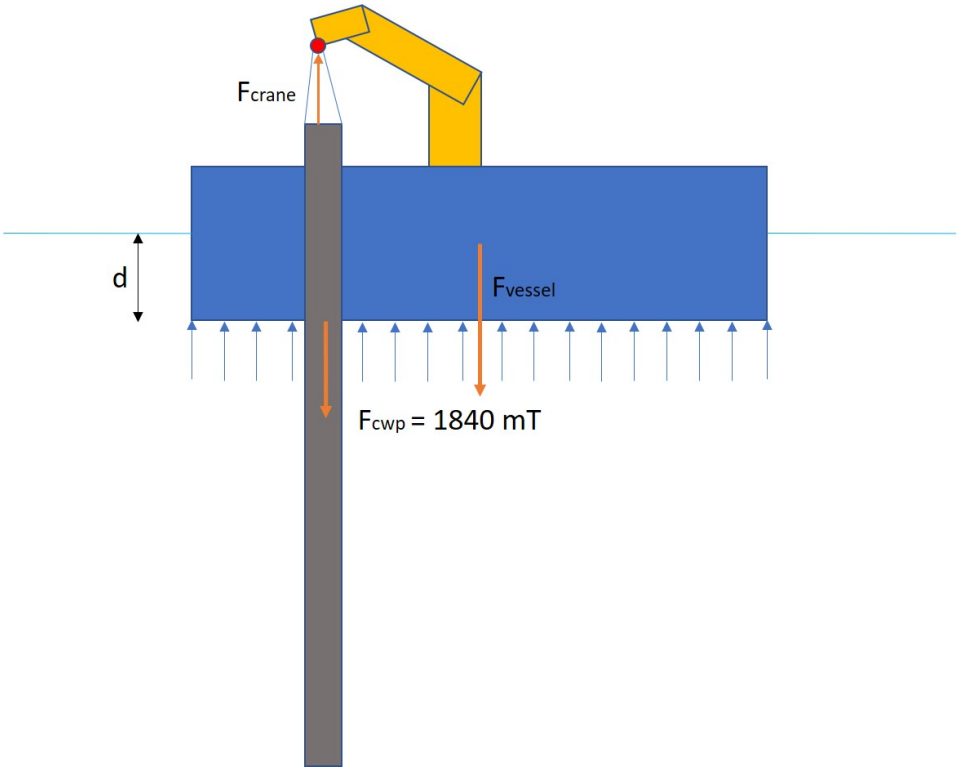

Figure G.3: Lifting situation of foldable pipe

The vertical equilibrium that should be satisfied is given by equation 6.13. The needed draft for Oceanic disregarding a mooring system is calculated to be 1.64 m, which is feasible.

$$\sum F = F_{cwp} + F_{vessel} - F_{crane} - \rho_w * g * d * A_{vessel} = 0 \quad \text{(G.1)}$$

in which:

- F_{cwp} is the force due to the weight of the foldable cold water pipe [N]
- F_{crane} is the lift capacity of a crane [N]
- F_{vessel} is the force due to the weight of the vessel in the water [N]
- ρ_w is the warm seawater density [kg/m^3]
- A_{vessel} is the surface area on the bottom of the vessel [m^2]

H

Buckling of a thin walled pipe

The assumptions of the general differential equations which lead to the expression of the collapse pressure are [35]:

- The shell is a round cylinder before buckling
- The shell is of uniform thickness throughout
- The material in the shell is homogeneous and isotropic, and
- The thickness of the shell wall is small compared to the diameter, so that the distribution of the normal stress over the thickness may be assumed as linear
- As a consequence the preceding assumption, the radial stress is considered to be negligible compared to the circumferential and longitudinal stress
- Displacements are small compared to the thickness so that certain small quantities may be neglected.
- The graphs shown in this study are performed for a material with a Poisson's ratio v = 0.3

H.1. Determination of K-values

The K-values as used in Chapter 5 are determined by Figure H.1 and H.2.

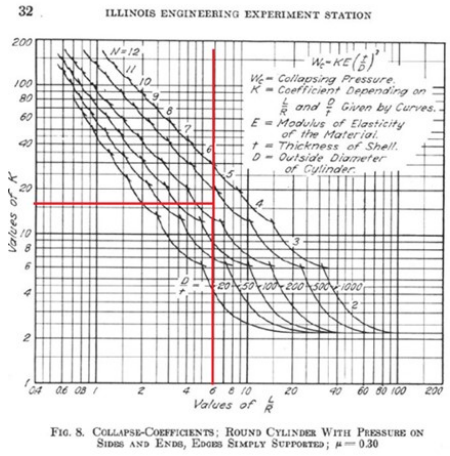

FIG. 8. COLLAPSE-COEFFICIENTS; ROUND CYLINDER WITH PRESSURE ON SIDES AND ENDS, EDGES SIMPLY SUPPORTED; $\mu = 0.30$

Figure H.1: K value collapse pressure for preliminary design values

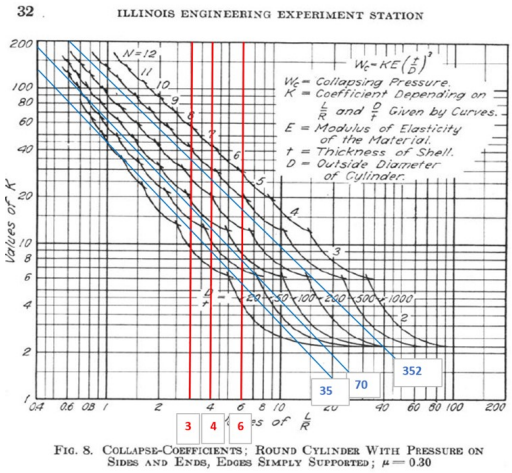

FIG. 8. COLLAPSE-COEFFICIENTS; ROUND CYLINDER WITH PRESSURE ON SIDES AND ENDS, EDGES SIMPLY SUPPORTED; $\mu = 0.30$

Figure H.2: K value collapse pressure for sensitivities

H.2. Buckling of a circular ring

The differential equation for the deflection curve for a thin circular ring is given by equation H.1. For an infinitely large r this equation reduces to that for a straight beam [19]. The following derivation is taken from the book [19]. The main importance of this derivation, is the expression given in equation H.2.

$$\frac{d^2u}{ds^2} + \frac{u}{r^2} = -\frac{M}{EI} \tag{H.1}$$

The method of obtaining the collapsing pressure is to assume that the true circular section is slightly deflected elastically, and then find the external pressure that will just hold the ring in equilibrium in this shape. Its value can be obtained by use of the equation for the deflection curve of a ring, as seen in equation H.1. There are four inflection points $(a, b, c,$ and $d,$ Figure H.3) at which the bending moment is zero and also the radial deflection is zero. The bending moment at any cross section B of the ring in Figure H.3 is:

$$M = M_0 + p\overline{AO} \cdot \overline{AD} - \left(\frac{p}{2}\right)\overline{AB}^2$$

In the triangle $AOB,$ the law of cosines gives:

$$\overline{OB}^2 = \overline{AO}^2 + \overline{AB}^2 - 2\overline{AO} \cdot \overline{AB}\cos\theta$$

but $\cos\theta = \overline{AD}/\overline{AB}$, so

$$\overline{OB}^2 = \overline{AO^2} + \overline{AB^2} - 2\overline{AO} \cdot \overline{AD}$$

or

$$\frac{\overline{AB}^2}{2} - \overline{AO} \cdot \overline{AD} = \frac{1}{2}\left(\overline{OB}^2 - \overline{AO}^2\right)$$

and substituting the values $\overline{OB} = (r - u)$ and $AO = (r - u_0)$ gives:

$$\frac{\overline{AB}^2}{2} - \overline{AO} \cdot \overline{AD} = \frac{1}{2}\left[(r-u)^2 - (r-u_0)^2\right]$$

Noting that u is small in comparison to $r,$ terms in u^2 and u_0^2 can be neglected to give:

$$\frac{\overline{AB}^2}{2} - \overline{AO} \cdot \overline{AD} = r\,(u_0 - u) \tag{H.2}$$

in which:

- $\overline{AB}$ denotes the length from A to B, as shown in Figure H.3 $[m]$
- $\overline{AO}$ denotes the length from A to O, as shown in Figure H.3 $[m]$
- $\overline{AD}$ denotes the length from A to D, as shown in Figure H.3 $[m]$
- r denotes the radius r of the thin walled cylinder $[m]$
- u_0 denotes the horizontal compression at the right and left edge $[m]$
- u denotes the compression along the circle as a function of the angle $[m]$

This expression is used for the relation between the compression at the edges left and right of the thin walled sheet and the outward displacement.

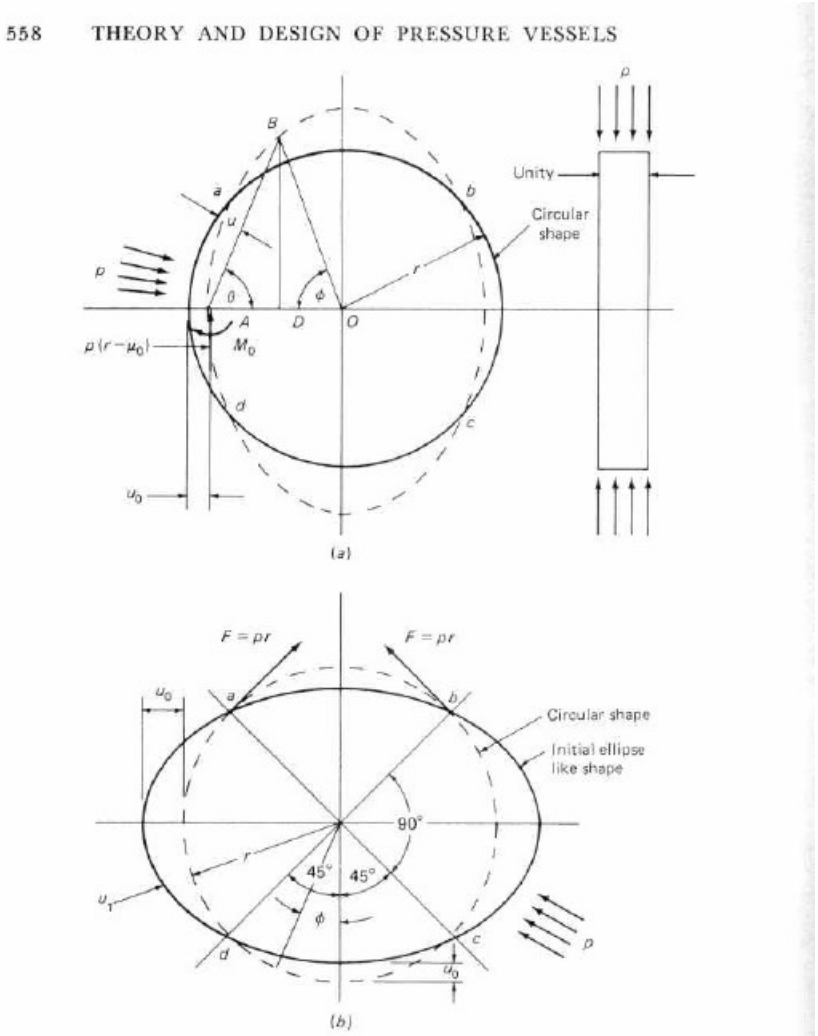

Fig. 8.4. (*a*) Cylindrical Ring under External Pressure During Buckling to an Ellipselike Shape. (*b*) Cylinder with Initial Ellipticity under External Pressure

Figure H.3: Cylindrical ring under external pressure ellipse shape

Visualizations of foldable pipe

Some visualizations of the foldable pipe have been made in Sketchup and can be seen in Figures I.1, I.2 and I.3.

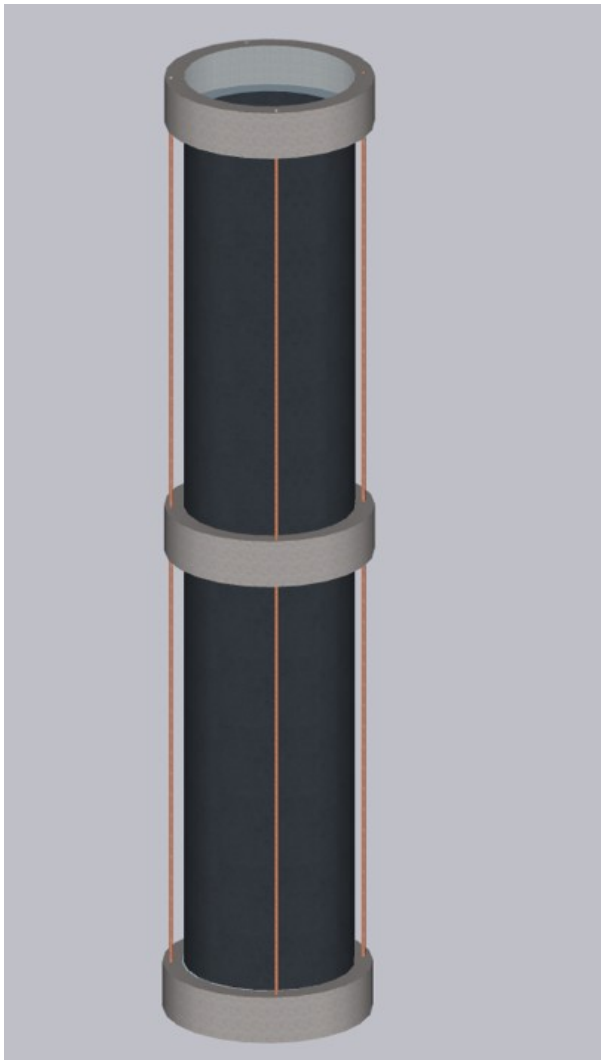

Figure I.1: Foldable concept drawing

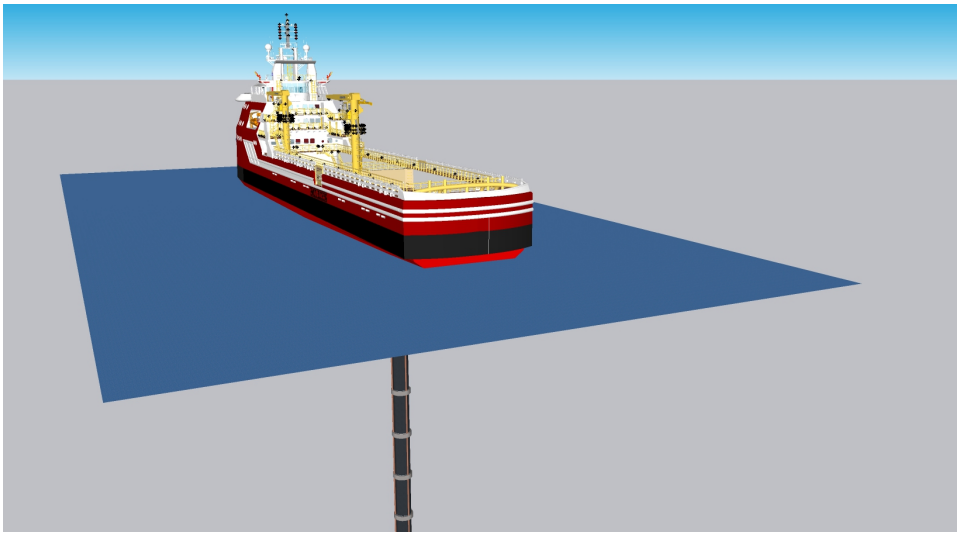

Figure I.2: Visualization foldable pipe concept with ship Allseas 1

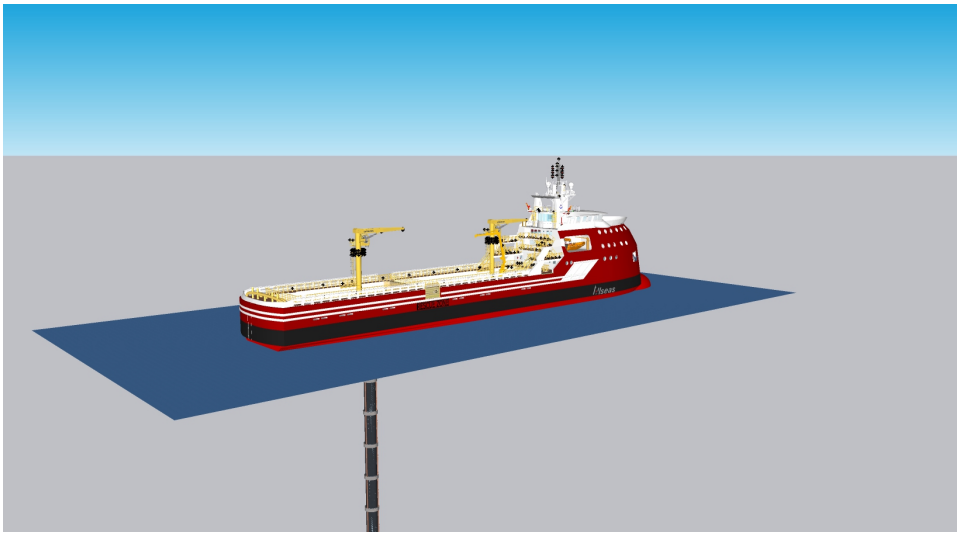

Figure I.3: Visualization foldable pipe concept with ship Allseas 2

J

Sheet model derivation

In this Appendix, the sheet model derivation is explained. Figure J.1 shows the sheet model representation. The thin walled sheet is split up into two sections: a left section and a right section. The displacement of the tin walled sheet is calculated on the cross section in the middle, as denoted by the red points in Figure J.1.

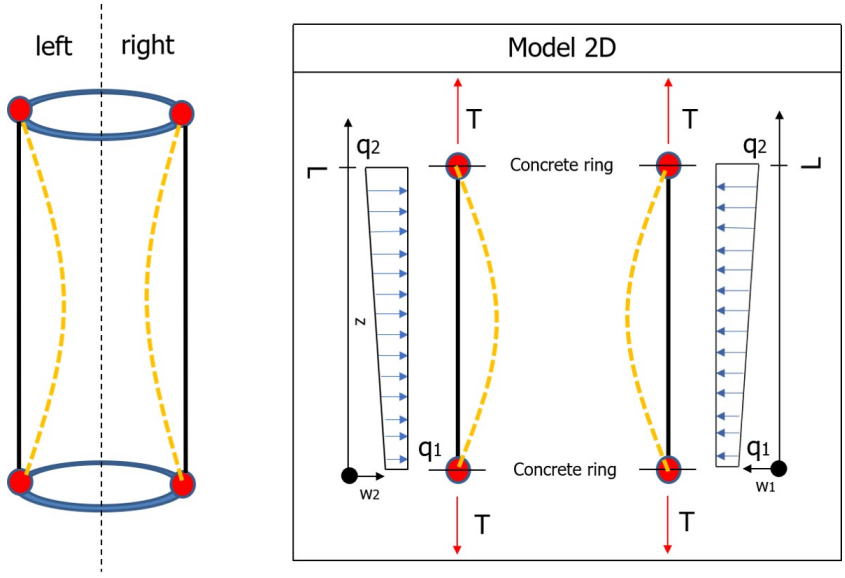

Figure J.1: 2D sheet model of the thin walled sheet

J.1. Equation of motion

The equation of motion for the left and the right part is the same and is shown in equation J.3. The static solution of the equation of motion is considered.

$$\rho A\ddot{w} - Tw'' = q_1 + \frac{q_2 - q_1}{L} * x \tag{J.1}$$

$$\ddot{w} - \frac{T}{\rho A}w'' = \frac{q_1}{\rho A} + \frac{q_2 - q_1}{L\rho A} \tag{J.2}$$

$$-c^2 w'' = \frac{q_1}{\rho A} + \frac{q_2 - q_1}{L\rho A} \tag{J.3}$$

As can be seen from equation J.3, the cross section falls out of the equation, meaning it does not have an influence on the displacement of the sheet. This is an uncertainty of the sheet model.

$$-c^2 = \frac{T}{\rho A} \tag{J.4}$$

J.2. Boundary conditions

$$w(0) = 0; w(L) = 0 \tag{J.5}$$

J.3. Solution of the equation of motion

$$w(x) = -\frac{1}{6}\frac{q_2 - q_1}{2T} * x^3 - \frac{1}{2}\frac{q_1}{T} * x^2 + \frac{L(2q_1 + q_2)}{6T} * x \tag{J.6}$$

Bibliography

[1] Adiputra, R. and Utsunomiya, T. (2019). Stability based approach to design cold-water pipe (CWP) for ocean thermal energy conversion (OTEC). *Applied Ocean Research*, 92:101921.

[2] Agency, U. S. E. P. (2015). Global Greenhouse Gas Emissions Data.

[3] Bergman, A. (2013). Design of a Modular Composite OTEC Cold Water Pipe.

[4] Bernardoni, C., Binotti, M., and Giostri, A. (2019). Techno-economic analysis of closed OTEC cycles for power generation. *Renewable Energy*, 132:1018–1033.

[5] Bluerise (2014). Offshore ocean thermal energy conversion - Feasbility study of a 10 MW installation. (March).

[6] Bluerise and GSR (2019). Sustainable OTEC power for Deep Sea Mining - Pre-feasibility study for Global Sea Mineral Resources NV. (January).

[7] Bluerise BV (2017). Ocean Thermal Energy - Renewable energy from the ocean. Technical report.

[8] Brakel, L. D. (2018). Design and modeling of a tension leg platform capable of supporting a 10 MW OTEC plant. Technical report.

[9] Commission, E. (2019). Reducing emissions from the shipping sector.

[10] Copernicus (2020). Copernicus data.

[11] DCNS (2011). Foldable_pipe_DCNS.pdf.

[12] De Sario, A. (2017). MSc Thesis Report Cold-Water Pipeline Deployment for Offshore OTEC Power Plants. Technical report.

[13] DNV-GL (2019). Energy transition outlook 2019 executive summary.

[14] DNV GL (2019). Maritime Forecast To 2050. *Energy Transition Outlook 2019*, page 118.

[15] Elengy (2019). LNG: AN ENERGY OF THE FUTURE.

[16] Energy, F. M. f. E. A. a. (2018). BMWi (2018) German DSM Study.

[17] Fachina, V. (2017). Deep-Subsea OTEC. *Mechanical Engineering Research*, 7(1):1.

[18] H. Ekeren (1983). Enige aspecten van het gedrag van een flexibele koudwaterpijp voor een 10 MW OTEC-centrale.

[19] Harvey, J. (1997). *John F. Harvey - Theory & Design of Pressure Vessels (1997)*.

[20] Keesmaat, K. (2015). Installation of a Large Diameter Cold Water Pipe in Deepwater for a Land-Based OTEC Plant.

[21] Keesmaat, K. and Janssen Ir BJ Kleute, i. M. (2015). Installation Limits of Large Diameter Cold Water Pipes in Deep Water for Land-Based OTEC Plants. Technical report.

[22] Kleute, B. J. (2014). System sensitivity and cold water pipe analysis of a 10MW Offshore OTEC-Ocean Thermal Energy Conversion plant. Technical report.

[23] KNVR (2019). IMO climate agreement.

[24] Kuiper, G. L. (2008). *Stability of offshore risers conveying fluid*. Eburon Uitgeverij BV.

[25] Lee, J. (1998). Modified thin wall pipe formula for deep water application. *Proceedings of the International Offshore and Polar Engineering Conference*, 2:82–85.

[26] Li, X., Jiang, X., and Hopman, H. (2018). A review on predicting critical collapse pressure of flexible risers for ultra-deep oil and gas production.

[27] Miller, A. K. (2011). OTEC Advanced Composite Cold Water Pipe : Final Technical Report Abstract and 1-page Executive Summary.

[28] Miller, K. A., Thompson, K. F., Johnston, P., and Santillo, D. (2018). An Overview of Seabed Mining Including the Current State of Development, Environmental Impacts, and Knowledge Gaps. *Frontiers in Marine Science*.

[29] NSW Government (2013). Common air pollutants and their health effects.

[30] Obrien, Patrick; Meldrum, E. O. C. P. J. A. K. M. I. (2011). Outcomes from the SureFlex Joint Industry Project - An International Initiative on Flexible Pipe Integrity Assurance,10.4043/21524-MS.

[31] Pipelife (2002). Pipelife Norge AS Technical Catalogue for Submarine Installations of Polyethylene Pipes. Technical report.

[32] Rubino, F., Nisticò, A., Tucci, F., and Carlone, P. (2020). Marine application of fiber reinforced composites: A review. *Journal of Marine Science and Engineering*, 8(1).

[33] Ryzin, J. V., Grandelli, P., Lipp, D., and Argall, R. (2005). The Hydrogen Economy of 2050: OTEC Driven? Technical report.

[34] Sparenberg, O. (2019). A historical perspective on deep-sea mining for manganese nodules, 19652019. *The Extractive Industries and Society*, pages 842–854.

[35] Sturm, R. G. (1941). A study of the collapsing pressure of thin-walled cylinders. *New York*, 1367:3225–3237.

[36] Trevor Brown (2019). Maritime fuel mix could be 25 % by 2050.